TEMPERATURE MODELING AND CONTROL OF THE SULFURIC ACID PLANT IN AN INDUSTRIAL SMELTER

by

Sarah Caron

Thesis submitted in partial fulfillment of the requirements for the degree of
Master of Applied Science (M.A.Sc.) in Natural Resources Engineering

Faculty of Graduate Studies
Laurentian University
Sudbury, Ontario, Canada

© Sarah Caron, 2019

THESIS DEFENCE COMMITTEE/COMITÉ DE SOUTENANCE DE THÈSE
Laurentian Université/Université Laurentienne
Faculty of Graduate Studies/Faculté des études supérieures

Title of Thesis Titre de la thèse	Temperature Modeling And Control Of The Sulfuric Acid Plant In An Industrial Smelter
Name of Candidate Nom du candidat	Caron, Sarah
Degree Diplôme	Master of Applied Science
Department/Program Département/Programme	MASc Natural Resources Engineering
Date of Defence Date de la soutenance	June 25, 2019

APPROVED/APPROUVÉ

Thesis Examiners/Examinateurs de thèse:

Dr. Helen Shang
(Supervisor/Directrice de thèse)

Dr. John Ashley Scott
(Committee member/Membre du comité)

Dr. Junfeng Zhang
(Committee member/Membre du comité)

Dr. Ali Elkamel
(External Examiner/Examinateur externe)

Approved for the Faculty of Graduate Studies
Approuvé pour la Faculté des études supérieures
Dr. David Lesbarrères
Monsieur David Lesbarrères
Dean, Faculty of Graduate Studies
Doyen, Faculté des études supérieures

ACCESSIBILITY CLAUSE AND PERMISSION TO USE

I, **Sarah Caron**, hereby grant to Laurentian University and/or its agents the non-exclusive license to archive and make accessible my thesis, dissertation, or project report in whole or in part in all forms of media, now or for the duration of my copyright ownership. I retain all other ownership rights to the copyright of the thesis, dissertation or project report. I also reserve the right to use in future works (such as articles or books) all or part of this thesis, dissertation, or project report. I further agree that permission for copying of this thesis in any manner, in whole or in part, for scholarly purposes may be granted by the professor or professors who supervised my thesis work or, in their absence, by the Head of the Department in which my thesis work was done. It is understood that any copying or publication or use of this thesis or parts thereof for financial gain shall not be allowed without my written permission. It is also understood that this copy is being made available in this form by the authority of the copyright owner solely for the purpose of private study and research and may not be copied or reproduced except as permitted by the copyright laws without written authority from the copyright owner.

Abstract

Roasting, smelting and converting are pyrometallurgical techniques used to eliminate gangue rock from sulfide ores and produce a saleable metal product. Due to the large amount of sulfur present in sulfide ores, the off-gas produced from pyrometallurgical processing is laden with sulfur dioxide (SO_2). Production of sulfuric acid (H_2SO_4), from off-gas laden with SO_2 is one of the methods used at smelters to reduce the amount of SO_2 being released into the atmosphere. The acid plant consists mainly of a catalytic converter, absorption towers and a network of heat exchangers. SO_2 is converted to sulfur trioxide (SO_3) which is absorbed to produce a sulfuric acid product. Efficient oxidation of SO_2 occurs within a tight temperature range so heat exchangers equipped with bypass valves are used to regulate the temperature throughout the acid plant.

In this dissertation, a steady-state model is developed from fundamental steady-state mass and energy balances. The steady-state model provides a relation between the process variables and the temperature of the outlet streams of the heat exchangers. Unknown variables are estimated using industrial operating data. The steady-state model is used to investigate the effect of process variables on the controlled variables. The disturbance variables that have the largest effect on the process are the feed gas flow rate and the SO_2 concentration. The results provide useful information since with recent process modifications that are part of the Clean AER project, variations in the feed gas flow rate and SO_2 concentration will increase. The effects of the manipulated variables were also investigated which provides a foundation of understanding

for process control. The results of the investigation of the effect of process variables on the controlled variables were quantified by calculating the steady-state gains.

The dynamics of the process were investigated through analyzing the industrial operating data. The output variables do not vary simultaneously with changes in the input variables. The correlation coefficients were determined for the variables. The correlation coefficient between variables provides an estimate of how much influence the input variables have on the output variables. Delayed correlation analysis was performed to explore the process dynamics. Dynamic models were identified using industrial operating data with and without prior information supplied using the System Identification toolbox in Matlab. Providing the steady-state gains and an estimate of the process time constants to the System Identification toolbox greatly improved the identified model. The dynamic model was validated by comparing the model-estimated output and the output from industrial operating data.

Temperature control within the acid plant is a multiple-input-multiple-output control problem. Bristol's Relative Gain Array and Singular Value Analysis are used to determine the most effective pairing of variables. A feedforward-feedback control scheme for temperature regulation is explored. Simulations for major disturbances, such as flow rate and SO_2 concentration of the feed gas, are carried out using two alternative controller pairings. The results of the simulations are reviewed and the advantages of each controller pairing are discussed.

Acknowledgements

First and foremost I would like to thank my supervisor, Dr. Helen Shang. Thank you for your patience, guidance, knowledge and continuous support of my research.

I would also like to thank my advisory committee: Dr. John A. Scott and Dr. Junfeng Zhang from Laurentian University and my external examiner Dr. Ali Elkamel from University of Waterloo for your time and insight.

The industrial data and process information for this dissertation was graciously provided by Vale's Copper Cliff operations group and Vale Technology and Innovation. Thank you for your encouragement and guidance, especially Chris Doyle, Dan Legrand and Paul Kenny, and Megan Dillabough and Heather Gauthier for arranging tours of the smelter and acid plant.

Thank you to my family for your support, encouragement and motivation throughout my studies.

The financial support from the National Sciences and Engineering Research Council of Canada (NSERC), Vale Canada Limited and Laurentian University is greatly appreciated.

Table of Contents

List of Figures

List of Tables

Chapter 1: Introduction

This introductory chapter provides general background information about the research topics and outlines the motivation and objectives of this dissertation.

1.1 Processing Metal Sulfide Ores

Nickel (Ni) is mined from laterite and sulfide ore deposits. More than of 60% of nickel production is from sulfide ores (Crundwell *et al.*, 2011). High-grade sulfide ore deposits of the Sudbury Basin has made Sudbury, Ontario a prominent area for mining and processing of nickel and copper. The most common Ni minerals present in metal sulfide ores are pentlandite ($(Ni,Fe)_9S_8$), pyrrhotite (Fe_8S_9), chalcopyrite ($CuFeS_2$) and silicate rock minerals (gangue rock). Sulfide ores contain 1.5 to 2.5% Ni and are refined to produce a high-grade nickel product containing 40 to 70% Ni (Crundwell *et al.*, 2011). Nickel bearing minerals are liberated from gangue rock by crushing and grinding after which the liberated minerals are concentrated by froth flotation to remove pyrrhotite, copper-bearing minerals and gangue rock. Smelting and converting the bulk concentrate produces to a low-iron (Fe) sulfide matte which is refined using hydrometallurgical processes to produce a saleable nickel product. The flowsheet used by Vale for the processing of sulfide ores is shown in Figure 1. Sulfur dioxide (SO_2) is produced at multiple points in the smelting of metal sulfide ores. Roasting, smelting and converting all produce an off-gas laden with SO_2.

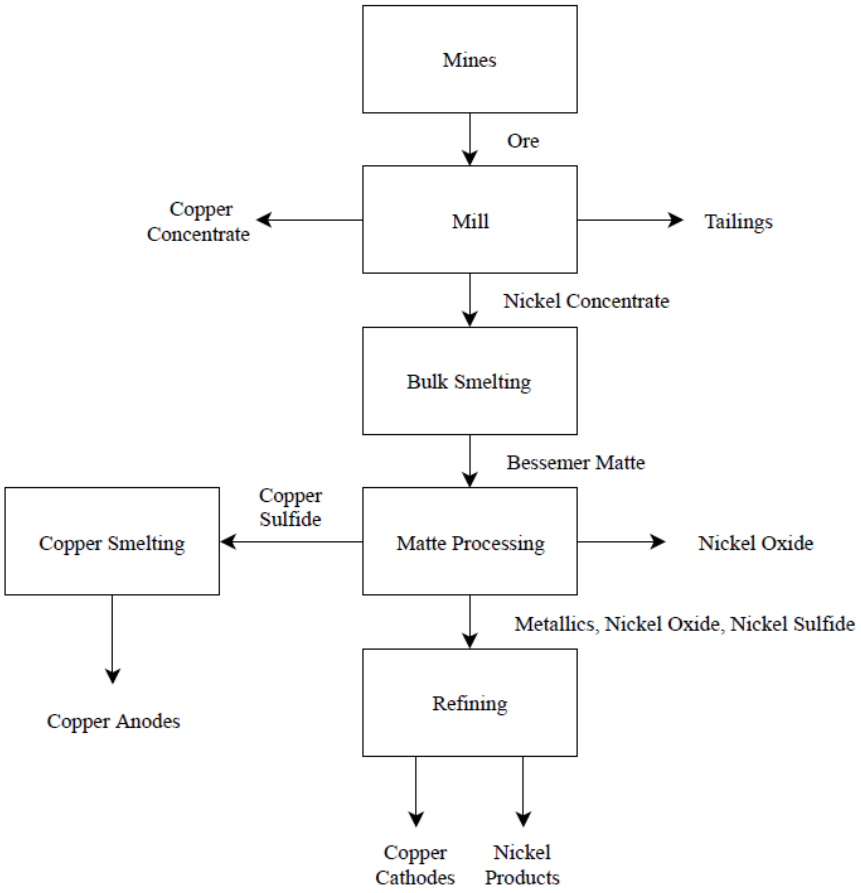

Figure 1 Vale's sulfide ore processing flowsheet (Vale Canada Limited, n.d.)

There are two steps in producing a high-grade nickel matte that is low in iron and sulfur, which makes it suitable for further refining by hydrometallurgical processes. Smelting produces a nickel rich molten sulfide matte by oxidizing and removing sulfur and iron and dissolving and removing gangue rock. Converting further removes sulfur and iron from the matte. In industry, there are two methods used for smelting nickel sulfide ores: roasting followed by smelting in an electric furnace and flash smelting, which combines the process of roasting and smelting. The flash smelting method is used by 75% of industrial processes (Crundwell *et al.*, 2011),

including Vale's Copper Cliff Smelter located in Copper Cliff, Ontario. Flash smelting requires less electricity and hydrocarbon fuel by utilizing the heat produced from oxidation reactions (Moats & Davenport, 2014). This method also avoids the production of weak SO_2 gas, which can cause upset to the acid plant. However, flash smelting requires an additional matte-from-slag settling step as there is greater loss of nickel and other metals to the slag due to the process being more oxidizing.

1.1.1 Roasting and Smelting

Roasting partially oxidizes the pentlandite and pyrrhotite minerals with air to produce a calcine containing nickel oxide (NiO) and iron oxide (FeO), which has a higher concentration of nickel, and removes sulfur via the off-gas (Crundwell *et al.*, 2011). The amount of oxidation that takes place is limited by the amount of air being supplied to the roaster. The partial oxidation reaction for pentlandite is,

$$Ni_{4.5}Fe_{4.5}S_8(s) + 12.5O_2(g) \xrightarrow{700℃} 4.5NiO(s) + 4.5FeO(s) + 8SO_2(g) + \Delta H \qquad (1.1)$$

and similarly for pyrrhotite,

$$Fe_8S_9(s) + 13O_2(g) \xrightarrow{700℃} 8FeO(s) + 9SO_2(g) + \Delta H \qquad (1.2)$$

Both oxidation reactions are exothermic, which heats up the incoming concentrate and air.

Smelting produces a molten Ni-rich sulfide matte, a molten Ni-lean silicate slag and off-gas laden with SO_2. In flash smelting, dried concentrate is mixed with a silica flux (SiO_2) and oxygen, and is blown horizontally into the furnace at 1300 °C. The smelting oxidation reactions are exothermic, producing -1,200 MJ per kmol of pentlandite and -2,500 MJ per kmol pyrrhotite (Moats & Davenport, 2014). The oxidation reaction for pentlandite is,

$$Ni_{4.5}Fe_{4.5}S_8(s) + 5.75O_2(g) \xrightarrow{1300℃} 4.5NiS(\ell) + 4.5FeO(\ell) + 3.5SO_2(g) + \Delta H \quad (1.3)$$

and for pyrrhotite,

$$Fe_8S_9(s) + 13O_2(g) \xrightarrow{1300℃} 8FeO(\ell) + 9SO_2(g) + \Delta H \quad (1.4)$$

Sulfur is removed through the off-gas by oxidizing sulfur to SO_2, which is sent to the acid plant for treatment. The furnace produces an off-gas that is strong in SO_2, approximately 20 to 50 vol% (Moats & Davenport, 2014). Iron is removed by oxidizing it to iron oxide (FeO) and fluxing the iron oxide with silica to form a molten iron-silicate slag (Fe_2SiO_4). Gangue rock is dissolved into the molten slag. The slag is then discarded. The molten matte (NiS) is 15 to 40% Ni and 20 to 40% Fe (Davenport & Partelpoeg, 2015), which is sent to converting to further oxidize sulfur and iron.

1.1.2 Converting

Converting is mainly an iron-oxidation process, removing iron as iron-silicate in the molten slag. The resulting matte is 40 to 70% Ni and 0.5 to 0.4% Fe (Davenport & Partelpoeg, 2015). During charging, the converter rotates away from the hood and furnace matte is ladled into the converter at 1200 °C with a silica flux. The converter rotates back into position for the blowing phase at which point air is injected. The iron present in the furnace matte is oxidized to a molten silicate slag (Moats & Davenport, 2014),

$$2Fe(\ell) + O_2(g) + SiO_2 \rightarrow Fe_2SiO_4(\ell) \tag{1.5}$$

Nickel and other metals that may be present are not oxidized as these reactions are thermodynamically unfavourable. Some of the sulfur present in the furnace matte is oxidized to SO_2, which provides the necessary heat for the iron oxidation reaction to proceed (Moats & Davenport, 2014),

$$S(\ell) + O_2(g) \rightarrow SO_2(g) \tag{1.6}$$

Flowing the blow stage, the converter is rotated away from the hood for the skimming phase. The unoxidized matte is immiscible with the slag matte due to differences in specific gravity. The slag is skimmed from the top of the converter and sent to a slag-cleaning vessel for

additional recovery of nickel as there are unavoidable matte droplet entrained in the slag by the turbulent converting conditions.

Peirce-Smith converters are the most commonly used vessel in industry due to their simplicity and efficiency. The converting process is a batch process so the converter emits SO_2 into the work environment and atmosphere during the charging and skimming phases. There are also fugitive emissions at the interface between the converter and hood during blowing. The SO_2 laden off-gas produced by the Peirce-Smith converter is captured by the hood and sent to the acid plant for treatment.

1.2 Sulfur Dioxide Emissions

Sulfur oxides (SO_x) are one of the six key air pollutants in addition to nitrogen oxides (NO_x), volatile organic compounds (VOC), carbon monoxide (CO), ammonia (NH_3) and fine particulate matter ($PM_{2.5}$). Emissions of SO_x into the atmosphere can have adverse effects on human health and the environment, especially in those communities close to smelters. The majority of SO_x emissions released by anthropogenic sources consists mostly of SO_2 (Environment and Climate Change Canada, 2019).

Sulfide ore mined from the Sudbury Basin contains eight times more sulfur in the ore than nickel, which results in a substantial amount of waste rock and concentrator tailings (Crawford, 1995) which can lead to acid mine drainage (Ripley *et al.*, 1996). Processing sulfide ores also

produces an off-gas laden with SO_2 and fine particulate matter. Where SO_2 cannot be converted to sulfuric acid (H_2SO_4), liquid SO_2, ammonium sulfate, jarosite or gypsum it is released into the atmosphere. The main contributor of SO_x emissions is the ore and mineral processing industry, contributing 482 kT (kilotonnes) of total SO_x emissions in 2016, of which 360 kT was produced by the non-ferrous mining and smelting industry (Environment and Climate Change Canada, 2019). In 1985, the INCO Copper Cliff Smelter was the largest single source of SO_2 emissions in Canada (Franklin *et al.*, 1985).

Once released into the atmosphere SO_2 is converted to other compounds and/or removed by various mechanisms including oxidation, wet or dry acid deposition, absorption by vegetation and soil and dissolution into water. The most dominant of the removal processes being acid deposition (WBK & Associates Inc., 2003). Although wet deposition (acid rain) is a concern, dry deposition can also contribute to the acidification process. SO_x released into the environment are oxidized in the atmosphere to form sulfuric acid, which may be transported distances and deposited in regions remote from their point sources. Heap roasting, an early smelting technique, released large amounts of SO_2 into the environment (Crawford, 1995) and contributed to the presence of acid deposition in Canada since the early 1970s (Franklin *et al.*, 1985). Acid deposition puts natural resources that are vital components of the Canadian economy at risk, about 50% of forest growth and agricultural production in eastern Canada is located in areas receiving excess acid rain (Franklin *et al.*, 1985). Acid deposition has shown to have harmful effects through direct deposition, the mobilization of metals (cadmium, lead and aluminum) and the transformation of a substance to a more toxic form.

When SO_2 is inhaled, it dissolves into the aqueous surfaces of the respiratory system as sulfite and bisulfite, which is absorbed and distributed throughout the body. The body's immune response can be compromised due to sulfites affecting metabolic processes through inhibition of systemic enzymes (WBK & Associates Inc., 2003). Acute exposure to SO_2 in the atmosphere is linked to respiratory illness. There are groups that are at increased risk and more susceptible to adverse effects of SO_2 at ambient levels. These include those with pre-existing cardiorespiratory disease, children, unborn children, the elderly and those with odour impairments. A study by Health Canada found that there may be a causal relationship between long-term, low-level exposure and prenatal and postnatal development issues (Read, 2016). Chronic exposure results in significantly impaired lung function and damage to the airways similar to chronic bronchitis (WBK & Associates Inc., 2003).

1.3 Sulfuric Acid Production

Sulfuric acid production is a necessary stage in the smelting process in order to reduce the amount of SO_2 released into the atmosphere. This method of emission abatement has proven effective in ensuring smelter operation is in regulatory compliance for SO_2 emission targets. Sulfuric acid is a salable by-product with a wide range of applications including fertilizers, metallic ore leaching, petroleum refining, pigment production, steel pickling and the manufacture of explosives, detergents, plastics and man-man fibres. This is an additional economic benefit to facilities processing sulfide ores.

The feed to the acid plant is a combination of the off-gases from different units of the smelter. The flash furnace produces a high-strength SO_2 off-gas while the roasters (matte processing), MK copper reactor and Pierce-Smith converters produce a low-strength SO_2 off-gas. Sulfuric acid is made from SO_2 bearing off-gases by catalytically reacting the SO_2 and oxygen (O_2) to form sulfur trioxide (SO_3) gas in the catalytic converter. In the absorption towers, SO_3 gas reacts with liquid water (H_2O) in 98.5 mass% H_2SO_4, 1.5 mass% H_2O to produce a strengthened sulfuric acid. The oxidation reaction in the catalytic converter determines the amount of SO_2 captured from the off-gas and the amount that is consequently prevented from being released into the atmosphere. Therefore, the amount of SO_2 oxidized and removed from the off-gas determines the overall performance of the acid plant.

1.4 Motivation

Research has been carried out on the modeling of catalytic converters in acid plants (Gosiewski, 1993; Günther *et al.*, 2012; Mann *et al.*, 1980; He & Shang, 2017; Silveston *et al.*, 1994; Mann *et al.*, 1986). In most existing studies the feed to the acid plant is from a sulfur burner, which has a controllable and easily maintainable SO_2 content. The feed gas to an acid plant in an industrial smelter however, presents an additional challenge due to highly varying feed conditions, so continued research is required to develop models for the acid plants in smelters (Sørensen *et al.*, 2015). This will help in achieving efficient SO_2 removal from off-gas to ensure smelter operation meets what is required by government regulations. An integrated process model of the various units of an acid plant can be used to forecast the effect

of various process changes and disturbances on the performance of the acid plant (Bergh *et al.*, 2004; Fenton *et al.*, 2016; Husnil *et al.*, 2017; Davenport & King, 2013; Kiss *et al.*, 2010; King, 1999). Process models can also be used to improve process control, optimize and simulate plant operation.

1.4.1 Sulfur Dioxide Emission Limits

Due in part to government actions and voluntary initiatives from industrial emitters SO_x emissions decreased by 65% to 1,067 kT between 1990 and 2016 (Environment and Climate Change Canada, 2019), and emission limits continue to decrease. Scientific information provides a basis to design and implement abatement programs and emission regulations. In Canada, the federal legislation controlling air pollution is the Clean Air Act under which ambient air quality objectives are set and the control of transboundary pollution originating in Canada. Under provincial legislation, the provincial governments enforce standards to prevent transboundary pollution. The act also gives the Minister of the Environment authority to recommend site-specific emission standards. Ontario Regulation (O. Reg.) 194/05 under the Environmental Protection Act sets industry standards for SO_2 emissions. The site-specific SO_2 emission limits for Vale's Copper Cliff Smelter are listed in

Table 1. Research conducted by Health Canada is the basis for setting a Canadian Air Quality Standard (CAAQS) for SO_2 (Read, 2016). O. Reg. 419/05 under the Environmental Protection Act sets local air quality limits for SO_2. The Schedule 2 and Schedule 3 local air quality limits for SO_2 emission limits are listed in Table 2.

Table 1 O. Reg. 194/05 SO_2 emission limits for Vale's Copper Cliff Smelter (Government of Ontario, 2017)

Year	SO_2 Emission Limit per Year (kT)
2006	265
2007 – 2009	175
2010 – 2014	175
2015 – Present	66

Table 2 O. Reg. 419/05 Air Pollution – Local Air Quality Schedule 2 and Schedule 3 for SO_2 emissions (Government of Ontario, 2019)

Applicable Date	Half Hour Standard (μgm^{-3})	One Hour Standard (μgm^{-3})	24 Hour Standard (μgm^{-3})	Annual Standard (μgm^{-3})
Current	830	690	275	N/A
July 1, 2023	N/A	100	N/A	10

The National Pollutant Released Inventory (NPRI) is Canada's public inventory of releases, disposals and transfers of more than 300 pollutants from over 7,000 facilities across the country. Vale's Copper Cliff Smelter (ID: 444) is one of the facilities that reports emissions to the NPRI. SO_2 emissions released from Vale's Copper Cliff Smelter from 2002 to 2017 are shown in Figure 2. Although the facility has reduced its SO_2 emissions today by almost a third since 2002, in 2017 it was still the largest contributor to SO_2 emissions by the "Non-Ferrous Metal (except Aluminum) Production and Processing" sector (Government of Canada, 2018). The large decrease in SO_2 in 2009, shown in Figure 2, is due largely to bad economy. Although acid plants are a proven method of SO_2 emission abatement, increasingly tightening regulations on SO_2 limits has proven challenging and acid plant operation may become the bottleneck for a smelter.

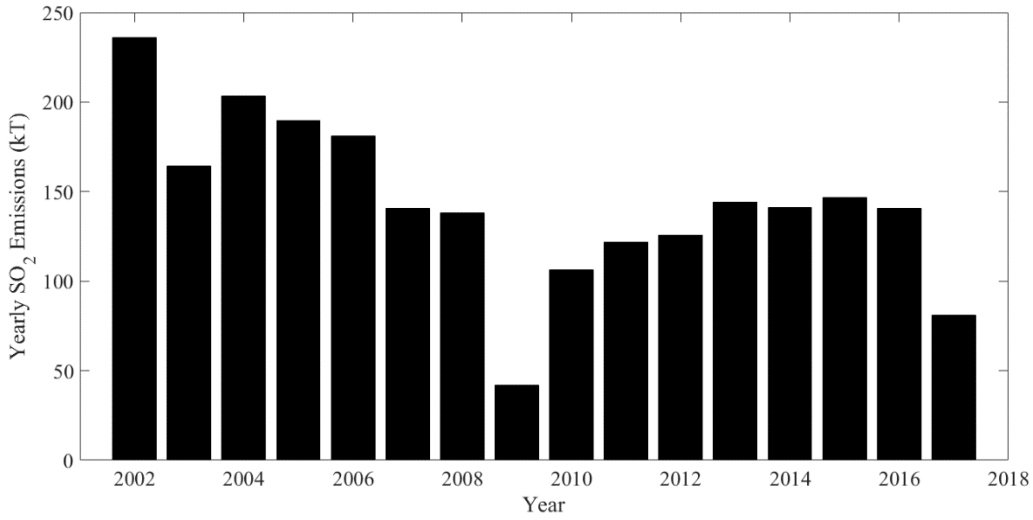

Figure 2 NPRI data for SO_2 released by Vale's Copper Cliff Smelter from 2002 to 2017 (Government of Canada, 2018)

1.4.2 Surface Facility Upgrade and Clean Atmospheric Emission Reduction Projects

Part of the motivation for this research is Vale's SFU (Surface Facility Upgrade) project and the CAD $1 billion dollar Clean AER (Atmospheric Emission Reduction) project. The projects were initiated as part of Vale's continued initiatives to reduce SO_2 emissions and in order to meet O. Reg. 194/05 site-specific SO_2 emission limit and the O. Reg. 419/05 local air quality standards. Also, in 2006 under the Canadian Environmental Protection Act of 1999 the federal government issued a Pollution Prevention Planning notice to 11 base metal smelter or refinery or zinc plant facilities, including the Copper Cliff Smelter (Government of Canada, 2006). The notice required the facilities to prepare a pollution prevention plan for meeting emission reduction targets for SO_2, submit interim progress reports and implement the pollution prevention plan by the end of 2018.

The SFU project reduced the smelter to a single higher-capacity flash furnace. While the Clean AER project, which began construction in 2012 saw a redesigned converter aisle with two new converters, now fitted with primary and secondary hoods to capture the off-gas. The off-gas from the converter aisle, which was previously emitted to the atmosphere through the Superstack, is sent to a new wet-gas cleaning plant and subsequently the acid plant. Figure 3 shows the flow of off-gas from the smelter units to the acid plant pre- and post-SFU and Clean AER changes. The projects also included new absorption towers, a secondary baghouse and fan building. The Clean AER project will reduce SO_2 emissions from the smelter by 85%, from 617 kT of SO_2 released from the site in the 1990s to an estimated 25 kT after completion (Vale, n.d.). The additional SO_2 being supplied to the acid plant will also result in an increase in sulfuric acid production. The completion of the project will also result in a 40% reduction in metals particulate emissions and greenhouse gases.

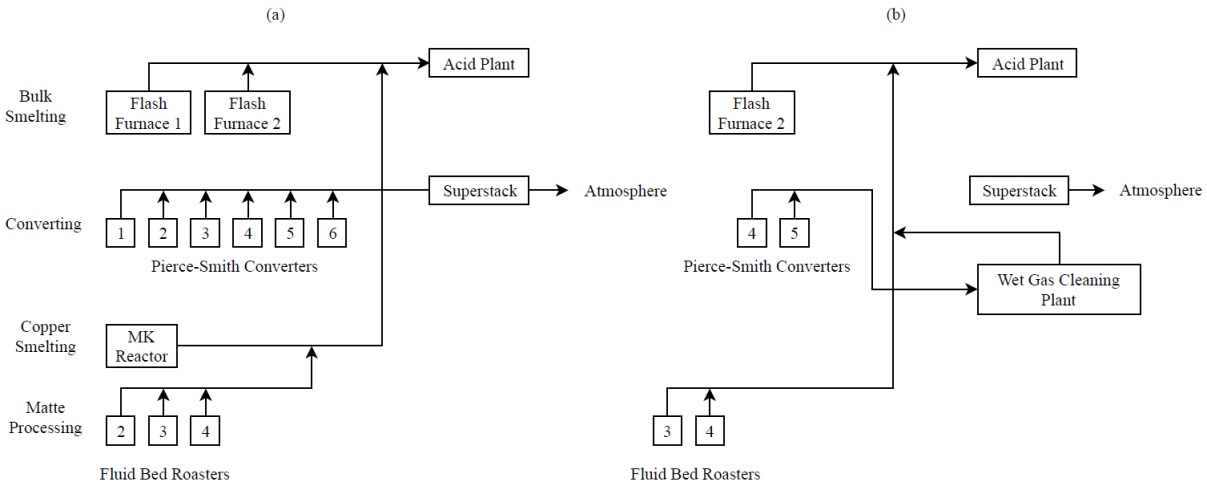

Figure 3 Off-gas flow to the acid plant at the Copper Cliff Smelter (a) pre- and (b) post-SFU and Clean AER (Vale, n.d.)

Figure 4 shows the feed gas composition and flow rate to the acid plant pre-Clean AER changes, which is highly varying. As a result of the Clean AER changes, there will be a significant increase in process variability. The feed from the Pierce-Smith converter is especially challenging due to the batch nature of the process. Once the converter off-gas is captured and sent to the acid plant the variations observed in Figure 4 will become even more dramatic. Figure 5 shows the variation of SO_2 concentration and flow rate in the converter aisle off-gas exiting the wet-gas cleaning plant, which will be sent to the acid plant post-Clean AER changes. Figure 5 also shows that the off-gas from the converter aisle is weak in SO_2, which alone is not ideal for efficient SO_2 oxidation.

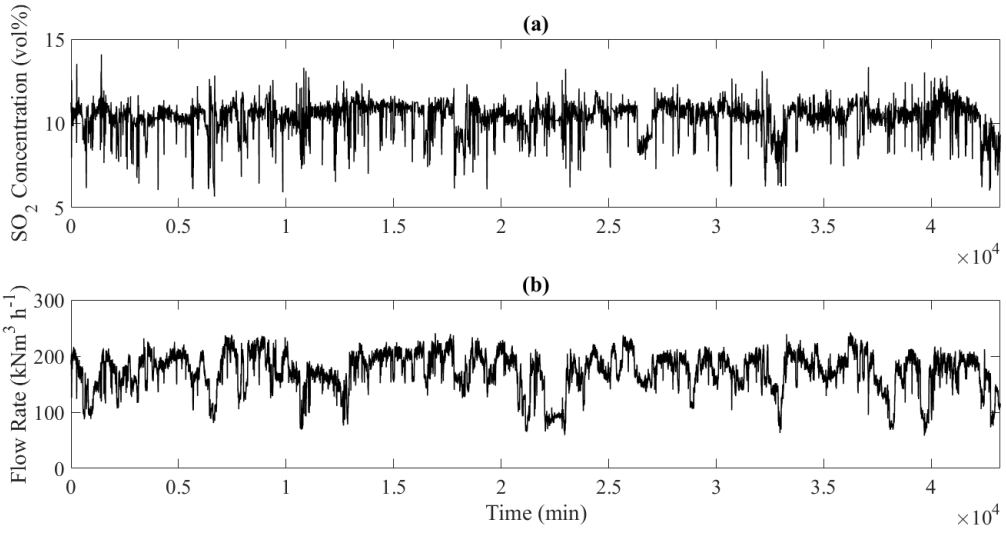

Figure 4 (a) SO_2 concentration and (b) flow rate variation in the feed gas to the acid plant pre-SFU and Clean AER

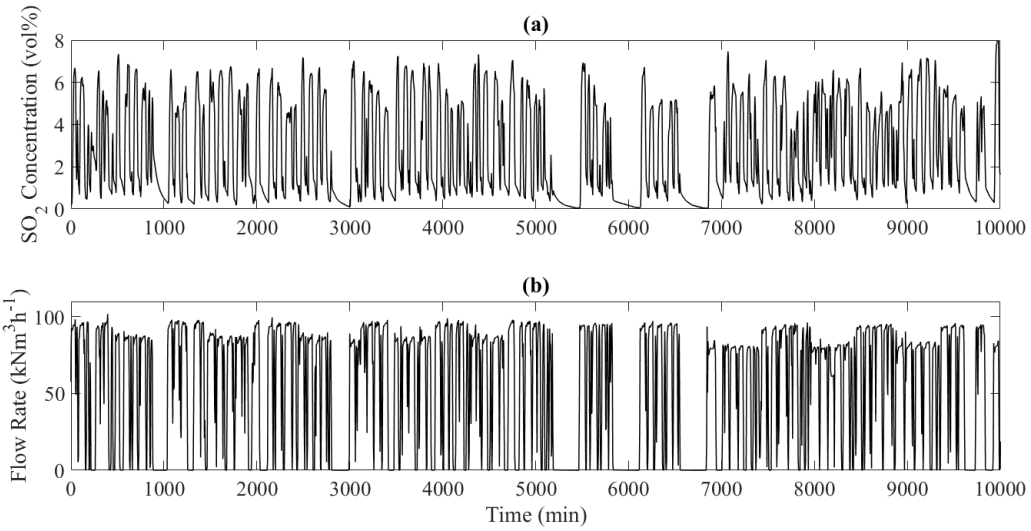

Figure 5 (a) SO_2 concentration and (b) flow rate variation in the converter aisle off-gas exiting the wet-gas cleaning plant

Since the implementation of off-gas capture from the converter aisle, oscillations in process parameters have been observed due to a non-continuous gas supply and highly varying gas conditions. In an attempt to mitigate oscillations and operate the converters in a more continuous fashion, converter aisle scheduling is used to regulate the flow of off-gas being produced. Prior to the Clean AER project, the converter aisle could operate as a single entity. However, with its off-gas now being sent to the acid plant, operational guidelines must be introduced and there must be communication between off-gas producers to maintain auto-thermal limit and reduce thermal cycling. For example if the flash furnace is offline, converting must also come to a halt, as the off-gas produced in the converting aisle is weak in SO_2 and is not sufficient for acid production. Under these conditions, the acid plant must enter a thermal cycle. Also, if the acid plant is not operating, the gas producers cannot be producing off-gas. Additional challenges include retuning of control loops and changes to equipment operation,

which are oversized for the current operating state. Modeling of the acid plant is a useful tool for validation and investigating proposed process and operational changes on acid plant performance. Modeling can also aid in enhancing acid plant performance by providing a foundation for improved process control and optimization.

1.5 Objectives

The objective of this dissertation is to develop steady-state and dynamic models for temperature in a metallurgical acid plant such that the model can well reflect industrial operation but still be simple enough for industrial applications. A second objective is to carry out simulations to determine the effect of process changes and variables on plant operation, and explore various control schemes. The ultimate objective of the research is to develop a detailed model for the sulfuric acid plant in an industrial smelter, determine the optimal operation conditions under the changing smelter operation and enhance the control of the acid plant to improve its operation.

Chapter 2: Process Description

This chapter provides an overview of the process utilized at the Copper Cliff Smelter to produce sulfuric acid from SO_2 laden off-gas.

The simplified flowsheet for the acid plant at Vale's Copper Cliff smelter is shown in Figure 6. The acid plant is mainly composed of a catalytic converter with four beds, two absorption towers, four heat exchangers and two gas coolers. Vale's Copper Cliff acid plant utilizes a double contact process, meaning there are three passes through the catalytic converter, an intermediate absorption step followed by an additional pass through the catalytic converter and a final absorption step. The off-gas from the smelter units is hot and dusty, before entering the acid plant the gas must be cooled, cleaned, diluted and dried. The gas from the smelter units also varies in SO_2 content, which can range from 10 to 75 vol%. The gas entering the catalytic converter should be much weaker in SO_2, about 8 to 13 vol% (Davenport & King, 2013). If SO_2 is present in higher concentrations the heat of the oxidation reaction in the converter would overheat the catalyst. Therefore, the feed gas must be diluted with either weak SO_2 off-gas and/or air before it is suitable for acid production.

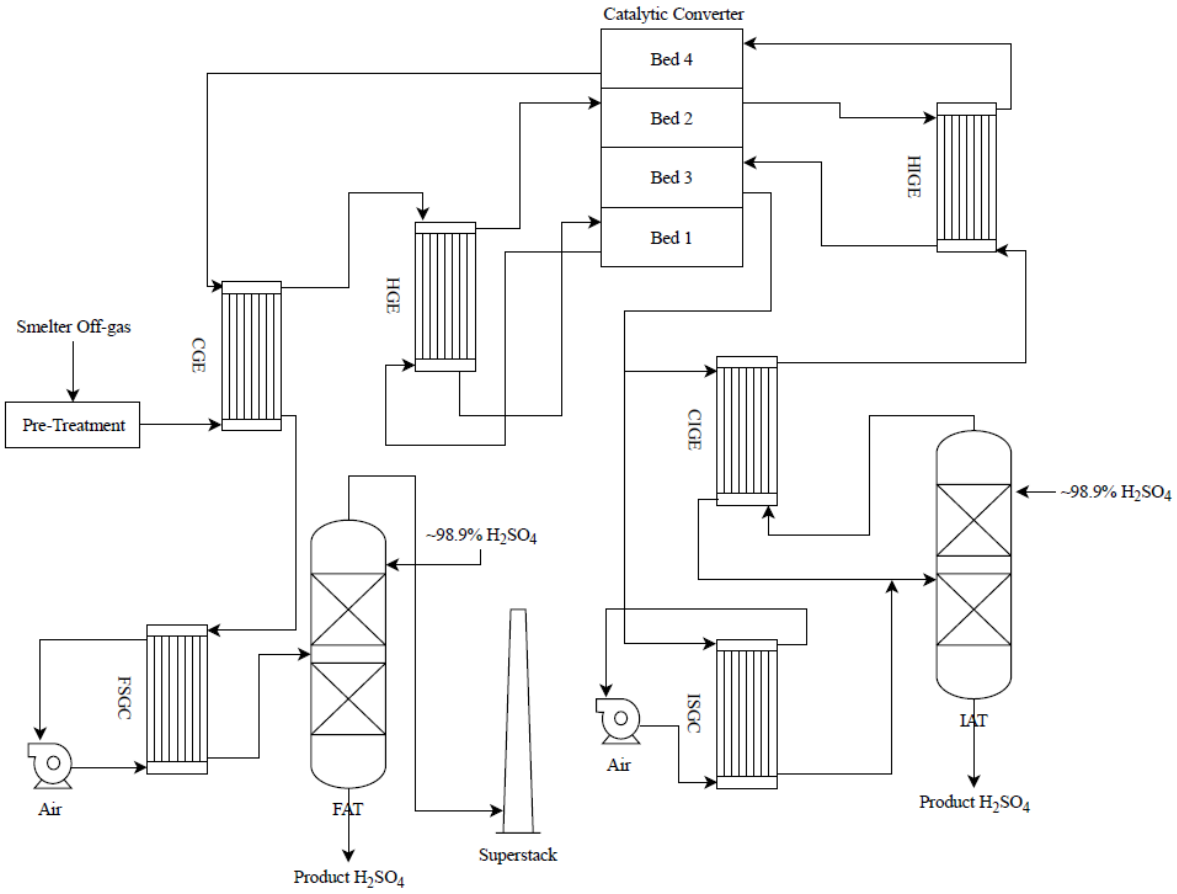

Figure 6 Acid plant gas flowsheet for Vale's Copper Cliff Smelter

2.1 Process Variables

All data for this dissertation was provided by Vale from their Copper Cliff Smelter facility. Temperature, flow rate, pressure, composition and valve position data were collected for a one-month period at the acid plant, pre-SFU and Clean AER process changes. The sampling time was one minute. The measuring points throughout the acid plant are numbered for convenience of description, as shown in Figure 7. There are controlled, manipulated and disturbance variables. The controlled variables are the outlet temperatures of the heat exchangers, in

particular the temperatures at the inlet of the catalytic converter, temperature at Node 6, Node 11, Node 13 and Node 31. The outlet temperatures are maintained at or near their set-points by adjusting the valve positions, which are the manipulated variables. The disturbance variables are the inlet temperatures to the heat exchangers, and the feed gas temperature, flow rate and composition. These variables cannot be adjusted but have an effect on the outlet temperatures.

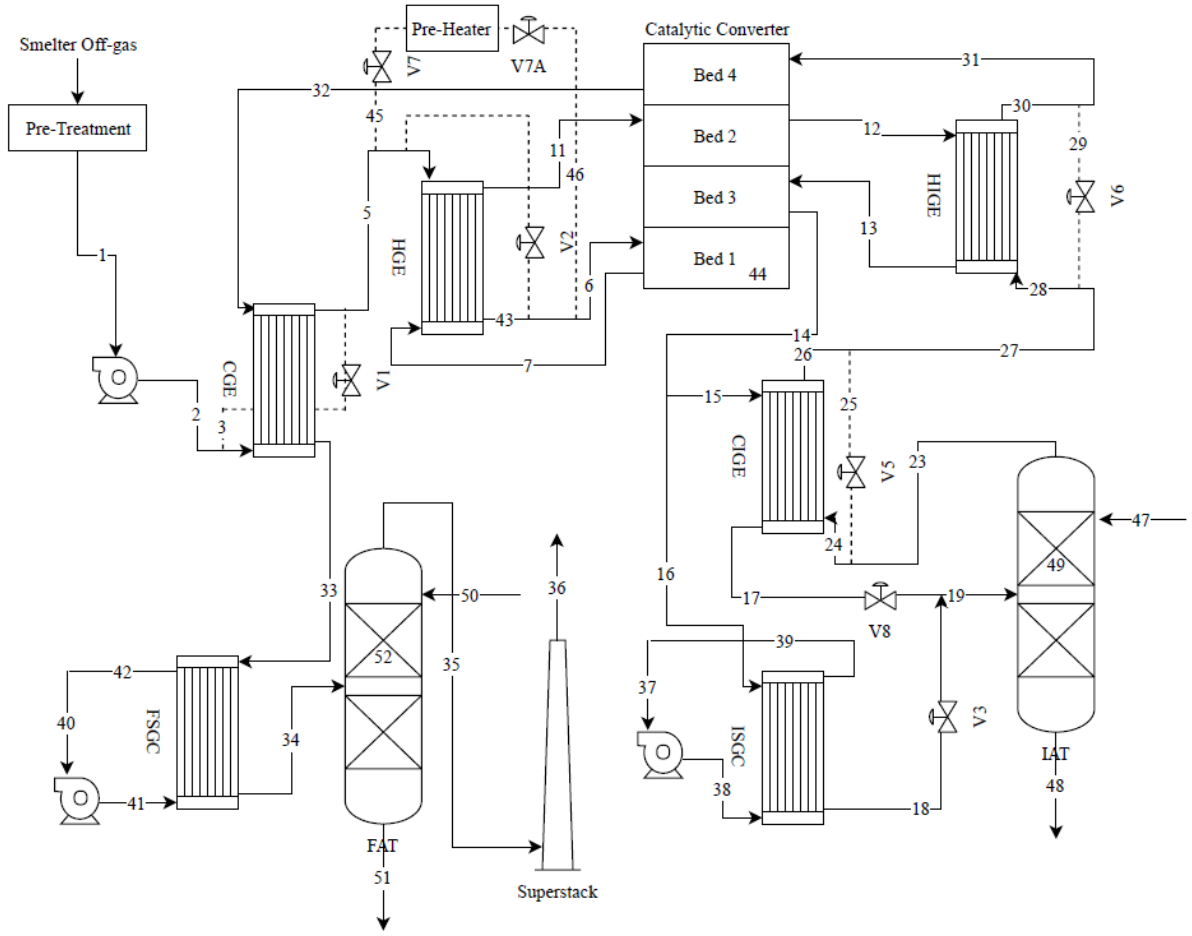

Figure 7 Measuring points for data collection at the Copper Cliff Smelter acid plant

2.2 Feed Gas Conditions

The gas composition, flow rate and heat capacities are estimated using the feed gas flow rate, temperature and SO_2 concentration from industrial operating data. The characteristics of the gas streams are inputs to the steady-state model and will be utilized in Chapter 3.

Composition

The feed to the acid plant is a combination of off-gas from the two flash furnaces, three fluid bed roasters in matter processing and a copper MK reactor. The gas contains SO_2, oxygen, carbon dioxide (CO_2) and nitrogen (N_2). However, the only component of the feed gas whose concentration is measured is SO_2. From industrial operating data, the mean SO_2 concentration is 10.36 vol%. Based on a mean SO_2 content of 10.36 vol%, the concentration of the remaining components were estimated using linear interpolation and an assay of a feed gas from a sulfuric acid plant with a similar SO_2 content. The resulting estimation of the feed gas composition is listed in Table 3. Assuming that the gas behaves ideally and the molar masses of each gas component are similar, the molar concentration used in this dissertation is equivalent to the volume percentage; 10 vol% SO_2 is equivalent to 10 mol% SO_2 or 0.10 mol fraction SO_2 (Davenport & King, 2013).

Table 3 Mean composition of the feed gas to the acid plant based on 10.36 vol% SO_2 from industrial operating data and a typical feed gas assay

Component	Typical Feed Gas Composition (Davenport & King, 2013) (vol%)	Mean Composition (vol%)
SO_3	0	0
SO_2	8 – 13	10.36
O_2	9 – 14	11.36
CO_2	0 – 7	3.30
$H_2O_{(g)}$	0	0
N_2	75	75

Heat Capacity

The heat capacity of the gas streams is calculated using gas phase thermochemistry data from the National Institute of Standards and Technology Chemistry WebBook, Standard Reference Database 69 (Linstrom & Mallard, 2018) and the Shomate Equation:

$$C_{m,i} = A + Bt + Ct^2 + Dt^3 + \frac{E}{t^2} \tag{2.1}$$

where $C_{m,i}$ (J mol^{-1} K^{-1}) is the molar heat capacity of component i, t is defined as temperature (K)/1000 and A, B, C, D and E are parameters. The values of the parameters for the components in the gas are listed in Table 4. The values of the parameters listed in Table 4 are only applicable for the associated temperature range, which has been selected based on the maximum and minimum temperature of the gas streams from industrial operating data.

Table 4 Values of parameters for the components in the gas and the applicable temperature range for use in the Shomate equation (Chase, 1998)

Component	Parameter					Temperature Range (K)
	A	B	C	D	E	
SO_3	24.02503	119.4607	-94.38686	26.96237	-0.11751	298 – 1200
SO_2	21.43049	74.35094	-57.75217	16.35534	0.086731	298 – 1200
O_2	31.32234	-20.23531	57.86644	36.50624	0.007374	100 – 700
CO_2	24.99735	55.18696	-33.69137	7.948387	-0.136638	298 – 1200
N_2	29.98641	1.853978	-9.647459	16.63537	0.000117	100 – 500
N_2	19.50583	19.88705	-8.598535	1.369784	0.527601	500 – 2000

The total molar heat capacity of a gas stream is the sum of the individual component molar heat capacities multiplied by their mol fraction:

$$C_m = \sum_i X_i C_{m,i} \tag{2.2}$$

where C_m (J mol^{-1} K^{-1}) is molar heat capacity of the gas steam and X_i is the molar fraction of each of the components in the gas stream. The total mass heat capacity of a gas stream can be calculated as follows:

$$C_p = \frac{C_m}{\sum_i X_i M_i} \tag{2.3}$$

where C_p (J g^{-1} K^{-1}) is the mass heat capacity of the gas stream and M_i (g mol^{-1}) is the molar mass of each component in the gas stream. The mean mass heat capacity for the inlet and outlet gas streams of the heat exchangers are listed in Table 5. In calculating the values of Table 5,

which are used throughout the steady-state model, the temperature used to calculate the heat capacity was the average of the inlet and outlet streams, listed in Table 6. It was assumed that the temperature change occurring within the heat exchanger does not affect the heat capacity of the gas. The heat capacity of the sulfuric acid is listed in Table 7. The data in Table 7 is within the range sulfuric acid concentrations relevant to the acid plant at the Copper Cliff Smelter.

Table 5 Mean mass heat capacity for the hot and cold steams of each heat exchanger

Gas Stream	Mean Mass Heat Capacity ($J\ kg^{-1}\ K^{-1}$)			
	CGE	HGE	CIGE	HIGE
Hot	1075.8	1064.2	1011.8	1052.0
Cold	985.91	1000.6	1072.7	1080.7

Table 6 Mean temperature between the inlet and outlet of each heat exchanger

Gas Stream	Mean Temperature (K)			
	CGE	HGE	CIGE	HIGE
Hot	633.4	805.7	604.2	747.0
Cold	438.2	586.7	485.7	653.1

Table 7 Heat capacity of sulfuric acid for varying acid strengths (Craig & Vinal, 1940)

Concentration of H_2SO_4 (vol%)	Molar Heat Capacity ($J\ mol^{-1}\ K^{-1}$)
89.36	135.56
91.81	132.63
94.82	131.38
97.44	132.55
100.00	137.57

Flow rate

The average flow rate of the feed gas is 172.5 $kNm^3\,h^{-1}$. The normalized unit, commonly used in industry, is converted to a molar flow rate by dividing by a conversion factor:

$$\dot{m} = \frac{N}{0.0224}\sum_i X_i M_i \tag{2.4}$$

where $\dot{m}$ ($kg\,h^{-1}$) is the mass flow rate and N ($kNm^3\,h^{-1}$) is the molar flow rate of the gas stream. Equation 2.4 can be used to calculate the flow rate at any point throughout the acid plant so long as the composition of the stream is known. The mass flow rate of gas at the inlet and outlet of the heat exchangers is listed in Table 8. It is assumed that the composition of the gas stream does not change between the inlet and outlet of the heat exchangers as no reaction is taking place.

Table 8 Mass flow rate of hot and cold gas streams of the heat exchangers

	Mean Mass Flow Rate ($kg\,s^{-1}$)			
Stream	CGE	HGE	CIGE	HIGE
Hot	62.01	72.52	66.93	73.89
Cold	70.31	70.31	55.10	55.10

Temperature Filtering

The temperature at the inlet of the HGE cold stream is highly varying. To remove large noises and smooth the noisy experimental data an exponential filter is applied. The filter's operation is described by (Seborg *et al.*, 2011):

$$y_F(k) = \varepsilon y_m(k) + (1 - \varepsilon) y_F(k - 1) \tag{2.5}$$

where y_F is the filtered value and y_m is the measured value, k is an instant in time and ε is a dimensionless parameter:

$$\varepsilon = \frac{\Delta t}{\tau_F + \Delta t} \tag{2.6}$$

where τ_F (min) is the time constant of the filter and Δt (min) is the sampling time. From Equation 2.5, the filter output is a weighted sum of the measured value at time k and the filter output at the previous sampling instant. The sampling time was chosen as 1 minute and the filter time constant as 3 minutes. This results in a dimensionless parameter of 0.25. Figure 8 compares the measured and filtered temperature cold stream at the inlet of the HGE. From Figure 8, the exponential filter removes large variations and smooths the temperature measurement data.

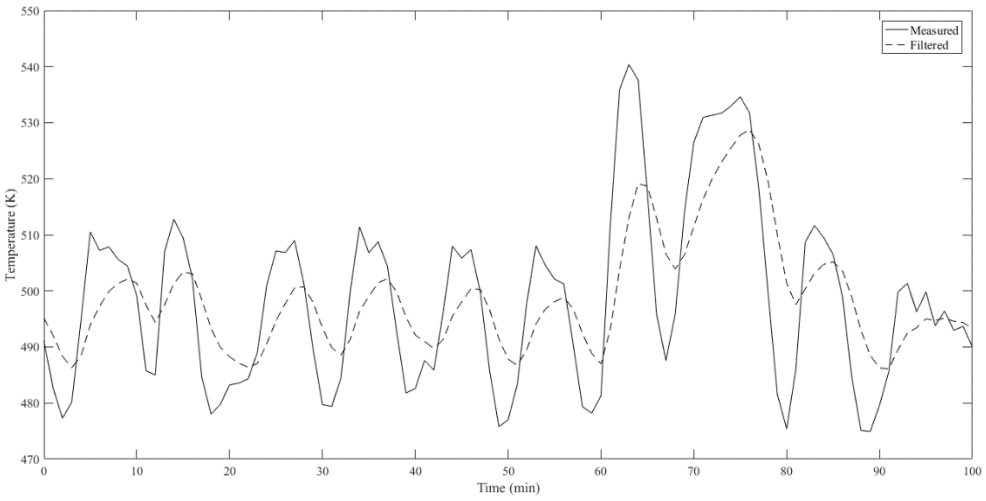

Figure 8 Comparison of the measured and filtered temperature of the inlet to the cold stream of the HGE for an exponential filter for a sampling period of 100 min

2.3 Catalytic Converter

The first step in the production of sulfuric acid is catalytically reacting the SO_2 within the off-gas with O_2 to form SO_3. The oxidation reaction is (Davenport & King, 2013):

$$SO_2 + \frac{1}{2}O_2 \xrightarrow{catalyst} SO_3, \Delta H = -100\ \frac{MJ}{mol\ SO_3} \tag{2.7}$$

Excess oxygen is supplied to the catalytic converter, typically two to four times the stoichiometric requirement, to ensure Reaction 2.7 proceeds rapidly. The reaction that takes place in the catalytic reactor is strongly exothermic, approximately 100 MJ per kmol of SO_3.

The gas is heated as the oxidation reaction proceeds and the gas descends through the catalyst bed, which provides much of the energy required for heating throughout the acid plant.

The SO_2 bearing gas is sent down through "beds" of catalyst. The catalyst contains vanadium (V), potassium (K), sodium (Na), caesium (Cs), S, O and SiO_2. The catalyst used in industry is typically a vanadium-oxide catalyst, V_2O_5-K_2SO_4 (Davenport & King, 2013). Without a catalyst and at normal temperatures gas phase oxidation of SO_2 is kinetically inhibited and the reaction is slow producing almost no SO_3 at all. Increasing the temperature increases the rate of reaction, but the state of the equilibrium shifts towards the production of SO_2 and O_2 as the oxidation reaction is reversible. This is described by the equilibrium constant for SO_2 oxidation, derived from Reaction 2.7:

$$K_E = \frac{P_{SO_3}^E}{P_{SO_2}^E \left(P_{O_2}^E\right)^{\frac{1}{2}}} \tag{2.8}$$

where K_E is the equilibrium constant and P^E represents the partial pressure of each component, as indicated by the subscripts at equilibrium. From Equation 2.8, the equilibrium constant and consequently the maximum attainable SO_3 production decreases with increasing pressure, which is directly proportional to temperature. Therefore, without a catalyst the temperature required for the reaction to proceed at a practical speed is so high that a poor conversion is obtained (Davenport & King, 2013). Using a catalyst promotes rapid SO_2 oxidation at cool temperatures where equilibrium SO_3 production is efficient.

The oxidation of SO_2 takes place in the molten film of the catalyst, where SO_2 and O_2 is absorbed and SO_3 is rapidly produced and desorbed. A molten film begins to form when the vanadium oxide and K, Na, Cs pyrosulfates combine to form a molten layer on the silica substrate between 660 and 690 K. The catalyst must at its active temperature before it is fed with SO_2 bearing gas otherwise the SO_2 will pass through the bed unreacted. The catalyst becomes fully active between 680 and 700 K. The feed gas entering the converter must be at or above 680 K otherwise the gas will cool and solidify the molten film on the catalyst, deactivating it. At temperatures above 900 K the molten catalyst and solid substrate irreversibly form a viscous inactive liquid. In addition to temperature, the composition of the feed gas influences the amount of SO_2 oxidized at equilibrium. The amount of SO_2 oxidized at equilibrium increases slightly with increasing O_2 and/or SO_2 content in feed gas because the oxidation reaction is shifted towards SO_3 production.

The amount of SO_2 oxidized and removed from the gas stream at any point throughout the catalyst bed is defined by the conversion ratio. The SO_2 conversion ratio is an important performance indicator for a converter. The conversion ratio can be expressed as a function of gas characteristics, heat of reaction and temperature (He *et al.*, 2019):

$$\Phi = \frac{C_p M}{(-\Delta H) X_{SO_2}{}^f} (T - T^f) \tag{2.9}$$

where M (kg mol^{-1}) is the molar mass and T^f (K) is temperature of the gas stream at the inlet of the converter, the subscript f denoting a feed stream, T (K) is the temperature of the gas stream at the outlet of the converter and ΔH (kJ mol^{-1} SO^3) is the heat produced by the oxidation reaction. After a single pass through the catalytic converter, the conversion ratio of SO_2 is only approximately 75%. Although there is rapid catalytic oxidation, the heat from the oxidation reaction increases the temperature and the equilibrium SO_2 conversion is approached. The SO_2 that is oxidized at equilibrium is the maximum extent to which the reaction oxidation can proceed. As a result, three additional catalyst beds are used with gas cooling in between each bed to lower the gas temperature and shift the equilibrium so additional oxidation can take place. The gas exiting the first bed of the converter has lower SO_2 and O_2 concentrations but the concentration of SO_3 is higher. Both of these slow the oxidation reaction. The gas exiting the first catalyst bed is cooled by transferring its heat to another gas in a heat exchanger. Cooling the gas shift the equilibrium of the oxidation reaction so more SO_2 oxidation is achievable. The conversion ratio of SO_2 calculated for each bed of the converter using Equation 2.9 are listed in Table 9.

Table 9 Calculated conversion ratio of SO_2 for each bed of the converter

Converter Bed	Calculated Conversion Ratio of SO_2 (%)
1	69.94
2	74.91
3	76.33
4	40.97

Gas Composition After Oxidation

The gas exiting the converter has been oxidized by Reaction 2.7, reducing the concentration of SO_2 and O_2 and increasing the concentration of SO_3. The concentration of SO_2 in the gas stream after oxidation can be estimated from a mass balance on a single bed of the catalytic converter and the conversion ratio:

$$X_{SO_2} = \frac{(1-\Phi)X_{SO_2}^f}{1-\frac{1}{2}X_{SO_2}^f} \tag{2.10}$$

where X_{SO_2} is the mol fraction of SO_2, the superscript f indicating a feed concentration. The concentration of SO_3 and O_2 are estimated similarly, each a function of the conversion ratio. Nitrogen does not participate in the oxidation reaction and it is assumed that CO_2 has a negligible effect. Thus, their concentration after oxidation is simply a function of feed concentrations. The composition of the streams after each pass through the converter is calculated using the conversion ratios of Table 9. The composition of the gas streams at the inlet and outlet of each converter bed are listed in Table 10.

Table 10 Composition of the gas streams at the inlet and outlet of the converter

Converter Bed	Stream	Mean Concentration (vol%)				
		SO_3	SO_2	O_2	CO_2	N_2
1	Inlet	0.000	10.36	11.36	3.299	75.00
	Outlet	7.550	3.203	8.015	3.403	77.80
2	Inlet					
	Outlet	10.07	0.8163	6.8981	3.471	78.78
3	Inlet					
	Outlet	10.72	0.1915	6.608	3.455	78.99
4	Inlet					
	Outlet	0.0880	0.1263	7.402	3.789	88.59

Flow Rate After Oxidation

The flow rate of gas streams exiting the converter are calculated using Equation 2.4, using the feed gas flow rate and the composition of the gas streams listed in Table 10. The flow rate of gas streams at the inlet and outlet of the converter are listed in Table 11.

Table 11 Mass flow rate of gas streams at the inlet and outlet of the converter

	Mean Mass Flow Rate at Converter Bed ($kg\ s^{-1}$)			
Stream	1	2	3	4
Inlet	70.31	72.52	73.89	55.10
Outlet	72.52	73.89	55.10	62.01

2.4 Absorption Towers

The SO_3 produced in the catalytic converter is made into sulfuric acid by contacting it with strong sulfuric acid. The SO_3 bearing gas is blow upward through descending 98.5 mass% H_2SO_4 (1.5 mass% H_2O) trickling through a packed bed. The absorption reaction is:

$$SO_3 + H_2O \xrightarrow{350-380\ K} H_2SO_4, \Delta H = -130\ \frac{MJ}{kmol\ SO_3} \quad (2.11)$$

which is strongly exothermic, approximately 130 MJ per kmol of SO_3. The small amount of water present in the descending acid limits the extent of the reaction as reacting sulfuric acid with water produces hot sulfuric acid vapour, which is difficult and expensive to condense. Limiting the absorption reaction ensures that the strengthened liquid sulfuric acid produced is relatively cool. The sulfuric acid produced by Reaction 2.11 is approximately 98.8 to 99.6 mass% H_2SO_4, with the remainder as water. The strong sulfuric acid is diluted to produce a 93% and 99% product, which is pumped to storage tanks and subsequently loaded into rail cars or trucks for delivery to market.

Composition After Absorption

It is assumed that all of the SO_3 entering the IAT and FAT is absorbed and that no SO_2, O_2, CO_2, N_2, or H_2O is absorbed. The composition of the remaining gas is recalculated based on the new volume of gas, see

Table 12.

Table 12 Gas composition at the inlet and outlet of the IAT and FAT

Absorption Tower	Stream	Mean Concentration (vol%)				
		SO_3	SO_2	O_2	CO_2	N_2
IAT	Inlet	10.72	0.1915	6.608	3.455	78.99
	Outlet	0.0000	0.2142	7.443	3.788	88.56
FAT	Inlet	0.0880	0.1263	7.402	3.789	88.59
	Outlet	0.0000	0.1265	7.409	3.793	88.67

In a double contact acid plant, such as the acid plant at Vale's Copper Cliff Smelter, SO_2 is oxidized to SO_3 and sulfuric acid by "double contact" of the SO_3 with strong sulfuric acid. After passing through three beds of the catalytic converter, SO_3 is removed in the interpass absorption tower (IAT). The remaining, unreacted SO_2 is passed through an additional catalyst bed for further SO_3 production. Sulfuric acid is made from the SO_3 by second contact with strong sulfuric acid in the final absorption tower (FAT). Although the increase in sulfuric acid production is not significant, removing SO_3 from the gas stream before it passes through the additional bed of the catalytic converter increases the oxidation efficiency of SO_2, lowering the amount of SO_2 emitted into the atmosphere.

Flow Rate After Absorption

Continuing to assume that the IAT and FAT are operating perfectly and all SO_3 is removed, the flow rate following the absorption towers is determined by calculating the mass of SO_3 removed and subtracting it from the flow rate at the inlet of the absorption tower. The mass flow rate of gas at the IAT and FAT are listed in Table 13.

Table 13 Mass flow rate of gas at the inlet and outlet of the IAT and FAT and the mass flow rate of SO_3 removed in each tower

Absorption Tower	Steam	Mean Mass Flow Rate ($kg\ s^{-1}$)	Mean Mass Flow Rate of SO_3 removed ($kg\ s^{-1}$)
IAT	Inlet	73.63	18.53
	Outlet	55.10	
FAT	Inlet	62.01	0.1494
	Outlet	61.86	

Final Flow Rate

The final flow rate of the gas stream is 61.86 $kg\ s^{-1}$, which is released into the atmosphere through the Superstack.

Final Composition

The final composition of the gas is the composition of the stream at the outlet of the FAT, see Table 14. This gas stream is released into the atmosphere through the Superstack.

Table 14 Final gas stream composition

Mean Concentration (vol%)				
SO_3	SO_2	O_2	CO_2	N_2
0	0.1265	7.409	3.793	88.67

2.5 Heat Exchangers

Temperature is one of the most important variables in an acid plant. As proper temperature is crucial for the oxidation reaction in the catalytic converter, the use of heat exchangers in the

acid plant is essential for efficient SO_2 oxidation. Temperature is measured at the inlet and outlet of both the shell and tube sides of each of the heat exchangers. The heat exchangers in the acid plant that regulate temperature by transferring heat to and from the gas entering and exiting different units in the acid plant. The heat exchangers used at Vale's Copper Cliff smelter are shown in Figure 9 and listed below:

1. Cold Gas Exchanger (CGE)
2. Hot Gas Exchanger (HGE)
3. Cold Interpass Gas Exchanger (CIGE)
4. Hot Interpass Gas Exchanger (HIGE)
5. Interpass SO_3 Gas Cooler (ISGC)
6. Final SO_3 Gas Cooler (FSGC)

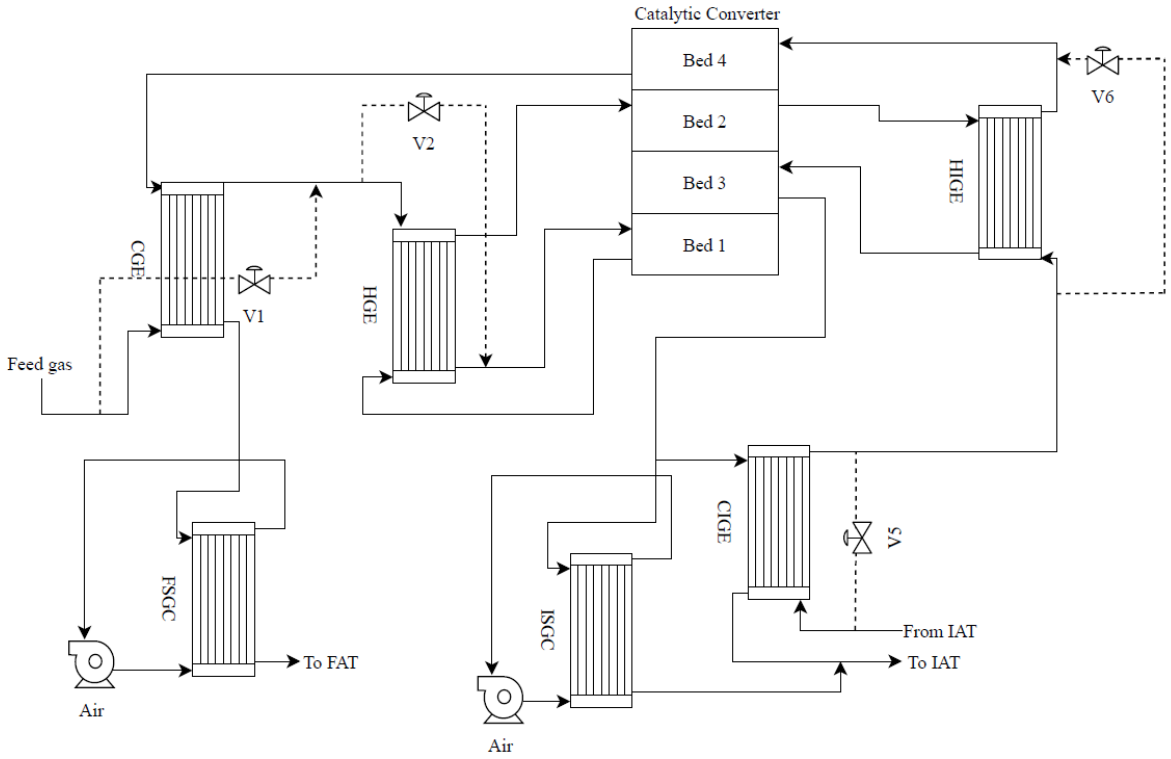

Figure 9 Network of six heat exchangers used at the Copper Cliff Smelter acid plant

All of the heat exchangers used in the acid plant are shell-and-tube type operating in countercurrent flow for a single pass through each. The cold stream of gas flows through the tube side for heating, typically sent to the catalytic converter, and the hot stream through the shell side for cooling, typically originating from the catalytic converter. Among the six heat exchangers there are two SO_3 coolers, which utilize ambient air and blowers to cool down the gas.

Table 15 lists the inlet and outlet streams of the six heat exchangers.

Table 15 Inlet and outlet stream sources and destinations for each of the heat exchangers

Heat Exchanger	Stream	Inlet	Outlet
CGE	Cold	Acid plant feed gas from pre-treatment equipment	Tube side of HGE
	Hot	Outlet from bed 4 of the converter	Shell side of FSGC
HGE	Cold	Tube side of CGE	Inlet to bed 1 of the converter
	Hot	Outlet from bed 1 of the converter	Inlet to bed 2 of the converter
CIGE	Cold	IAT gas outlet	Tube side of HIGE
	Hot	Outlet from bed 3 of converter	IAT gas inlet
HIGE	Cold	Tube side of CIGE	Inlet to bed 4 of the converter
	Hot	Outlet from bed 2 of the converter	Inlet to bed 3 of the converter
ISGC	Cold	Ambient air from air blower	Atmosphere
	Hot	Outlet from bed 3 of the converter	IAT gas inlet
FSGC	Cold	Ambient air from air blower	Atmosphere
	Hot	Shell side of CGE	FAT gas inlet

The amount of heat transfer that takes place in the heat exchangers can be manipulated by adjusting the valves located on each of the heat exchangers and sending a portion of the gas through a bypass stream, represented in Figure 9 by dashed lines. Bypass is the main manipulated variable in regulating the temperature throughout the acid plant. A portion of the cold stream is bypassed around the heat exchanger and therefore not heated. Then, the bypassed

portion and the heated portion are combined. The resulting stream is cooler than when all of the gas is passed through the heat exchanger. Consequently, when gas is passed through the bypass, the hot stream is warmer as less cooling occurs. The greatest amount of heat transfer occurs when the bypass valve is closed and no gas is bypassing the heat exchanger. Bypass in combination with automatic control techniques can also generate an outlet temperature of reduced variability when the inlet gas temperature is varying.

2.5.1 Temperature Control in the Catalytic Converter

The main control objective of the catalytic converter is to maintain a constant inlet gas temperature to the catalytic converter that is within the operating range of the catalyst. If the inlet temperature is too low, the catalyst may be cooled and solidify, deactivating the catalyst. If the input temperature is too high, the outlet temperature will be higher resulting in lower SO_2 oxidation efficiency, and possibly a temperature above the catalyst degradation temperature. A proper input temperature to the catalytic converter is desirable as well as a regulated temperature will help in efficient SO_2 oxidation. The first pass outlet temperature is especially important since the majority of SO_2 oxidation occurs in the first bed of the catalytic converter. The outlet temperature of first bed of the catalytic converter must be closely monitored as it is possible that the bottom of the bed may reach degradation temperature as the gas entering the first bed has the highest amount of SO_2. The HGE and HIGE directly regulate the inlet temperatures to each of the beds of the catalytic converter. Therefore, they play an important role in the efficient conversion of SO_2.

2.5.2 Temperature Control in the Absorption Towers

The temperature of the acid entering the absorption towers is around 350 K, which is high enough for rapid acid making but avoids excessive H_2O, SO_3 and H_2SO_4 gas formation. The temperature of the output acid is approximately 380 K. The input acid temperature is controlled by indirect water cooling. The output acid temperature is controlled by adjusting the absorption tower's sulfuric acid input to output rate. Increasing the ratio results in the output sulfuric acid temperature being cooler, and vice versa. The input gas temperature is between 450 and 500 K. This input temperature is hot enough to avoid liquid sulfuric acid condensation in the flues between the catalytic converter and absorption towers and cool enough to void excessive acid mist formation. The output gas temperature is around 350 K, which is cool enough for liquid H_2SO_4 condensation in downstream flues so flues are constructed of stainless steel.

Chapter 3: Steady-State Modeling

Modeling of the catalytic converter was carried out for the acid plant in the Copper Cliff Smelter in a previous study (He J. , 2018). In this chapter, a steady-state model is developed for the heat exchangers of the acid plant and the effects of process variables are investigated. Integration of the heat exchangers and a converter bed is also studied.

3.1 Model Development

The steady-state model described in this chapter was developed using fundamental mass and energy balances with unknown parameters, which were estimated from industrial operating data. The steady-state models are useful in exploring the relationship among key variables effecting temperature of the gas streams passing through the heat exchangers and to provide a foundation for dynamic model identification. In developing a steady-state model, the following assumptions and simplifications were made:

1. The heat exchangers are adiabatic;
2. The gas characteristics do not change from the inlet to the outlet of the heat exchangers;
3. The absorption towers operate perfectly, removing all of the SO_3 present in the gas.

Figure 10 is a schematic of a heat exchanger with a bypass stream represented by the dashed line. Heat exchanger modeling is focused on the temperature of the outlet streams and position of the valve, which is located on the bypass stream. There are four heat exchangers in the acid plant, but the operating principles for each of the heat exchangers is the same. Therefore,

modeling can be carried out on a single heat exchanger using steady-state mass and energy balances and applied to the remaining heat exchangers.

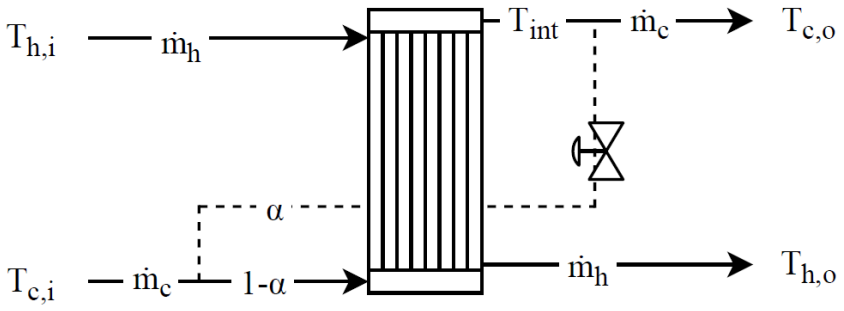

Figure 10 Schematic diagram of a heat exchanger with a bypass stream and its inputs and outputs

For an energy balance of the heat exchanger, the overall rate of heat transfer is:

$$q = UA\Delta T_{lm} \tag{3.1}$$

where q (W) is the rate of heat transfer, U (W m^{-2} K^{-1}) is the overall heat transfer coefficient, ΔT_{lm} (K) is the log-mean temperature difference and A is the heat transfer area (m^2). The parameter UA (W K^{-1}) is an unknown and unmeasured parameter. The log mean temperature difference for a heat exchanger operating in countercurrent flow is:

$$\Delta T_{lm} = \frac{(T_{h,i} - T_{c,o}) - (T_{h,o} - T_{c,i})}{ln\frac{(T_{h,i} - T_{c,o})}{(T_{h,o} - T_{c,i})}} \tag{3.2}$$

where T (K) is the temperature, the subscripts h and c denoting the hot and cold streams, respectively, and i and o denoting the inlet and outlet streams, respectively. The temperature difference across a heat exchanger can be simplified by replacing the log-mean temperature difference with the arithmetic mean temperature difference:

$$\Delta T_{am} = \frac{\left(T_{h,o} + T_{h,i}\right) - \left(T_{c,i} + T_{c,o}\right)}{2} \tag{3.3}$$

where ΔT_{am} (K) is the arithmetic mean temperature difference. Figure 11 compares the log-mean and arithmetic mean temperature difference for a sampling period of 10 min for the HGE. Examining the figure, the arithmetic mean temperature difference approximates the log-mean temperature difference well and can be used to simplify Equation 3.1.

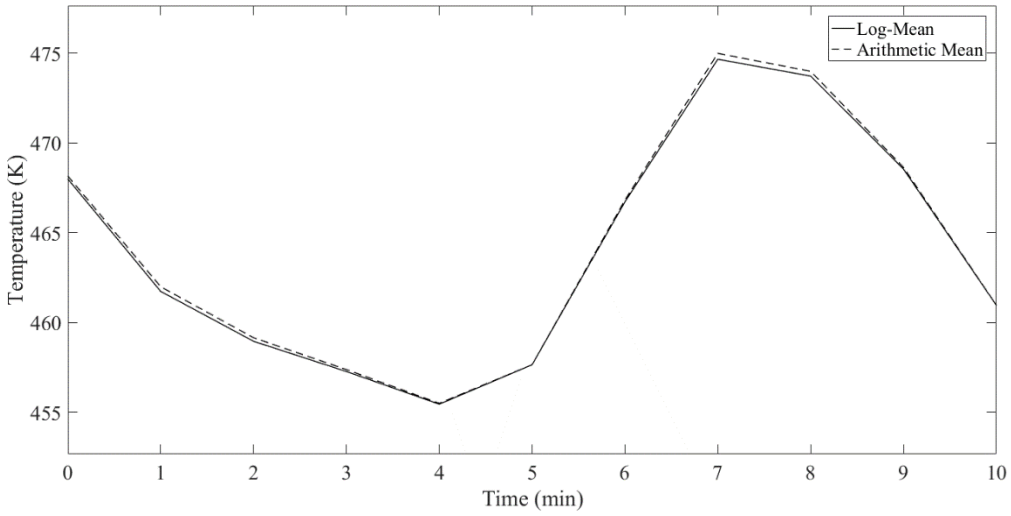

Figure 11 Comparison of the log-mean and arithmetic mean temperature difference for the HGE for a sampling period of 10 min

From an energy balance, the amount of heat released from the hot stream and absorbed by the cold stream is equal to the rate of heat transfer:

$$q = \dot{m}_h C_{p,h}\left(T_{h,i} - T_{h,o}\right) = \dot{m}_c C_{p,c}\left(T_{c,o} - T_{c,i}\right) \tag{3.4}$$

where $\dot{m}$ (kg s^{-1}) is the mass flow rate. The mass flow rate of the cold stream in any of the heat exchangers is the addition of the bypassed stream, represented in Figure 10 by a dashed line, and the portion that was passed through the heat exchanger. From a mass balance around the cold stream:

$$T_{c,o}\dot{m}_c C_{p,c} = (1-\alpha)T_{int}\dot{m}_c C_{p,c} + \alpha T_{c,i}\dot{m}_c C_{p,c} \tag{3.5}$$

where α is the bypass fraction and T_{int} (K) is the intermediate temperature, the temperature before the bypassed stream is mixed with the stream passed through the heat exchanger. Typically, the intermediate temperature is not measured. Assuming that the heat capacity of the cold stream is constant through the heat exchanger, the cold stream outlet temperature can be expressed as:

$$T_{c,o} = (1-\alpha)T_{int} + \alpha T_{c,i} \tag{3.6}$$

Considering the bypassed fraction of the gas stream, the energy balance on the heat exchanger becomes:

$$(T_{h,i} - T_{h,o})\dot{m}_h C_{p,h} = (1-\alpha)(T_{int} - T_{c,i})\dot{m}_c C_{p,c} \tag{3.7}$$

The bypass fraction is assumed to be linearly related to the valve position:

$$\alpha = \beta V \tag{3.8}$$

where β is a parameter and V is the valve position (% open).

Equation 3.4, Equation 3.6 and Equation 3.7 are solved for each of the stream outlet temperatures: hot, cold and intermediate. Replacing the bypass fraction with Equation 3.8, the steady-state model for outlet temperatures is:

$$T_{h,o} = T_{h,i} - \frac{2UA(T_{h,i} - T_{c,i})}{UA\left(1 + \frac{\dot{m}_h \bar{C}_{p,h}}{(1-\beta V)\dot{m}_c \bar{C}_{p,c}}\right) + 2\dot{m}_h \bar{C}_{p,h}} \tag{3.9}$$

$$T_{c,o} = T_{c,i} + \frac{\dot{m}_h \bar{C}_{p,h}}{\dot{m}_c \bar{C}_{p,c}}\left(\frac{2UA(T_{h,i} - T_{c,i})}{UA\left(1 + \frac{\dot{m}_h \bar{C}_{p,h}}{(1-\beta V)\dot{m}_c \bar{C}_{p,c}}\right) + 2\dot{m}_h \bar{C}_{p,h}}\right) \tag{3.10}$$

$$T_{int} = T_{c,i} + \frac{\dot{m}_h \bar{C}_{p,h}}{(1-\beta V)\dot{m}_c \bar{C}_{p,c}}\left(\frac{2UA(T_{h,i} - T_{c,i})}{UA\left(1 + \frac{\dot{m}_h \bar{C}_{p,h}}{(1-\beta V)\dot{m}_c \bar{C}_{p,c}}\right) + 2\dot{m}_h \bar{C}_{p,h}}\right) \tag{3.11}$$

where $\bar{C}_p$ (J kg^{-1} K^{-1}) is the mean mass heat capacity, subscripts h and c denoting the hot and cold streams, respectively. Noise is reduced by utilizing the mean values of the heat capacities.

The steady-state model in Equations 3.9 – 3.11 is a function of the unknown parameters β and UA, input temperatures and gas characteristics. Examining Equation 3.9, the temperature of the hot stream at the outlet is the initial hot stream inlet temperature less a value related to the temperature difference between the hot and cold streams at the inlet and the bypass valve position. Assuming all other variables are held constant if the valve were opened Equation 3.9 suggests that the hot stream outlet temperature would decrease less from the inlet temperature, resulting in the hot stream being warmer. If the valve were closed, the hot stream outlet temperature would decrease more from the inlet temperature and the hot stream would be cooler. Equations 3.10 and 3.11 for the cold stream outlet and intermediate temperatures have a similar structure. The cold stream outlet temperature is also related to the temperature difference between the hot and cold streams at the inlet. However, the cold stream outlet temperature increases from its inlet temperature. If the valve were opened the cold stream outlet temperature would increase less from the inlet temperature and the outlet temperature would be cooler. If the valve were closed the cold stream outlet temperature would increase more, resulting in the outlet stream being warmer. The temperature of the intermediate stream also increases from the inlet temperature of the stream. Comparing Equation 3.10 and Equation 3.11, the intermediate temperature is a function of an additional bypass fraction term. If the valve were opened the intermediate temperature would be warmer. The opposite is true for closing the valve, the intermediate temperature would be cooler.

3.2 Parameter Estimation

For the steady-state model in Equations 3.9 – 3.11 there are two unknown parameters, β and UA. The dimensionless parameter β is related to the % opening of the valve and the fraction of the stream bypassed around the heat exchanger, α. The second parameter UA (kW K^{-1}) is a heat exchanger parameter, a combination of the heat transfer coefficient and the heat transfer area. The parameters of the steady-state model are estimated from industrial operating data so the obtained model can be readily adapted to different industrial sulfuric acid plants with varying process and operating conditions.

The first-half of the industrial data from the 30-day data collection period is used to estimate the unknown parameters UA and β. The unknown parameters are solved in MATLAB using a non-linear least-squares solver, "lsqnonlin", which solves curve fitting problems using a trust-region-reflective algorithm to minimize the sum of squared error between the measured and estimated temperature:

$$SSE = \sum \left(T(x) - \hat{T}(x)\right)^2 \tag{3.12}$$

where SSE is the sum of squared errors, T and $\hat{T}$ are the measured and estimated temperature, respectively, and x is the vector of parameters, UA and β, whose values are adjusted by the solver. The vector returned by the solver contains the values of the parameters that minimize

Equation 3.12. A vector containing an initial guess for the values of the parameters is supplied to MATLAB. The initial guess for the parameter UA is estimated by simplifying Equation 3.1:

$$(UA)_0 = \frac{\dot{m}_h C_{p,h}\left(T_{h,i} - T_{h,o}\right)}{\left(T_{h,o} - T_{c,i}\right)} \tag{3.13}$$

where the temperature difference across the heat exchanger replaces the log-mean temperature difference. Equation 3.13 is of the form $Ax = B$, which can be solved using a system of linear equations solver in MATLAB. The initial point for the parameter β is estimated from the HGE where the intermediate temperature is measured at Node 43. Equation 3.6 can be rearranged to solve for the bypass fraction, which is a function of cold stream outlet, inlet and intermediate temperatures:

$$\alpha = \frac{T_{c,o} - T_{int}}{T_{c,i} - T_{int}} \tag{3.14}$$

Assuming all of the heat exchangers are operated similarly and for simplicity, the bypass fraction calculated for the HGE is utilized to estimate an initial point for β for the remaining heat exchangers. β can be estimated using Equation 3.8, utilizing the valve position data for the associated heat exchanger, and a linear systems of equations solver in MATLAB. The initial points used for estimating the unknown parameters are listed in

Table 16.

Table 16 Initial points supplied to the non-linear least-squares solver

Heat Exchanger	Parameter	
	$(UA)_0$ (kW K^{-1})	$(\beta)_0$
CGE	50.49	0.0050
HGE	60.71	0.0060
CIGE	103.8	0.0094
HIGE	55.97	0.0054

For the CGE and HIGE heat exchangers the intermediate temperature is not measured. For these exchangers only Equations 3.9 – 3.10 are used to estimate the parameters. For the HGE and the CIGE heat exchangers the intermediate temperature is measured so in addition to Equations 3.9 – 3.10, Equation 3.11 is included in the system of equations used to estimate the parameters. The values of the parameters that minimize the SSE for each heat exchanger are listed in Table 17.

Table 17 Values of the unknown parameters estimated by the non-linear least-squares solver

Heat Exchanger	Parameter	
	UA (W K^{-1})	β
CGE	49.67	0.0060
HGE	74.15	0.0055
CIGE	132.3	0.0039
HIGE	83.14	0.0052

3.3 Model Validation

With the estimated parameters in Table 17 the outlet temperatures can be predicted using Equations 3.9 – 3.11. To examine the validity of the obtained model, the model predicted

temperature is compared with industrial measurement data. The first-half of the industrial operating data was used for parameter estimation and the remaining half is used for model validation. The validation plots shown in Figure 12 - 15. Examining the plots, there is some disagreement between the measured and calculated outlet temperatures. An error calculation can be used to quantify the disagreement between the model-predicted and measured temperature. The root mean squared error (RMSE), also known as the standard error of regression, is an estimate of the standard deviation of the random component in the data. The RMSE is calculated by:

$$RMSE = \sqrt{\frac{\sum_{i=1}^{n}\left(T(x) - \hat{T}(x)\right)^2}{n}} \tag{3.15}$$

where n is the number of data points used for model validation. The RMSE for each of the heat exchangers is listed in Table 18. Examining the validation figures and the RMSE values, the largest discrepancies between model-predicted and measured temperature are observed for the CGE and HGE, Figure 12 and Figure 13, respectively. The outlet streams of the CGE/HGE heat exchanger network are the inlet streams to the catalytic converters. This explains the disagreement between the model predicted and measured temperature as the measurement data is for temperature where control action has been applied to maintain a more constant value. Thus, the measurement data is not the real outlet temperatures of the heat exchangers. However, the model was successful in tracking the variations of measurements and replicates them well in the predicted temperatures. For the CIGE/HIGE heat exchanger network outlet

temperatures the model provides a good prediction of temperature when compared to the measured temperature, shown in Figure 13 and Figure 14. The close match between the model-predicted and measured temperature shows that the model developed with the estimated parameters is valid in describing the process. Thus, the model can be used to determine the effect of process changes and variables on the outlet temperatures. Understanding the effect of process variables on temperature can be used as a foundation for process control and optimization to enhance the operation of the plant. The model can also be used to estimate the SO_2 conversion ratio, SO_2 concentration and temperature at unmeasured points, which provides additional monitoring.

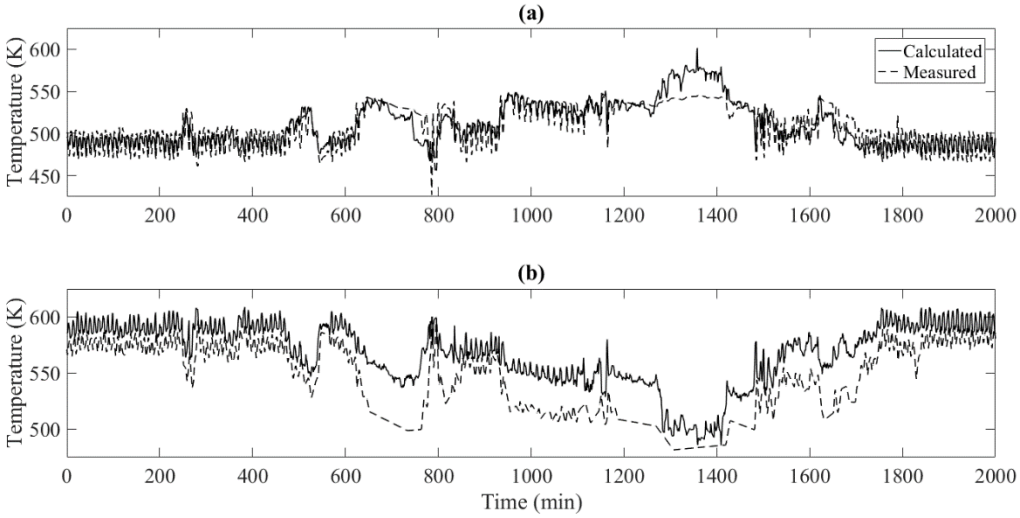

Figure 12 Comparison of the measured and calculated (a) cold and (b) hot outlet stream temperatures for the CGE

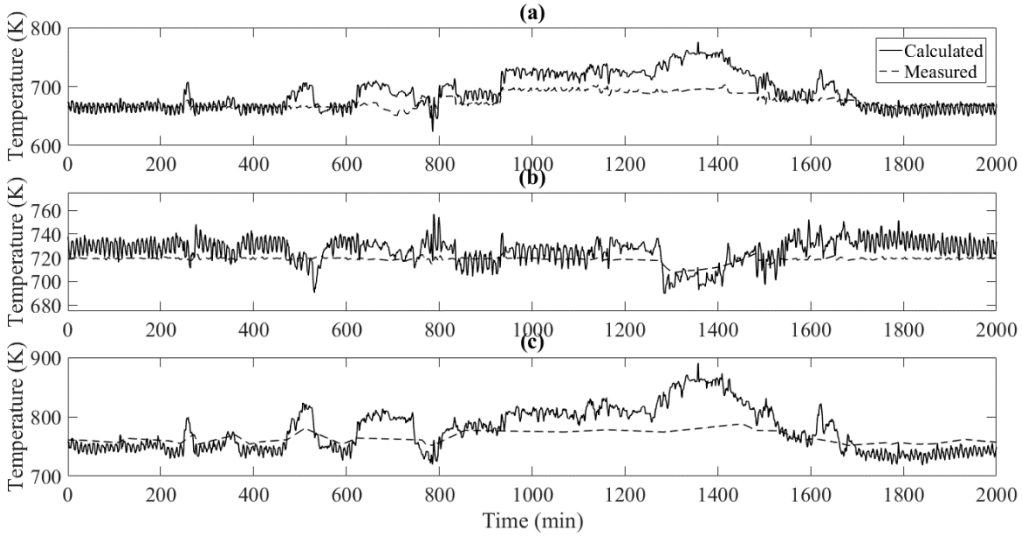

Figure 13 Comparison of the measured and calculated (a) cold, (b) hot and (c) intermediate outlet stream temperatures for the HGE

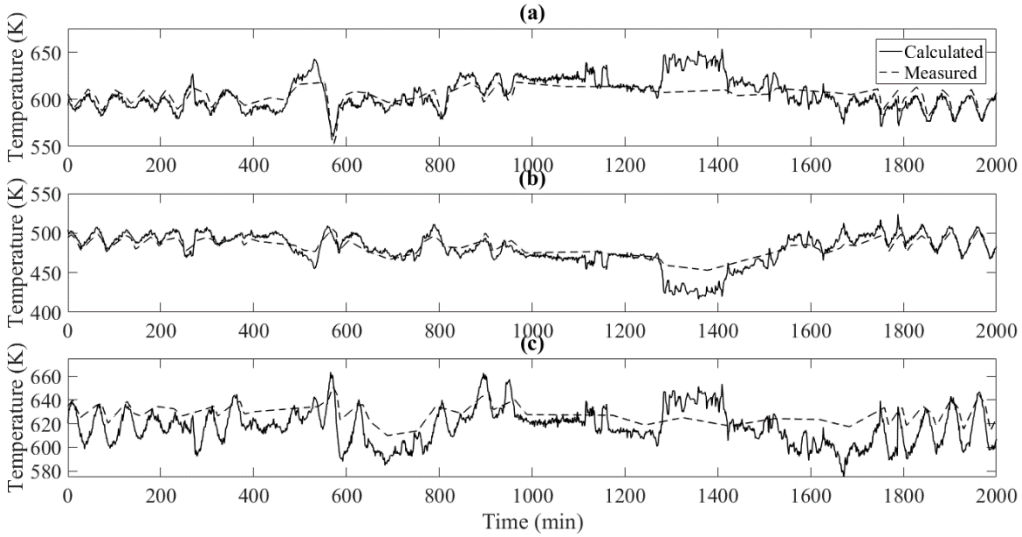

Figure 14 Comparison of the measured and calculated (a) cold, (b) hot and (c) intermediate outlet stream temperatures for the CIGE

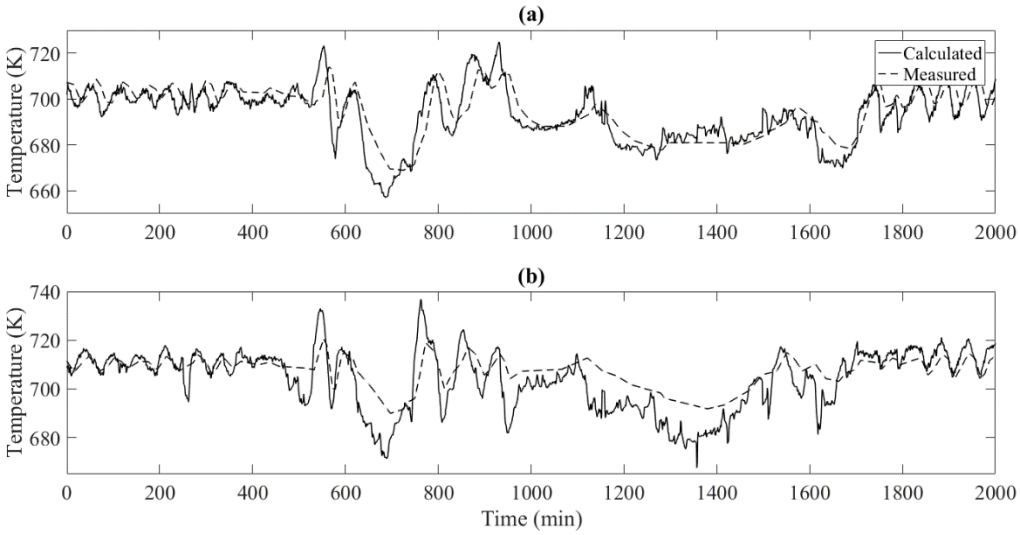

Figure 15 Comparison of the measured and calculated (a) cold and (b) hot outlet stream temperatures for the HIGE

Table 18 RMSE for gas streams of the heat exchangers

Heat Exchanger	RMSE			
	Cold Stream	Hot Stream	Intermediate Stream	Average
CGE	15.68	21.44	N/A	18.57
HGE	20.17	13.22	25.28	19.56
CIGE	13.73	11.54	16.09	13.79
HIGE	8.269	7.580	N/A	7.924

3.4 Effect of Process Variables

The steady-state model described by Equations 3.9 – 3.11 has been validated and follows temperature trend well so it can be used to determine the effect of process variables on the controlled variables, the outlet temperatures of the heat exchanger networks, which feed the catalytic converter. There are two types of process variables to investigate: the manipulated

variables and the disturbance variables. Examining the effect of process variable changes on temperature is useful when process changes are being explored or introduced. When process changes are implemented the disturbance variables also change and their effect on the controlled variables is not well known. With Clean AER project changes, the off-gas from the converter aisle will soon be captured and sent to the acid plant. The additional off-gas being captured results in changes to the feed gas flow rate, temperature and SO_2 concentration, all of which are disturbance variables and have some effect on the controlled variables. The effect of the manipulated variables, valve position, on the controlled variables should also be explored as these variables are adjusted in order to mitigate the effects of the disturbance variables and maintain the controlled variables at their desired set-points.

The outlet streams of the HGE and HIGE are the inlet to the converter, which requires tight temperature control. The CGE and CIGE do not directly affect the temperature at the inlet of the converter, however they do effect the outlet temperatures of the HGE and HIGE. Together the CGE/HGE and the CIGE/HIGE form two networks of heat exchangers. The two heat exchanger networks are shown in Figure 16 and Figure 17, respectively. For each of the heat exchanger networks there are two controlled variables and two manipulated variables. The controlled and manipulated variables and their measuring points for each of the heat exchanger networks are listed in Table 19. In addition to manipulated variables, disturbance variables are also inputs to the CGE/HGE and CIGE/HIGE heat exchanger networks. The disturbance variables have an effect on the controlled variables but they cannot be adjusted. The

disturbance variables for each of the heat exchanger networks and their measuring points are listed in Table 20.

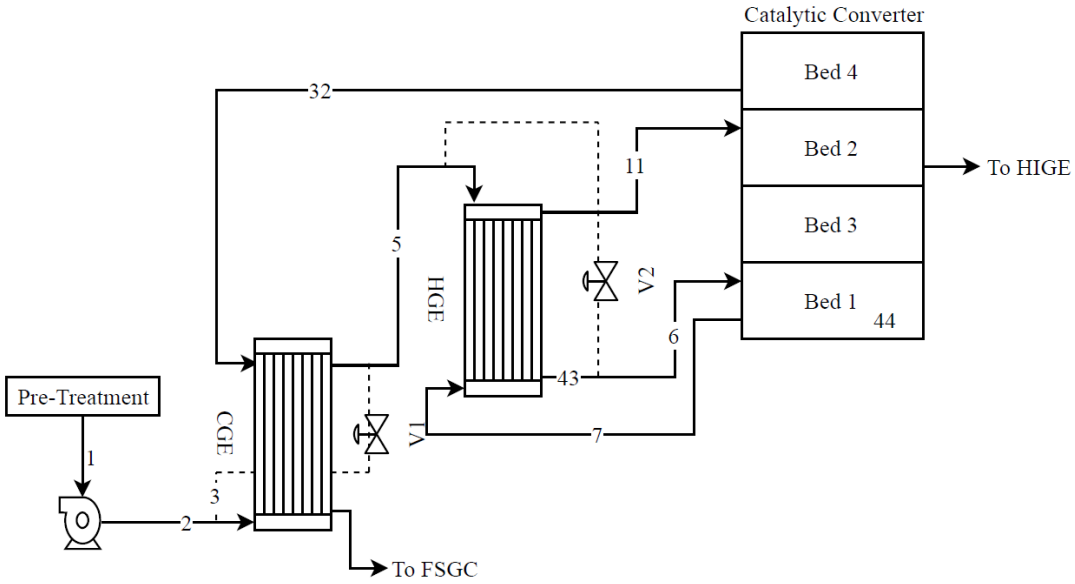

Figure 16 CGE/HGE heat exchanger network configuration

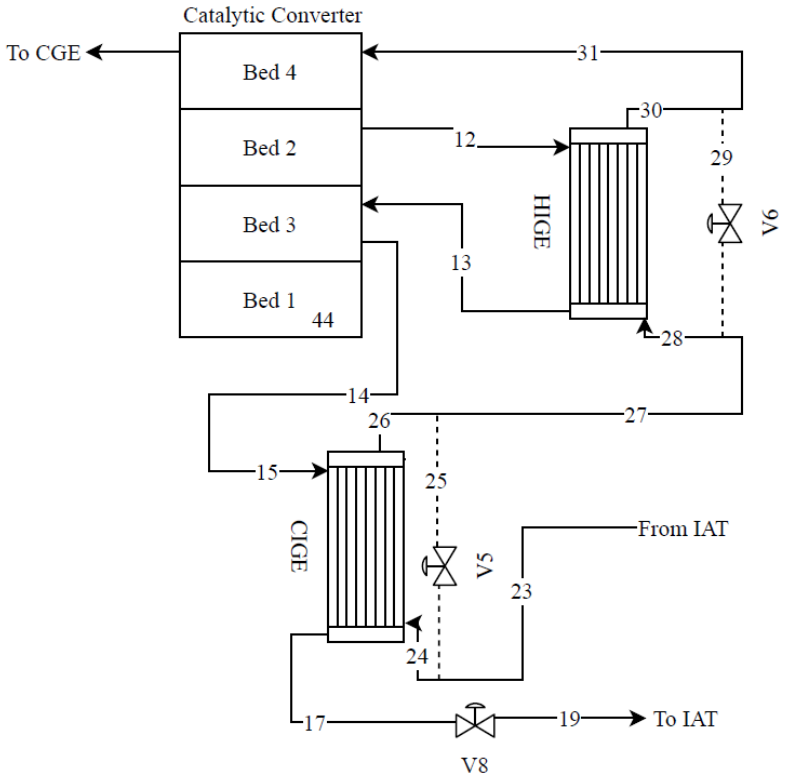

Figure 17 CIGE/HIGE heat exchanger network configuration

Table 19 Controlled and manipulated variables for the CGE/HGE and CIGE/HIGE heat exchanger networks and their measuring points

Heat Exchanger Network	Controlled Variables		Manipulated Variables	
	Location	Type	Location	Type
CGE/HGE	Node 6	T	V1	V
	Node 11	T	V2	V
CIGE/HIGE	Node 13	T	V5	V
	Node 31	T	V6	V

Table 20 Controlled and disturbance variables for the CGE/HGE and CIGE/HIGE heat exchanger networks and their measuring points

Heat Exchanger Network	Controlled Variables		Disturbance Variables	
	Location	Type	Location	Type
CGE/HGE	Node 6	T	Node 2	T
			Node 7	T
			Node 32	T
	Node 11	T	Node 1	N
			Node 6	X
CIGE/HIGE	Node 13	T	Node 12	T
			Node 15	T
	Node 31	T	Node 24	T
			Node 1	N

The steady-state model in Equations 3.9 – 3.11 is used to determine the effects of changes of the disturbance and manipulated variables on the controlled variables. The process variables were varied from their minimum to maximum values obtained from industrial operating data. Each process variable was examined individually while all other variables were held constant at their mean value from industrial operating data. Two configurations were considered: open-loop and closed-loop. Using the open-loop configuration the outlet temperatures of the CGE/HGE and CIGE/HIGE heat exchanger networks were estimated and plotted. Using the closed-loop configuration the outlet temperature of the CGE/HGE heat exchanger network, the outlet temperature of the first bed of the catalytic converter and the SO_2 conversion ratio for the first bed of the catalytic converter were estimated.

3.4.1 Open-Loop

The open-loop configuration used to determine the effects of process variables on the controlled variables is depicted in Figure 18 for the CGE/HGE heat exchanger network. The inputs to the CGE/HGE heat exchanger network are the temperatures at Node 2, Node 32 and Node 7, the positions of V1 and V2 and the flow rate at Node 1. Of these inputs the temperature at Node 2 and the flow rate at Node 1 are feed gas disturbance variables. The positions of V1 and V2 are manipulated variables. The outputs of the CGE/HGE heat exchanger network are the temperatures are Node 6 and Node 11, which are the inlet streams to the first two beds of the catalytic converter.

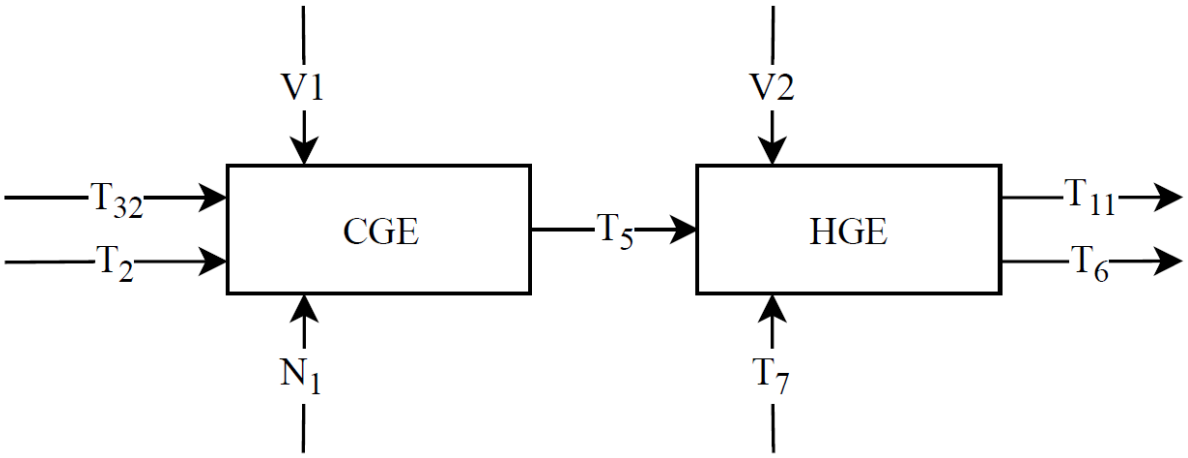

Figure 18 Open-loop configuration for the CGE/HGE heat exchanger network and the input and output variables used to determine the effect of process variables on the temperatures at Node 6 and Node 11

The positions of V1 and V2 are adjusted to control the outlet temperatures of the CGE/HGE heat exchanger network. These temperatures are crucial as they are the inlet streams to the first

and second bed of the catalytic converter. The first bed of the catalytic converter is especially important as the gas stream contains the greatest amount of SO_2, which can cause excess heating of the catalyst, and approximately 75% of SO_2 conversion takes place. The outlet temperatures are manipulated so that the streams entering the converter are within the operating range of the catalyst and efficient SO_2 oxidation occurs. It is also desirable to have a constant temperature entering the catalytic converter so the valves are used to reduce variations in temperature. From industrial operating data the mean valve positions of V1 and V2 are 54.90% and 57.23%, respectively. When V1 is 54.90% open, the temperatures at Node 6 and Node 11 are 685.2 K and 725.9 K, respectively. When V2 is 57.23% open, the temperatures at Node 6 and Node 11 are 681.2 K and 725.1 K, respectively. Figure 19 shows the effect of varying the valve positions from their minimum to maximum operating values on the outlet temperatures. From industrial operating data the operating range of V1 is 0 – 100% while the operating range of V2 is 40 – 80%.

V1 is located on the cold gas stream of the CGE in the CGE/HGE heat exchanger network, see Figure 16. The outlet streams of the CGE are not direct inlets to the catalytic converter. Opening V1 bypasses cold gas at Node 2 around the CGE so it does not increase in temperature as it would if it were passed through the heat exchanger. The cold gas that is bypassed is combined with the cold gas passed through the heat exchanger, which has been warmed. Therefore, the combined gas stream and the temperature at Node 5 is cooler. Node 5 is the cold gas inlet stream of the HGE so a colder inlet temperature results in both the hot and cold stream outlet temperatures being cooler. At the minimum valve position of 0% open, the temperature

at Node 6 is 691.1 K and at Node 11 is 730.6 K. At the maximum valve position of 99.27% open, the temperature at Node 6 is 674.1 K and at Node 11 is 717 K. From these values and from examination of Figure 19, the position of V1 does not greatly affect the temperatures at Node 6 and Node 11, although it does result in the streams being slightly cooler. Closing V1 has the opposite effect, a slightly warmer temperature at Node 6 and Node 11. Opening V1 from 0 to 100% decreases the temperature at Node 6 by 17.8 K while the temperature at Node 11 decreases 13.6 K. Thus, V1 has a larger impact on the cold stream, the stream on which the valve is located, and the temperature at Node 6.

V2 is located on the cold gas stream of the HGE of the CGE/HGE heat exchanger network, see Figure 16. The outlet streams of the HGE heat exchanger are Node 6 and Node 11, which are the inlet streams to the first and second bed of the catalytic converter, respectively. Opening V2 bypasses cold gas at Node 5 around the HGE so it is not heated. The cold gas that is bypassed is combined with the cold gas passed through the heat exchanger, which has been warmed. Consequently, the temperature of the gas passing through the heat exchanger, the intermediate temperature, at Node 43 is warmer, shown in Figure 20. The cold gas stream also has a longer residence time than the hot gas stream since its flow rate is smaller, so the temperature of the stream would increase to a point where there would no longer be a driving force for heat transfer. Thus, the temperature of the hot gas stream at Node 11 would be warmer than if all of the cold as was passed through the HGE as less cooling takes place. At the minimum valve position of 40.39% open, the temperature at Node 6 is 690.6 K and at Node 11 is 716.5 K. At the maximum valve position of 78.09% open the temperature at Node 6 is

669.4 K and at Node 11 is 735.8 K. From these values and from examination of Figure 19, the position of V2 has a greater impact on the temperature at Node 6 and Node 11 than V1. It can also be concluded that the position of V2 has a larger effect on the temperature at Node 6, which is the cold stream of the HGE heat exchanger, than the temperature at Node 11. For the operating range of V2 the temperature at Node 6 decreases by 21.2 K and the temperature at Node 11 increases by 19.3 K. Although V2 has a smaller operating range than V1, the temperatures at Node 6 and Node 11 vary by greater amounts.

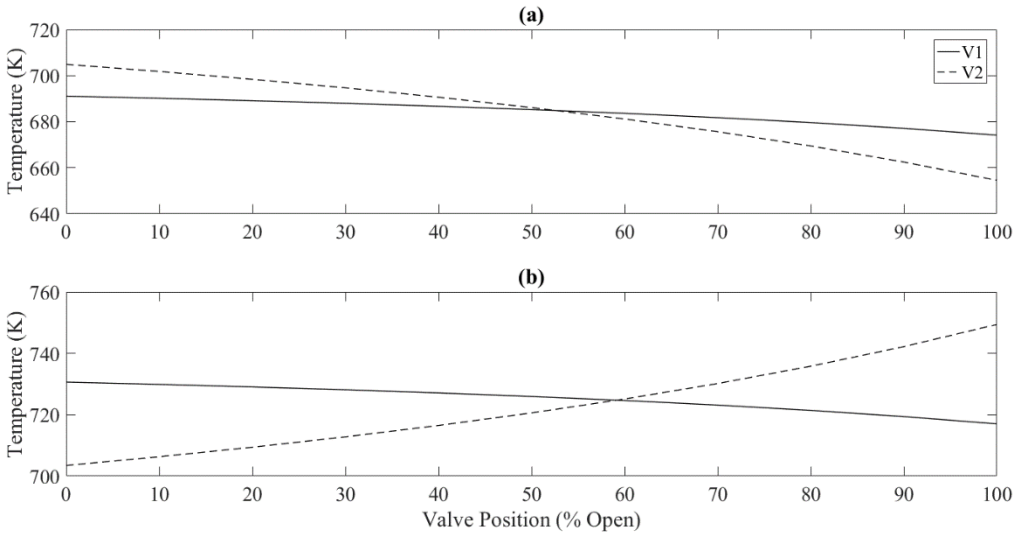

Figure 19 Open-loop effect of CGE/HGE bypass valves, V1 and V2, on the outlet temperature at (a) Node 6 and (b) Node 11

Opening or closing V1 and V2 on the CGE/HGE heat exchanger network also effects the flow rate of the cold gas streams. When V1 or V2 is opened, there is a greater amount of gas bypassing the CGE and HGE and consequently, less gas flowing through the heat exchangers. Thus, the residence time of the cold gas stream is increased and a greater amount of heat

transfer occurs. This would make the intermediate temperature warmer. This is confirmed by calculating the intermediate temperatures of the CGE/HGE for various valve positons. The results are plotted in Figure 20.

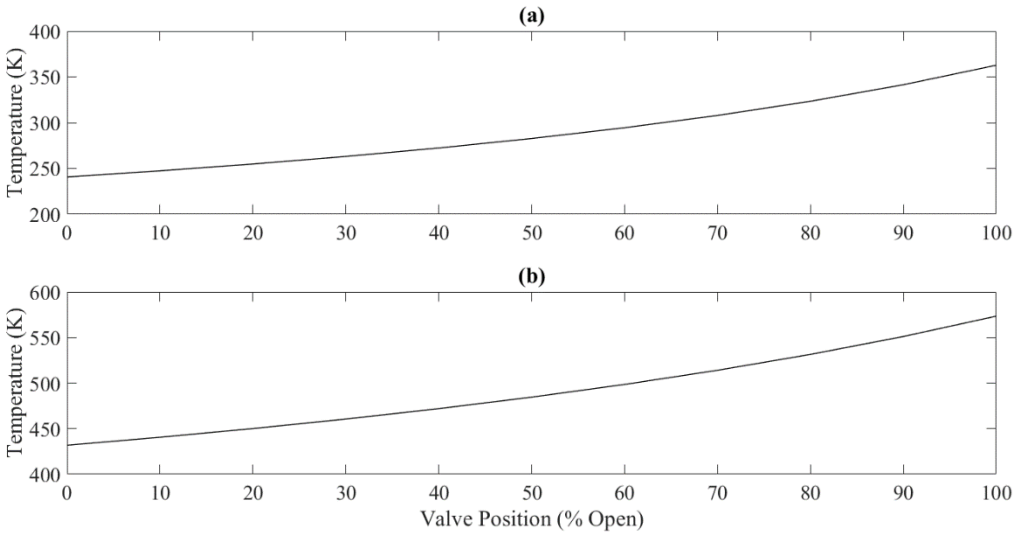

Figure 20 Open-loop effect of the CGE/HGE bypass valves, V1 and V2, on the intermediate temperature of the (a) CGE and (b) HGE

From Figure 19 it can be concluded that both V1 and V2 have a greater impact on the temperature at Node 6. Comparing the effect of V1 and V2, V2 has a larger effect on the outlet temperatures. Opening V1 decreases the temperatures at both Node 6 and Node 11. Opening V2 decreases the temperature at Node 6 and increases the temperature at Node 11. These results provide a better understanding of how each valve effects the outlet temperature, which provides a foundation for process control and should be considered when process changes are made.

The temperature of the feed gas at Node 2 is a disturbance variable, which would have an impact on the temperature at Node 6 and Node 11. From industrial operating data the mean temperature at Node 2 is 378.6 K while the minimum and maximum temperatures are 327.8 K and 384.9 K, respectively. At the mean feed gas temperature the temperatures at Node 6 and Node 11 are 675.5 K and 719.1 K, respectively. The outlet temperatures at Node 6 and Node 11 are the inlet gas streams to the catalytic converter. For efficient SO_2 oxidation the gas streams entering the catalytic converter should be within the catalyst operating range of 680 – 700 K.

Examining Figure 21, as the feed gas temperature increases both outlet temperatures increase. If the feed gas temperature increases and the temperature at Node 32 is held constant at its mean value, the outlet temperature at Node 6 and Node 11 would consequently also increase. Implications of a higher outlet temperature at Node 6 and Node 11: the temperature of the gas streams could be at or approach the catalyst degradation temperature within the catalytic converter. From Figure 21, increasing the feed gas temperature from its mean to maximum value, the temperatures at Node 6 and Node 11 would increase by approximately 10 K to 686.0 K and 726.5 K, respectively. Thus, at the maximum feed gas temperature the temperature at Node 11 is outside of the ideal operating range of the catalyst and the temperature at Node 6 is nearing its upper limit. The temperature at Node 6 should not approach the upper limit of the catalyst operating range. This gas stream contains the most amount of SO_2 and approximately 75% of conversion occurs in the first bed. Thus, this gas stream will experience the greatest temperature increase as the reaction proceeds. However, it is desirable to have a

higher temperature at Node 11. Since there is less SO_2 in the gas stream, the stream enters the second bed at a higher temperature to push the equilibrium of the oxidation reaction towards the production of SO_3 (Davenport & King, 2013). Although the temperatures are not above the catalyst degradation temperature of ~900 K they are the temperatures at the inlet of the catalytic converter and the oxidation reaction has the potential to increase the gas temperatures above 900 K.

Conversely, from Figure 21 as the feed gas temperature decreases the temperatures at Node 6 and Node 11 would decrease. At the minimum feed gas temperature of 384.9 K the temperature at Node 6 and Node 11 is 666.1 K and 710.5 K, respectively. Again, Node 11 is slightly above of the ideal operating range of the catalyst, although it is a strategy to force the production of SO_3. The temperature at Node 6 is 15 K below the ideal operating range of the catalyst. The oxidation reaction would warm the stream significantly however, the gas stream should be within the ideal operating range of the catalyst at the inlet. At temperatures below 660 K, the catalyst would cool and deactivate resulting in no oxidation taking place. The molten layer in which the oxidation reaction occurs begins to form at approximately 660 K, so oxidation would occur at any temperature above this although it may not be the most efficient. The most oxidation takes place in the first bed of the catalytic converter which is essential for efficient SO_2 removal from the gas stream and ultimately, this determines the amount of SO_2 being released into the atmosphere.

Figure 21 shows the temperature at Node 6 and Node 11 for the range of feed gas temperature from industrial operating data. It is possible due to plant start-up and/or shut-downs or process changes that the feed gas temperature could fall much below or above the ideal catalyst operating range, which could cause catalyst degradation or deactivation. As the feed gas temperature increases the outlet temperatures increase and vice versa. A large increase or decrease in the feed gas temperature could cause the outlet temperatures to be outside of the ideal operating range temperature of the catalyst at the inlet or within the bed of the catalytic converter. It is very important that efficient oxidation takes place in the first bed of the catalytic converter, since this stream contains the greatest amount of SO_2. Thus, tight temperature control of the gas stream at Node 6 is very important.

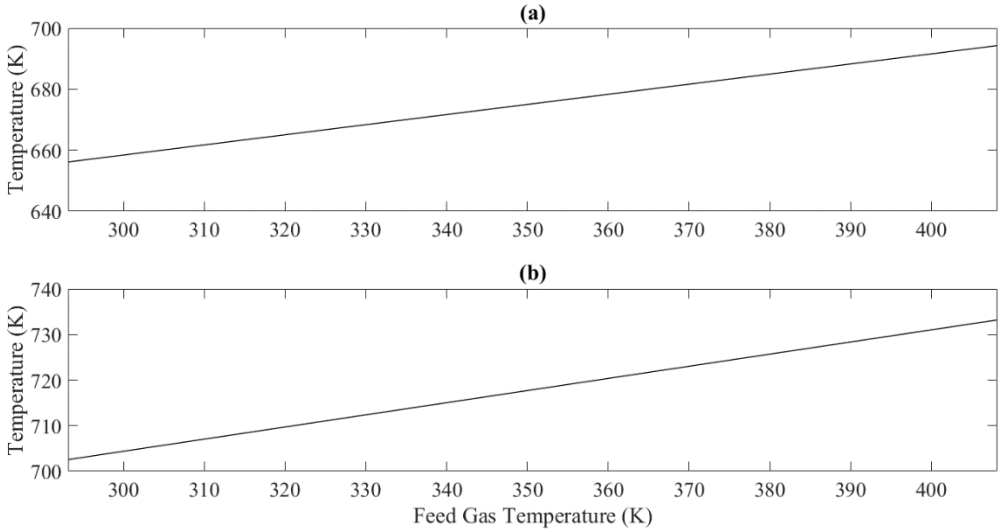

Figure 21 Open-loop effect of feed gas temperature on the outlet temperature at (a) Node 6 and (b) Node 11 for the CGE/HGE heat exchanger network

Understanding the effect of the feed gas flow rate on temperature is of considerable interest since Clean AER modifications will result in the off-gas from the converter aisle being captured and sent to the acid plant for treatment. The flow of off-gas from the converter aisle is not continuous and there are periods of high, low and no flow as the converting cycle is completed. Flow rate will have a large effect on outlet temperature since the flow rate determines the residence time of a gas stream in the heat exchangers and thus the amount of heat transfer. Knowing how flow rate effects each of the outlet temperatures can aid in understanding how to manipulate the valve positions in order to maintain an outlet temperature that is within the ideal operating range of the catalyst. From previous work, it has also been concluded that the flow rate is highly correlated with temperature throughout the acid plant (He J. , 2018). From industrial operating data the mean feed gas flow rate is 172.5 $kNm^3 h^{-1}$. At this mean feed gas flow rate the temperatures at Node 6 and Node 11 are 682 K and 725.3 K. An increase or decrease in the feed gas flow rate would increase or decrease each of the flow rates throughout the acid plant.

The maximum feed gas flow rate from industrial operating data is 242.34 $kNm^3 h^{-1}$ at which the temperatures at Node 6 and Node 11 are 652.4 K and 752.2 K, respectively. From Figure 22, as the feed gas flow rate effects the outlet temperatures considerably, a temperature difference of more than 100 K for the feed gas flow rate operating range. For a higher feed gas flow rate, the gas has less residence time and therefore less heat transfer occurs from the hot stream to the cold stream. The gas steam at Node 5 is also a cold stream, which has been heated in the CGE. If the feed gas flow rate is increased, the temperature at Node 5 will be cooler and

thus, the cold stream entering the HGE will also be cooler. The cooler gas stream being fed to the HGE in combination with a smaller residence time would result in the temperature at Node 6 being much cooler. As the flow rate increases, the temperature at Node 11 increases. At Node 11 the stream is hot and has been cooled from the outlet of the first bed of the catalytic converter in preparation for the next oxidation step. Again, for a higher flow rate there the gas streams have a smaller residence time within the heat exchanger and less heat transfer occurs. Thus, for the hot stream being cooled in the HGE there would be less of a decrease in temperature from the inlet at Node 7 and the outlet temperature at Node 11 would be warmer.

The minimum feed gas flow rate from industrial operating data is 58.19 $kNm^3 h^{-1}$ which leads to the temperatures at Node 6 and Node 11 being 768.5 K and 646.9 K, respectively. For a decrease in feed gas flow rate the gas streams would have an increase residence time in the heat exchanger and more heat transfer would occur. The temperature of the cold gas stream at Node 5, which has passed through the heat exchanger would be warmer than it would have been with a lower feed gas flow rate. Thus, the cold stream entering the HGE would be warmer, and in combination with the lower gas flow rate more heat transfer would occur, resulting in the temperature at Node 6 being much higher. The opposite effect occurs for the temperature at Node 11. For a lower flow rate there is more residence time and therefore more heat transfer occurs. Since there is more heat transfer from the hot to cold gas streams the temperature at Node 11 would decrease.

Flow rate has a significant effect on outlet temperature, the outlet temperatures varying by nearly 100 K over the flow rate operating range. Flow rate is also a disturbance that will be common with the Clean AER modifications. Increasing the feed gas flow rate impacts the flow rate throughout the acid plant. For increasing flow rate, the residence time of the gas streams decreases and as a result less heat transfer occurs. Thus, the cold stream will be cooler and the hot stream will be warmer. The opposite is true for decreasing flow rate. The residence time increases and more heat transfer occurs. The cold steam will be warmer and the hot stream will be cooler.

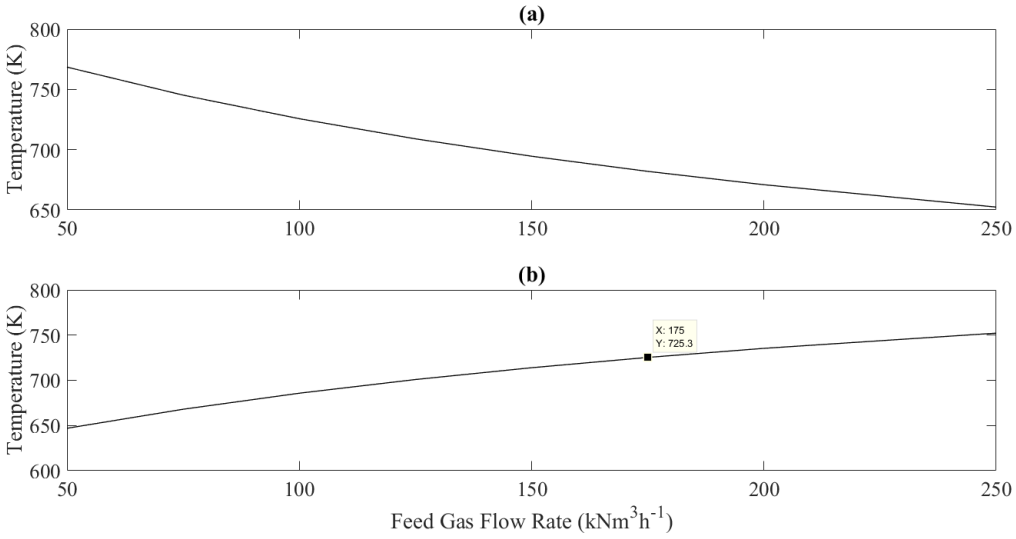

Figure 22 Open-loop effect of feed gas flow rate on the outlet temperature at (a) Node 6 and (b) Node 11 for the CGE/HGE heat exchanger network

The manipulated and disturbance variables have similar effects on the outlet temperatures of the CIGE/HIGE heat exchanger network, shown in Figure 17. The gas streams at Node 13 and Node 31 are the inlets to the third and fourth bed of the catalytic converter, respectively. Much

like the temperatures at Node 6 and Node 11, these gas streams should be constant and within the ideal operating range of the catalyst. Figure 23 depicts the open-loop configuration for the CIGE/HIGE heat exchanger network. The inputs to the CIGE/HIGE heat exchanger network are the temperatures at Node 12, Node 15 and Node 28, the positions of V5 and V6 and the flow rate at Node 1. The feed gas temperature and flow rate also have an effect on the outlet temperatures of the heat exchanger network. The positions of V5 and V6 are manipulated variables. The outputs of the CIGE/HIGE heat exchanger network are the temperatures of Node 13 and Node 31, which are the inlet streams to the third and fourth bed of the catalytic converter, respectively.

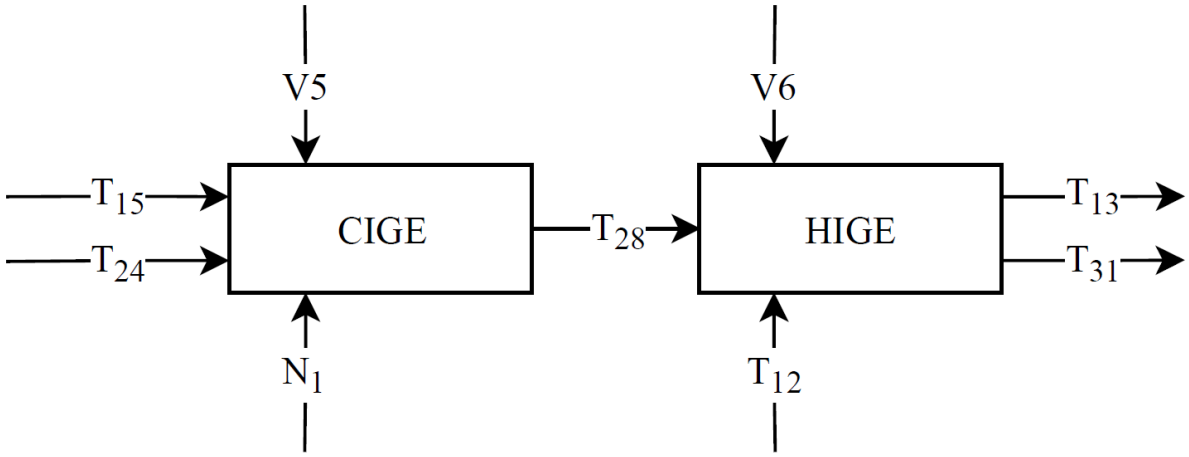

Figure 23 Open-loop configuration for the CIGE/HIGE heat exchanger network and the input and output variables used to determine the effect of process variables on the temperatures at Node 13 and Node 31

V5 is located on the cold stream of the CIGE in the CIGE/HIGE heat exchanger network, shown in Figure 17. The mean valve position for V5 is 17.50% and has an operating range of

0 – 100%. The valve operates in the same manner as V1, bypassing cold gas around the heat exchanger. Opening the valve would result in the combined gas stream at Node 27 being cooler than if the valve were opened less. Since the gas stream at Node 27 is cooler, which passes through the HIGE, the outlet temperatures at Node 13 and Node 31 will also be cooler. From Figure 24, at the maximum valve position of 99.44% the temperature at Node 13 is 697.4 K and at Node 31 is 647.6 K. Closing the valve would have the opposite effect on the outlet temperatures; they would increase in temperature. The minimum valve position for V5 is 0%. From Figure 24 at the minimum valve position the temperature at Node 13 is 717.4 K and at Node 31 is 679.1 K. Also, from Figure 24, for the operating range of V5, 0 – 100%, Node 13 and Node 31 experience a temperature change of 20 K and 31.5 K, respectively. Thus, V5 has a larger effect on the temperature at Node 31 than on Node 13.

V6 is located on the cold stream of the HIGE, of which the outlet temperatures are the inlet gas streams to the catalytic converter. The mean valve positon for V6 is 57.66% and has an operating range of 10 – 100%. Adjusting the valve position of V6 passes more or less cold gas around the HIGE, similar to V2 on the HGE. The bypassed gas is not heated and upon combining it with the gas that passes through the HIGE, the gas stream at Node 31 is cooler than it would be if less gas was sent through the bypass. Since there would be less gas flowing through the HIGE when the valve is opened less heat transfer would occur and the hot stream and temperature at Node 13 would be warmer. Less heat transfer would occur since there is less gas flowing through the HIGE, which means a larger residence time, and hence, the cold gas stream would increase in temperature to a point at which there would no longer be a driving

force for heat transfer, shown in Figure 25. From Figure 24, at maximum valve 99.91%, the maximum valve position the temperature at Node 13 is 721.3 K and 665.0 K. The opposite effect is observed for closing the valve. The minimum valve position for V6 is 10.16%. At the minimum valve position the temperature at Node 13 is 707.8 K and at Node 31 is 678.0 K. Examining Figure 24 for the operating range of V6, 10 – 100%, the temperatures at Node 13 and Node 31 experience a temperature change of 13.5 K and 13.0 K, respectively. Thus, V6 has a similar effect on the temperatures at Node 13 and Node 31. And comparing V5 and V6, both valves have a similar effect on the outlet temperatures of the HIGE.

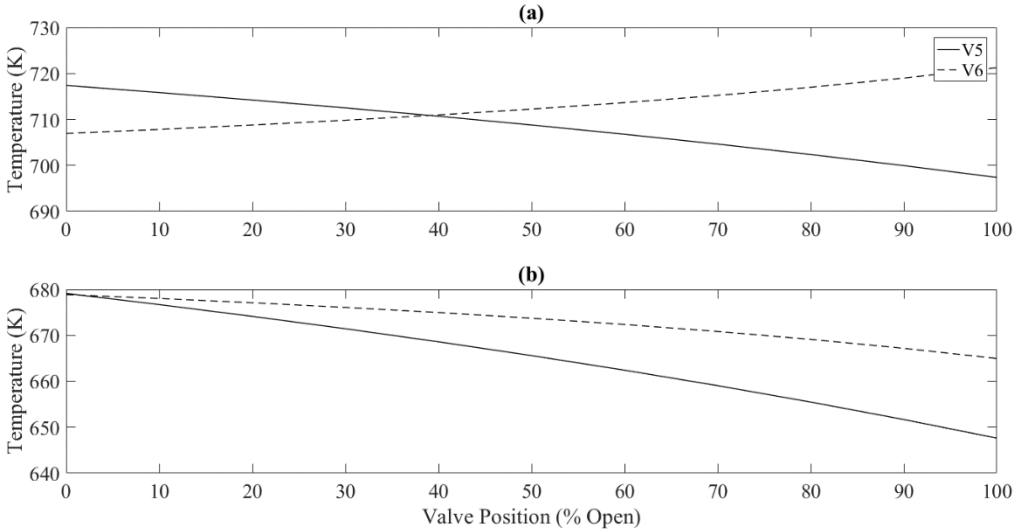

Figure 24 Open-loop effect of CIGE/HIGE bypass valves, V5 and V6, on the outlet temperature at (a) Node 13 and (b) Node 31

Like V1 and V2, adjusting the position of V5 and V6 on the CIGE/HIGE heat exchanger network also effects the flow rate of the cold gas streams. This is confirmed by calculating the

intermediate temperatures of the CIGE/HIGE for various valve positons. If V5 or V6 is opened the intermediate temperatures would increase. The results are plotted in Figure 25.

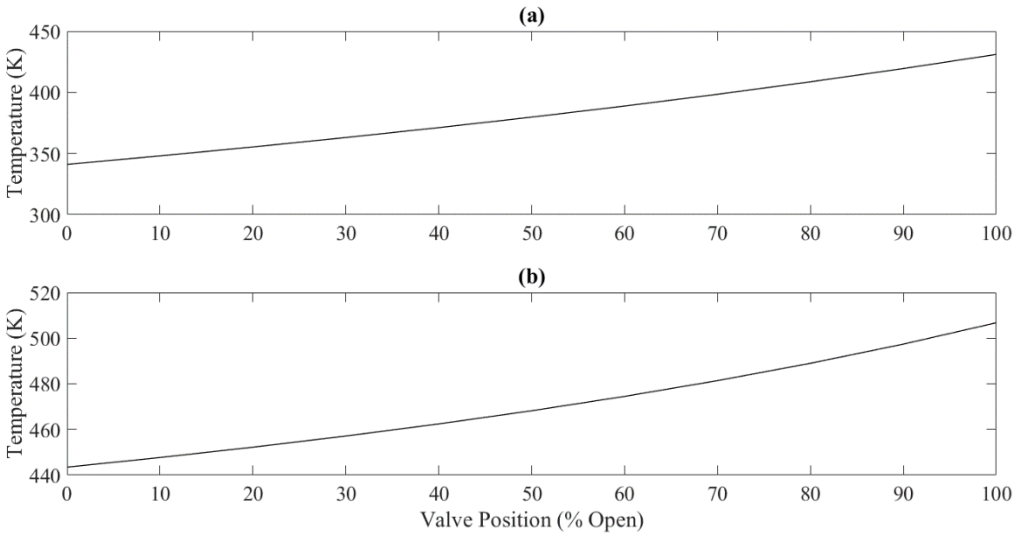

Figure 25 Open-loop effect of the CIGE/HIGE bypass valves, V5 and V6, on the intermediate temperature of the (a) CIGE and (b) HIGE

Thus, from Figure 24, V5 has a larger effect on the temperature at Node 31 than at Node 13. However, V6 has a larger effect on Node 31 than Node 13. Also, V5 has a larger impact on the temperatures than V6, comparing the temperature change over each of the valves operating ranges. Opening V5 decreases the temperature at Node 13 and Node 31. Opening V6 increases the temperature at Node 13 and decreases the temperature at Node 31. These results provide a better understanding of how V5 and V6 effect the CIGE/HIGE outlet temperatures. This provides a foundation for process control techniques and should be considered when adjusting the valves.

The feed gas flow rate will have an impact on the gas flow rates throughout the acid plant, so its effect on the outlet temperatures at Node 13 and Node 31 should also be investigated. The mean feed gas flow rate to the plant is 172.5 $kNm^3\ h^{-1}$. For this feed gas flow rate the temperatures at Node 13 and Node 31 are 699.9 K and 685.7 K.

The maximum feed gas flow rate from industrial operating data is 242.34 $kNm^3\ h^{-1}$ the temperatures at Node 13 and Node 31 are 723.4 K and 672.7 K, respectively. From Figure 26, the feed gas flow rate has a large effect on the outlet temperatures of the CIGE/HIGE, nearly 50 K for the operating range. However, this is considerably less than the effect of feed gas flow rate on the CGE/HGE outlet temperatures. If the feed gas flow rate is increased, the temperature at Node 27 will be cooler and thus, the cold stream entering the HIGE will also be cooler than if the flow rate were decreased. The cooler gas stream being fed to the HIGE in combination with a smaller residence time would result in the temperature at Node 31 being much cooler. As the flow rate increases, the temperature at Node 13 increases. At Node 13 the stream is hot and has been cooled from the outlet of the catalytic converter in preparation for the next oxidation step. Again, for a higher flow rate there the gas streams have a smaller residence time within the heat exchanger and less heat transfer occurs. Thus, for the hot stream being cooled in the HIGE there would be less of a decrease in temperature from the inlet at Node 12 and the outlet temperature at Node 13 would be warmer.

The minimum feed gas flow rate from industrial operating data is 58.19 $kNm^3\ h^{-1}$ which leads to the temperature at Node 13 and Node 31 is 661.1 K and 713.3 K, respectively. For a decrease

in feed gas flow rate the gas streams would have an increase residence time in the heat exchanger and more heat transfer would occur. The temperature of the cold gas stream at Node 27, which has passed through the heat exchanger would be warmer than it would have been with a lower feed gas flow rate. Thus, the cold stream entering the HIGE would be warmer, and in combination with the lower gas flow rate more heat transfer would occur, resulting in the temperature at Node 31 being much higher. The opposite effect occurs for the temperature at Node 13. For a lower flow rate there is more residence time and therefore more heat transfer occurs. Since there is more heat transfer from the hot to cold gas streams the temperature at Node 13 would decrease.

Flow rate has a considerable effect on outlet temperatures of the CIGE/HIGE heat exchanger network, the outlet temperatures varying by approximately 50 K over the flow rate operating range. However, its effect is less than that on the outlet temperatures of the CGE/HGE. Flow rate is also a disturbance that will be common with the Clean AER modifications. Increasing the feed gas flow rate impacts the flow rate throughout the acid plant. For increasing flow rate, the residence time of the gas streams decreases and as a result less heat transfer occurs. Thus, the cold stream will be cooler and the hot stream will be warmer. For decreasing flow rate; the residence time increases and more heat transfer occurs. Thus, the cold steam will be warmer and the hot stream will be cooler.

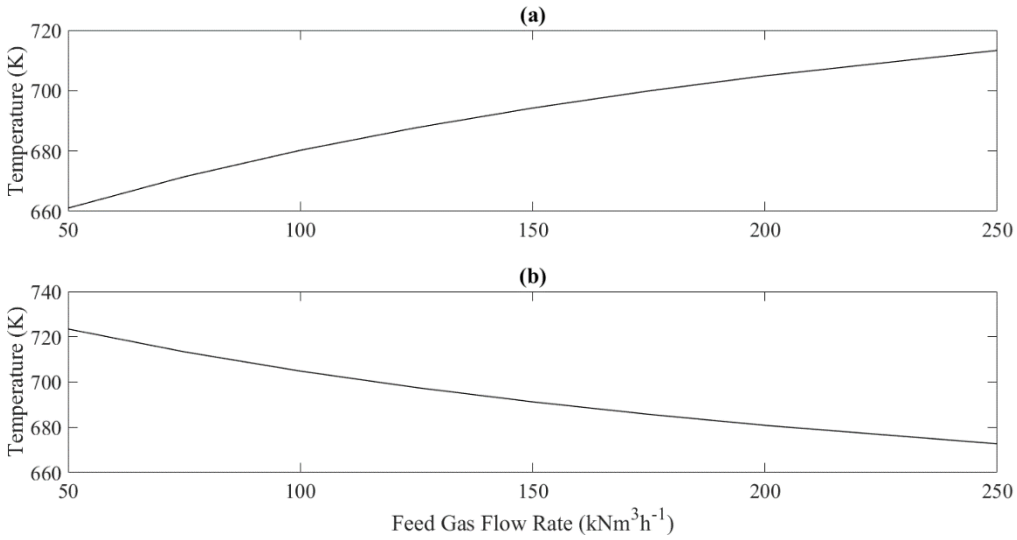

Figure 26 Open-loop effect of feed gas flow rate on the outlet temperature at (a) Node 13 and (b) Node 31 for the CIGE/HIGE heat exchanger network

3.4.2 Closed-Loop

An important thing to note about the CGE/HGE heat exchanger network is that the gas stream at the outlet, Node 7, of the first bed of the catalytic converter is the hot stream inlet to the HGE. So, a closed-loop forms and the temperature at Node 7 depends on the temperature of Node 6. Although the temperature at Node 7 is not an important temperature itself, it does effect the outlet temperatures of the CGE/HGE heat exchanger network. Thus, it would be useful to know the effect of the process variables on the temperature at Node 7.

Figure 27 shows the closed-loop configuration for the CGE/HGE heat exchanger network. The inputs to the CGE/HGE heat exchanger network are the temperatures at Node 2 and Node 32, the positions of V1 and V2, the flow rate at Node 1 and the concentration of SO_2 in the feed

gas. Comparing to the open-loop configuration, the concentration of SO_2 in the feed gas is an additional disturbance variable. The manipulated variables and controlled variables are the same as the open-loop configuration. In the closed-loop configuration of Figure 27, the temperature of Node 7 is an output, rather than an input.

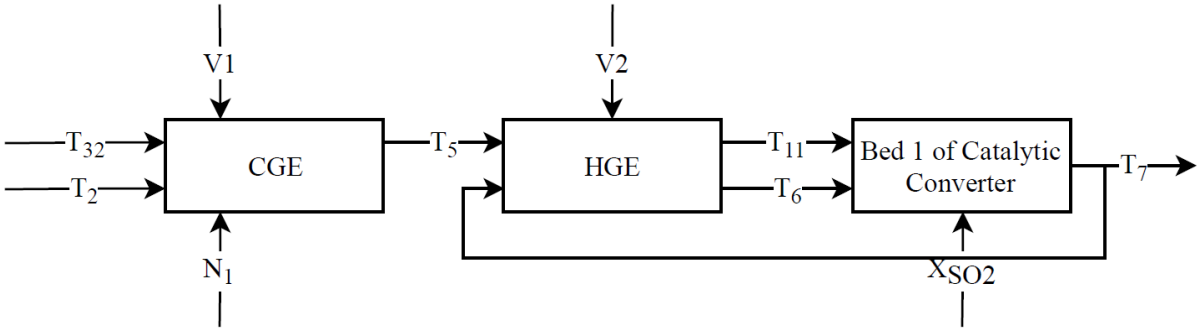

Figure 27 Closed-loop configuration of the CGE/HGE heat exchanger network and its inputs and output variables used to determine the effect of process variables on the temperature at Node 7

Based on steady-state mass and energy balances, the conversion ratio and temperature evolves following the heat-up path (He, Zhang, & Shang, 2019):

$$\Phi = \frac{C_p M}{(-\Delta H) X_{SO_2}{}^f}(T - T^f) \tag{3.16}$$

As the oxidation reaction proceeds, the SO_2 conversion ratio and temperature increase. The equilibrium state is reached when the SO_2 consumption rate in the forward reaction of Equation 2.7 is equal to the SO_3 generation rate in the reverse reaction. At the equilibrium state the

equilibrium conversion ratio is related to the equilibrium temperature by (He, Zhang, & Shang, 2019):

$$T_E = \frac{-b}{a + Rln\left[\frac{{X_{SO_3}}^f + {X_{SO_2}}^f \Phi_E}{(1-\Phi_E){X_{SO_2}}^f}\left(\frac{1 - 0.5{X_{SO_2}}^f \Phi_E}{{X_{O_2}}^f - 0.5{X_{SO_2}}^f \Phi_E}\right)\right]} \tag{3.17}$$

where a and b are empirical constants related to the SO_2 oxidation reaction, R is the ideal gas constant, Φ_E is the SO_2 conversion ratio at equilibrium, and ${X_{SO_3}}^f$ and ${X_{O_2}}^f$ are the feed concentrations of SO_3 and O_2, respectively. The heat-up path intercepts the equilibrium curve at the equilibrium point. The equilibrium point can be calculated by combining Equation 3.15 and Equation 3.16. As the oxidation reaction proceeds, SO_3 is produced which impedes the oxidation of SO_2. This effect becomes more significant as the equilibrium point it approached. Thus, it is not possible to achieve the equilibrium point in an acid plant. The calculated equilibrium point provides a theoretical maximum conversion ratio. The actual conversion achieved in an acid plant is ideally close to but slightly smaller than the equilibrium ratio. The actual conversion ratio is related to the equilibrium ratio by a parameter:

$$\Phi = \xi \Phi_E \tag{3.18}$$

where ξ is a parameter less than one, that is estimated from industrial operating data. The parameter indicates how close the SO_2 conversion ratio is to the equilibrium ratio. For the

industrial operating data the parameter for the first bed of the catalytic converter is equal to 0.99 (He, Zhang, & Shang, 2019).

Beginning with the effect of V1 on outlet temperature of the catalytic converter, as V1 increases the temperature at Node 7 decreases. If V1 is opened the combined gas stream at Node 5 would be cooler, resulting in the temperature at Node 6, the inlet of the catalytic converter, being cooler. Assuming all other variables are held at their mean values and the oxidation reaction proceeds, the temperature at Node 7 would also be cooler, shown in Figure 28. As V2 increases, the temperature at Node 7 also decreases. If V2 is opened the combined gas stream at the inlet of the catalytic converter would be cooler. Thus, assuming that all other process variables are held at their mean values from industrial operating data, the temperature at Node 7 would also be cooler. Over their operating ranges V1 and V2 cause a temperature change of 12 K and 35.1 K at Node 7, respectively. So V2 has a more significant effect on the outlet temperature of the converter. From Figure 19 it was concluded that V2 had a larger effect on the temperature a Node 6 than V1. Thus, it follows that V2 would also have a larger impact on the temperature at Node 7 since it is the same gas stream.

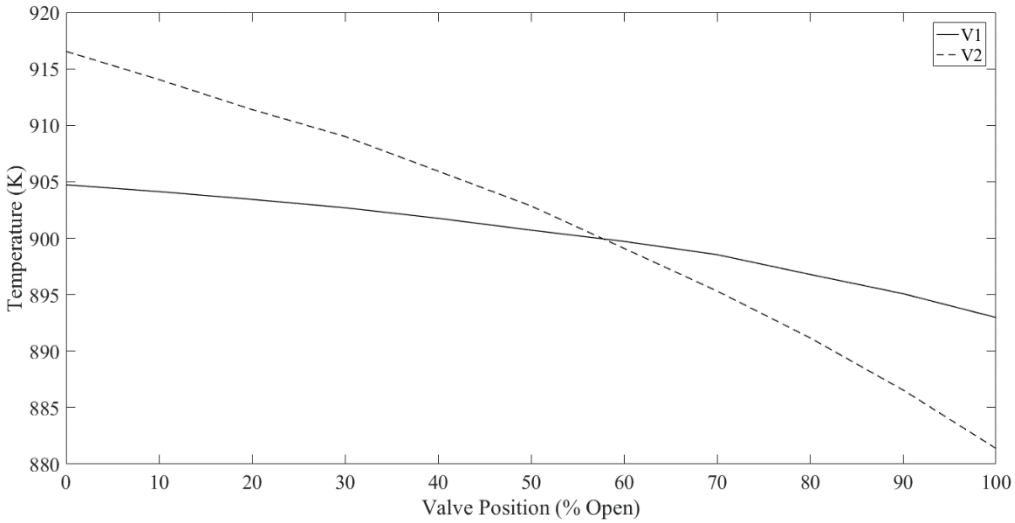

Figure 28 Closed-loop effect of CGE/HGE bypass valves, V1 and V2, on the outlet temperature at Node 7 for the CGE/HGE heat exchanger network

If the feed gas temperature were increased, the temperature of the cold stream flowing through the CGE/HGE heat exchanger network would also increase. This would result in the temperature at Node 7 increasing, shown in Figure 29. From Figure 29 the temperature at Node 7 varies by 27 K over the operating range.

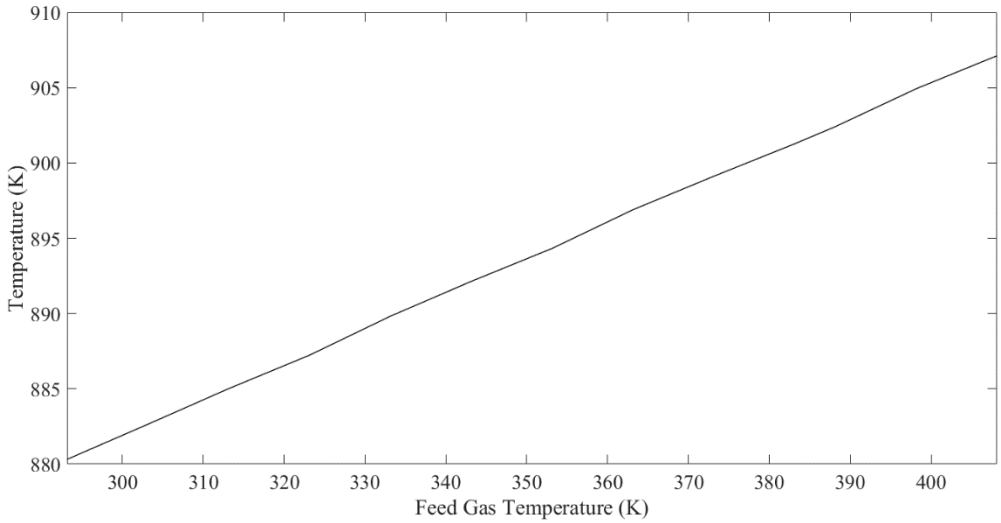

Figure 29 Closed-loop effect of feed gas temperature on the outlet temperature at Node 7 for the CGE/HGE heat exchanger network

Flow rate has a large effect on the temperature at Node 7 much like it did for the outlet temperatures of the CGE/HGE and CIGE/HIGE heat exchanger networks. If the feed gas flow rate were increased the temperature of the cold gas stream running through the CGE/HGE heat exchanger network would be cooler, resulting in the temperature at Node 7 being cooler. Over the operating range in Figure 30 the temperature at Node 7 varies by nearly 100 K. The feed gas flow rate has a more significant effect on the temperature at Node 7 in comparison to the valve positions and feed gas temperature.

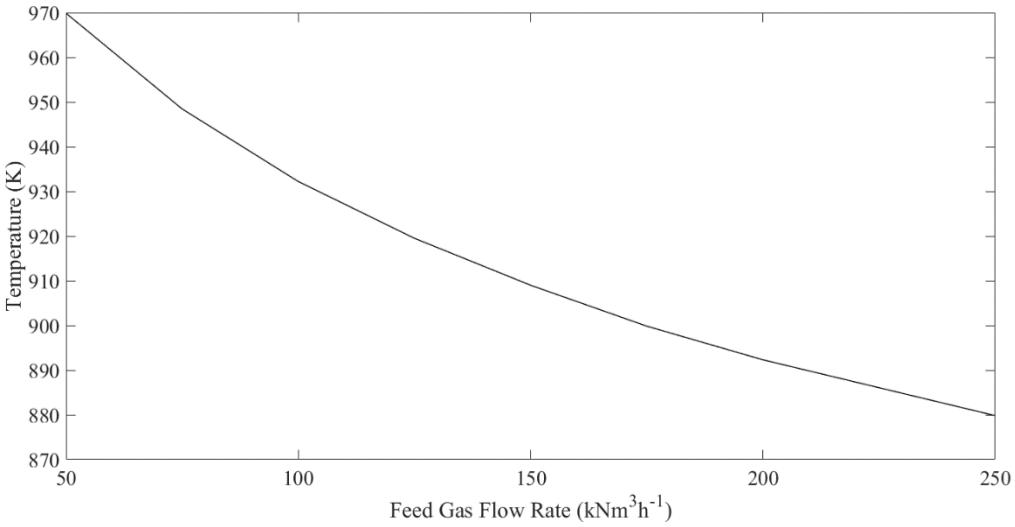

Figure 30 Closed-loop effect of feed gas flow rate on the outlet temperature at Node 7 for the CGE/HGE heat exchanger network

Knowing the equilibrium point of the first bed of the catalytic converter, Equation 3.15 can be used to estimate the outlet temperatures for a varying feed gas SO_2 concentration. Variation in SO_2 concentration significantly raises the operational challenges for the acid plant in the smelter. From the industrial operating data, the concentration of SO_2 in the feed gas typically varies from 5 to 15 vol%. The off-gases supplied from the roasters and MK reactor are weaker in SO_2 while the off-gas supplied from the furnaces is stronger in SO_2. The combination of off-gases produces an off-gas that is typically 10 vol% SO_2. However, once the Clear AER modifications are implemented, the off-gases produced by the Pierce-Smith converters will be collected and sent to the acid plant. The Pierce-Smith converters produce a large amount of off-gas that is inconsistently flowing and is weak in SO_2. Therefore, it is important to understand the implications of a weaker in SO_2 gas being sent to the acid plant.

From Figure 31 the temperature of the gas stream at the outlet of the converter increases with increasing SO_2 concentration. More SO_2 conversion occurs due to a higher concentration at the inlet, and thus there is more heat evolved from the oxidation reaction and a higher temperature at the outlet. For a feed gas that is weaker in SO_2 (~5%) the temperature at Node 7 is 793.4 K. In comparison, a feed gas that is stronger in SO_2 (~15%) results in the temperature at Node 7 being 932.8 K. Thus, for the operating range of SO_2 concentration the temperature at Node 7 can vary by nearly 150 K. Thus, the feed gas concentration of SO_2 has the largest effect on the outlet temperature of the first bed of the catalytic converter.

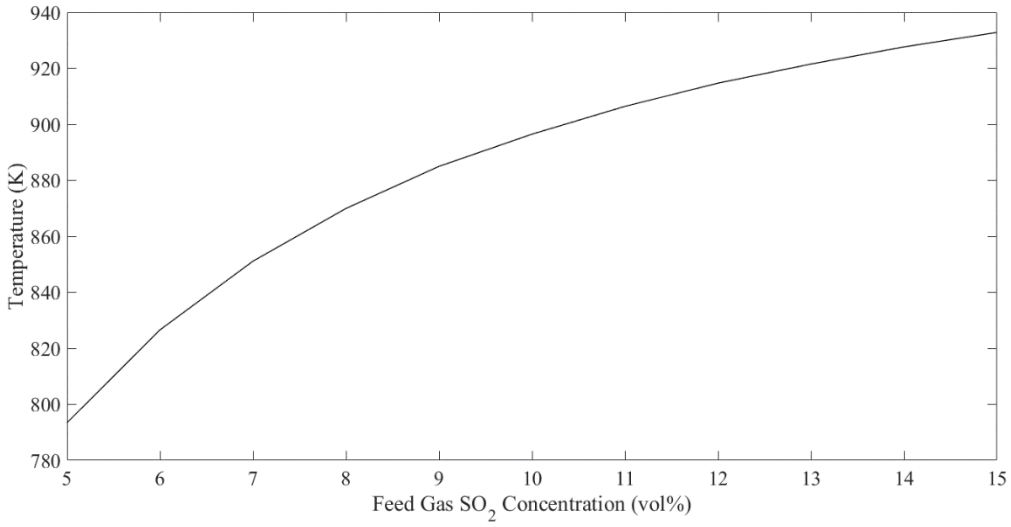

Figure 31 Closed-loop effect of feed gas SO_2 concentration on the outlet temperature at Node 7 for the CGE/HGE heat exchanger network

Equation 3.15 and Equation 3.16 to determine the equilibrium SO_2 conversion ratio and equilibrium temperature of the first bed of the catalytic converter. Using the parameter estimated by industrial data, Equation 3.17 can be used to determine the actual conversion ratio. Equations 3.9 – 3.11 can be used to estimate the outlet temperatures at Node 6 and Node

11 as well as the SO_2 conversion ratio of the first bed of the catalytic converter. The closed-loop configuration used to determine the outlet temperatures of the CGE/HGE heat exchanger network is shown in Figure 32. The inputs are the same as those for the open-loop configuration except rather than the temperature at Node 7 being an input it is an estimated output which is used to calculate the temperature at Node 7. The additional output of the closed-loop configuration is the SO_2 conversion ratio in the first bed of the catalytic converter.

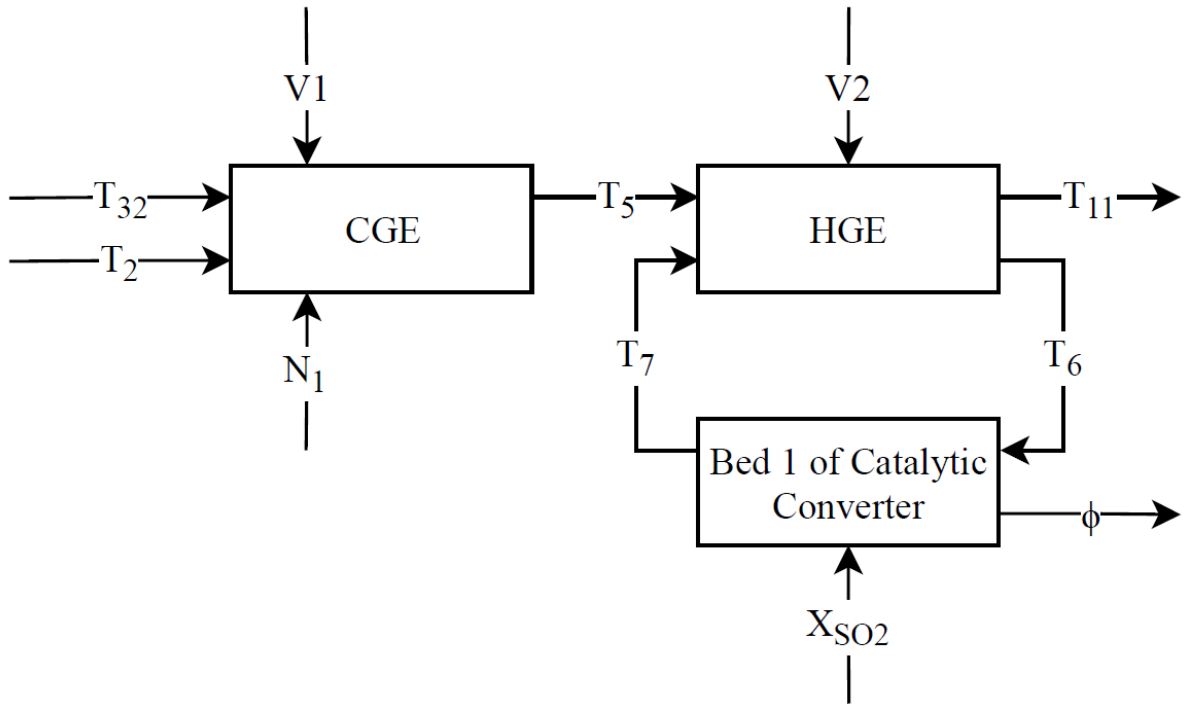

Figure 32 Closed-loop configuration of the CGE/HGE heat exchanger network and its input and output variables used to determine the effect of process variables on the temperatures at Node 6 and Node 11 and the SO_2 conversion ratio

The effects of V1 and V2 on the outlet temperature for the closed-loop configuration follow the same trend as the open-loop configuration, see Figure 33. Opening V1 decreases both the temperature at Node 6 and at Node 11. The valve has a larger effect on the temperature at Node

6, which is the stream the valve is located on. Opening V2 decreases the temperature at Node 6 while the temperature at Node 11 increases. Again, the valve has a greater impact on the temperature at Node 6. Comparing V1 and V2, V2 has a larger effect on the outlet temperatures. The temperature change is approximately 20 K for the operating range of V2, which is much smaller than the operating range of V1. The temperature at Node 7 does not greatly affect the operation of the valves, it only effects the outlet temperatures slightly since this is a stream that is used to warm the cold gas stream of the HGE. Consistent with the decrease in temperature at Node 6 with opening V1 and V2, if temperature at Node 6 decreases then temperature at Node 7 would also decrease.

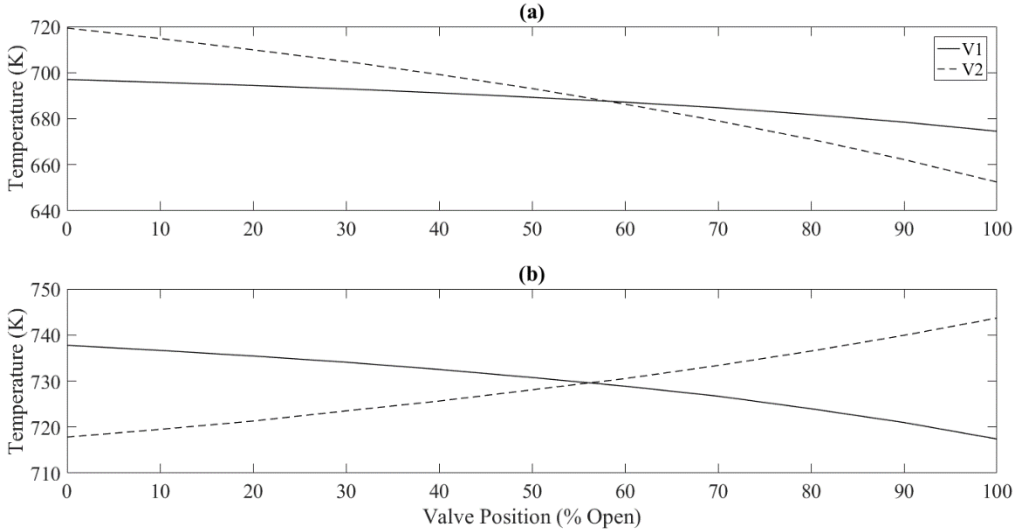

Figure 33 Closed-loop effect of CGE/HGE bypass valves, V1 and V2, on the outlet temperature at (a) Node 6 and (b) Node 11

The effect of feed gas temperature is also similar to the open-loop results. From Figure 34, as the temperature of the feed gas increases, the temperature at Node 6 and Node 11 would increase. Using the closed-loop to determine the effect of feed gas temperature on Node 7, it

would increase if the feed gas temperature increased, as concluded. Thus, if the hot stream of the HGE increases, the temperatures at both Node 6 and Node 11 would increase. The increase in temperature has a similar effect on the outlet temperatures, a change of approximately 50 K over the operating range. Comparing the effect of feed gas temperature results from open-loop and closed-loop it is clear that the feed gas temperature has a greater effect than initially predicted.

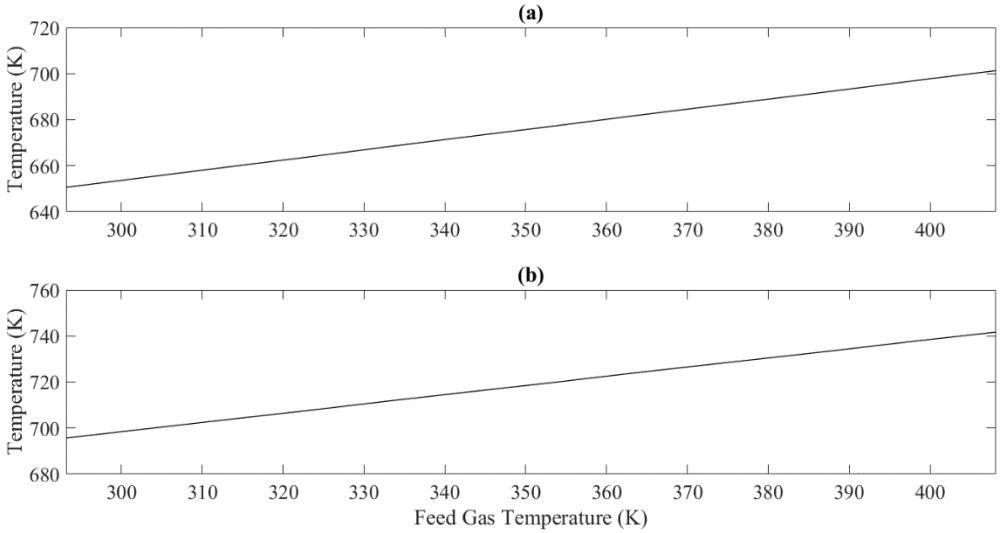

Figure 34 Closed-loop effect of feed gas temperature on the outlet temperature at (a) Node 6 and (b) Node 11 for the CGE/HGE heat exchanger network

The feed gas flow rate has the same effect on the outlet temperatures as the open-loop configuration. From Figure 35, as the feed gas flow rate increases the cold stream outlet temperature at Node 6 decreases and the hot stream outlet temperature at Node 11 increases. However, using the closed-loop configuration we can see that the feed gas flow rate has an even larger effect on the temperature at Node 6 than the open-loop configuration predicted.

For the operating range of the flow rate, the open-loop configuration predicted that the temperature at Node 6 would decrease by approximately 120 K compared to the closed-loop configuration which predicts the temperature at Node 6 would decrease by nearly 180 K. It was concluded from the open-loop configuration that the feed gas flow rate has significant effect on the outlet temperatures. Thus, it makes sense that using the closed-loop configuration the effect would be amplified. As the feed gas flow rate increases the temperature at Node 7 decreases by almost 100 K, see Figure 30. Then, since the temperature at Node 7 is cooler the temperature at Node 11 would be cooler as well; for open-loop it was increased approximately 100 K and for closed-loop it is closer to 70 K. In addition, if the temperature at Node 7 is decreased then the temperature at Node 6 would decrease since there is less heat transferred from the hot stream to the cold stream.

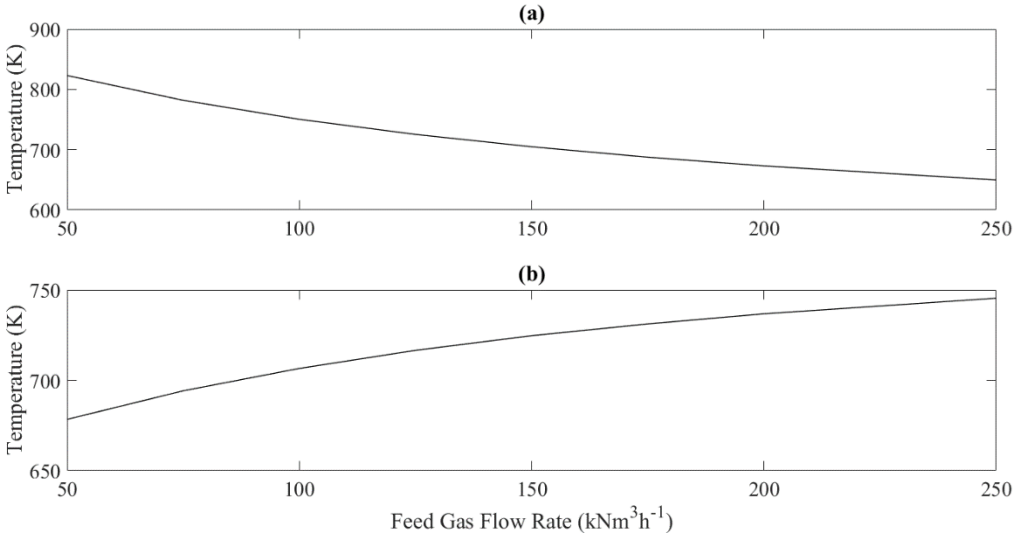

Figure 35 Closed-loop effect of feed gas flow rate on the outlet temperature at (a) Node 6 and (b) Node 11 for the CGE/HGE heat exchanger network

The concentration of SO_2 in the feed gas does not directly affect the outlet temperature at Node 6 since the cold gas stream has not passed through the catalytic converter. The concentration of SO_2 in the feed gas does however effect the temperature at the outlet of the first bed of the catalytic converter, which is the hot stream inlet to the HGE. Thus, for an increase in feed gas SO_2 concentration the hot stream of the HGE would be warmer, see Figure 36. Thus, the temperature of both Node 6 and Node 11 would increase. If the temperature at Node 7 were warmer, the temperature at Node 11 would be warmer since it has to cool a warmer stream. Also, Node 6 would be warmer since the stream would be heated more. The concentration of SO_2 in the feed gas has a greater effect on the temperature at Node 11 than Node 6. For the SO_2 concentration operating range Node 11 changes by 80 K while the temperature at Node 6 changes by 65 K.

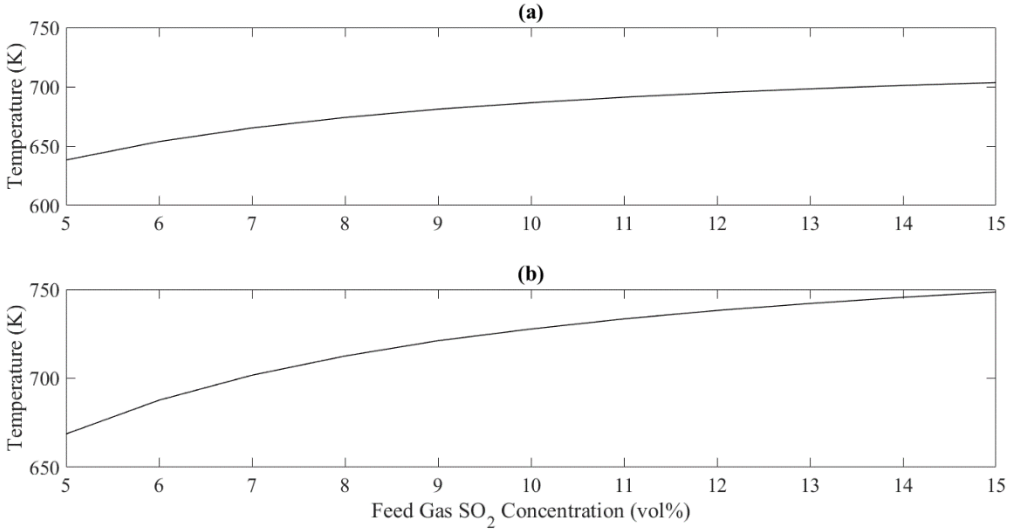

Figure 36 Closed-loop effect of feed gas SO_2 concentration on the outlet temperature at (a) Node 6 and (b) Node 11 for the CGE/HGE heat exchanger network

The SO_2 conversion ratio is an important performance indicator for the catalytic converter. It represents the amount of SO_2 being oxidized to SO_3 and removed from the off-gas stream before it is sent into the atmosphere through the Superstack. The conversion ratio is of high industrial interest since it can be used to determine how efficiently the acid plant is operating.

Although the valve positions do not directly effect the SO_2 conversion ratio of the first bed of the catalytic converter, the valve positions effect the temperature at Node 6, which is the inlet stream to the catalytic convert. Thus, if V1 or V2 is opened, the temperature at Node 6 decreases, as shown in Figure 28. Examining Figure 37, if either valve is opened the SO_2 conversion ratio increases. Thus, a cooler temperature at the inlet of the first bed of the catalytic converter results in a greater amount of SO_2 being oxidized to SO_3. Since V2 has a larger effect on the temperature at Node 6, it follows that V2 would have a larger effect on the SO_2 conversion ratio. For the operating ranges of the valves, the SO_2 conversion ratio varies by 3.47% and 7.12% for V1 and V2, respectively.

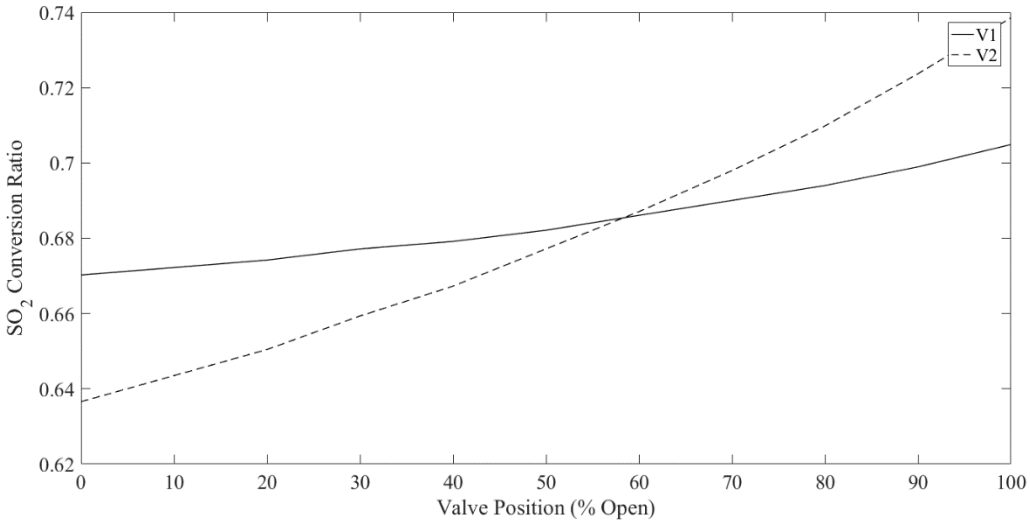

Figure 37 Closed-loop effect of CGE/HGE bypass valves, V1 and V2, on the SO_2 conversion ratio for the first bed of the catalytic converter

The results of Figure 38 further confirm that a lower temperature at the inlet of the first bed of the catalytic converter. It follows from Figure 29 that increasing the feed gas temperature increases the temperature at Node 6 and from Figure 37 that an increase in temperature at Node 6 reduces the SO_2 conversion ratio. The SO_2 conversion ratio varies by 7.72% for the feed gas temperature operating range.

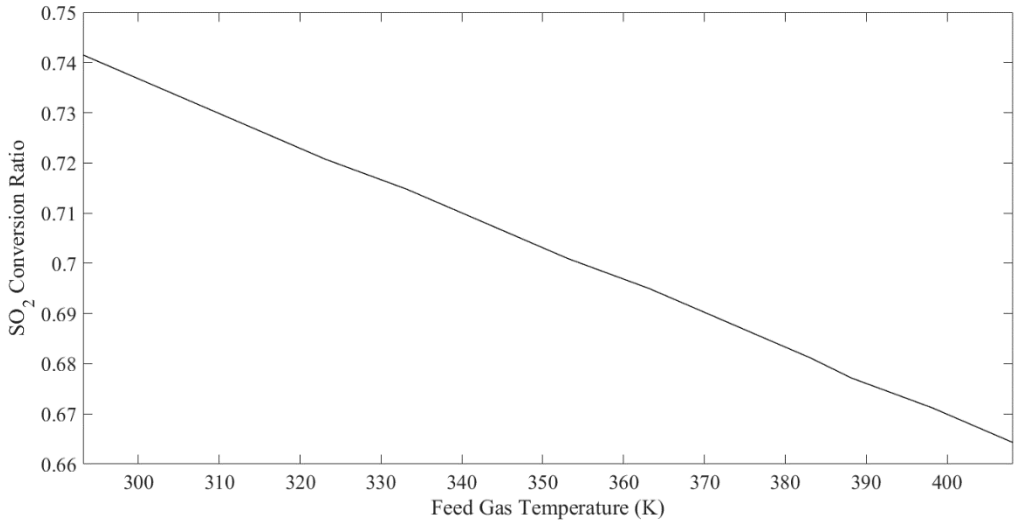

Figure 38 Closed-loop effect of feed gas temperature on the SO_2 conversion ratio for the first bed of the catalytic converter

Flow rate does not directly affect SO_2 conversion but it effects temperature. Since flow rate has a large effect on temperature it will have a significant effect on conversion. From Figure 39 for the feed gas flow rate operating range, the SO_2 conversion ratio varies 26.83%, which is much larger than the effects from the valve positions and feed gas temperature. From Figure 34, if the feed gas flow rate is increased, the temperature at Node 6 would decreased due to a larger amount of heat transfer occurring in the CGE/HGE heat exchanger network. Then, if the temperature at Node 6 decreases the SO_2 conversion ratio would increase, Figure 39.

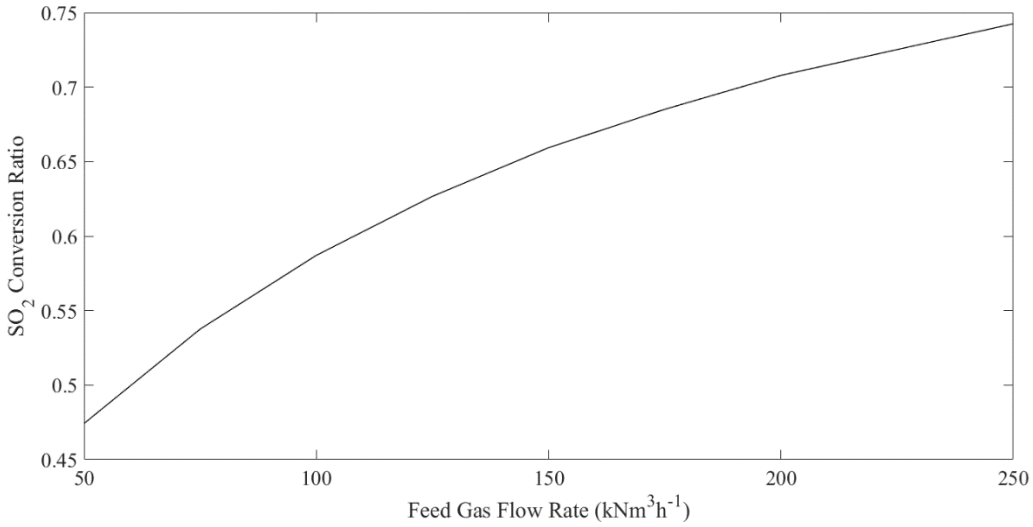

Figure 39 Closed-loop effect of feed gas flow rate on the SO_2 conversion ratio for the first bed of the catalytic converter

High SO_2 concentration favours a higher SO_2 conversion as a larger amount of SO_2 is converted. However, the outlet concentration of SO_2 also increases with increasing feed concentration. Despite more SO_2 conversion for a larger SO_2 feed concentration, the conversion ratio decreases, a larger value in the denominator of Equation 3.15. From Figure 36, for an increasing SO_2 concentration in the feed gas the temperature at Node 6 would increase. Thus, for increasing temperature at Node 6, the SO_2 conversion ratio should decrease. This is confirmed by the plot in Figure 40. From Figure 40, SO_2 concentration in the feed gas has a large effect on the SO_2 conversion ratio. Over the operating range, the SO_2 conversion ratio varies 37.12%.

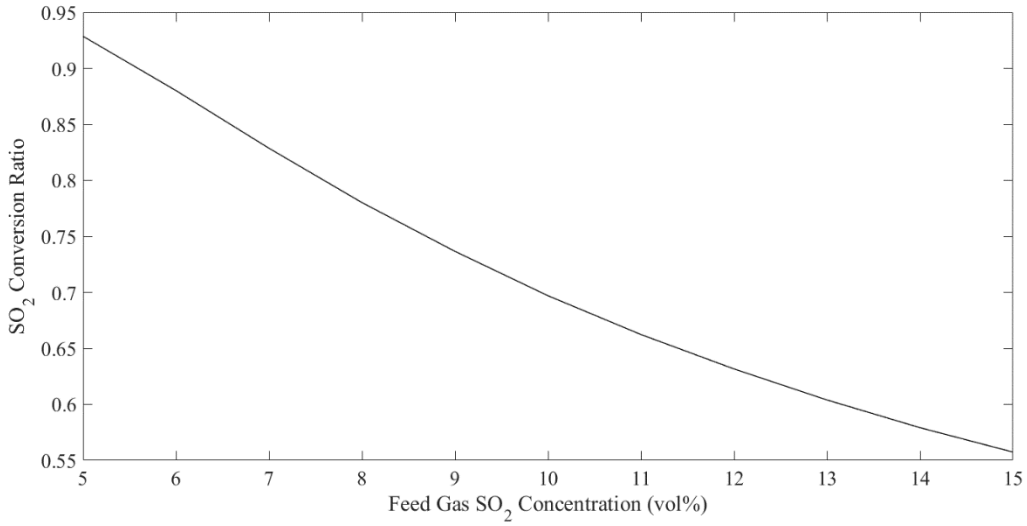

Figure 40 Closed-loop effect of feed gas SO_2 concentration on the SO_2 conversion ratio for the first bed of the catalytic converter

The closed-loop configuration can also be applied to the CIGE/HIGE heat exchanger network. The effect of the disturbance and manipulated variables is significantly reduced for the third and fourth beds of the catalytic converters since the gas streams entering the last two beds of the catalytic converter are weaker in SO_2, less conversion takes place. Thus, understanding the effects process variables on the outlet temperatures and the SO_2 conversion ratio for the CGE/HGE heat exchanger network is most crucial.

3.5 Steady-State Gain

The steady-state process gain can quantify the effects of the process variables on the outlet temperatures and the SO_2 conversion ratio. The open-loop steady-state process gain is the ratio of the output variable change to an input variable change when the input is adjusted to a new

value. It describes the sensitivity output to a change in the input. To determine the steady-state gain, an input is changed in a stepwise fashion while holding all other inputs constant. The process is then allowed to reach a new steady-state and the response of the model is observed. Then, step changes can be made for the remaining inputs and open-loop response data can be obtained for the controlled variables. The steady-state gain of a process corresponds to:

$$K_{ij} = \frac{\Delta y_i}{\Delta u_j} \tag{3.19}$$

where the K_{ij} is the steady-state gain of the (i, j) element of a gain matrix and Δy_i and Δu_j are changes in the *ith* output and *jth* input variable, respectively. The steady-state gain is constant for linear processes regardless of their operating conditions (Seborg *et al.*, 2011). When the steady-state gain is large, the output will experience a large change for a small change in the input. For the same change in input, the output will experience a small change if the steady-state gain is small. The sign of the steady-state gain may be positive or negative. If the steady-state gain is negative and the input is increased, the output will decrease. If the steady-state gain is positive and the input is increased, the output will also increase.

Consider the CGE/HGE and CIGE/HIGE heat exchanger networks in Figure 16 and Figure 17 and the corresponding process variables and their notation in Table 19. There are two controlled variables and two manipulated variables for each of the heat exchanger networks. The controlled variables are the outlet temperatures and the manipulated variables are the valve

positions. To determine whether the steady-state gain is constant for linear processes regardless of their operating conditions, several step tests for the same manipulated variables were performed (Seborg *et al.*, 2011; McAvoy, 1981). The valve positions were adjusted by ±Δ5-25%, and the results were averaged. Step changes were chosen so that the steady-state gains did not change significantly with the size of the perturbation of the manipulated variables (McAvoy, 1981). The average steady-state manipulated variable gains for the CGE/HGE and CIGE/HIGE are listed in Table 21 and Table 22, respectively. From the results, for the CGE/HGE heat exchanger network V2 has a larger effect on the outlet temperatures than V1. Also, for an increase in V1, both of the outlet temperatures will decrease whereas for an increase in V2, the temperature at Node 6 will decrease and the temperature at Node 11 will increase. For the CIGE/HIGE heat exchanger network, V5 and V6 have a similar effect on the outlet temperatures. For an increase in V5 the outlet temperatures decrease whereas for an increase in V6 the temperature at Node 13 increases and the temperature at Node 31 decreases. These result is consistent with the conclusions made by Figure 19 and Figure 24.

Table 21 Steady-state gains for the CGE/HGE heat exchanger network for manipulated variables

Controlled Variable	Manipulated Variable	
	V1	V2
Node 6	-0.1663	-0.5267
Node 11	-0.1435	0.4747

Table 22 Steady-state for the CIGE/HIGE heat exchanger network for manipulated variables

Controlled Variable	Manipulated Variable	
	V5	V6
Node 13	-0.1848	0.2292
Node 31	-0.1882	-0.2969

Gain was also calculated for feed gas variables as well as the input temperatures for each of the heat exchanger networks. The inlet temperatures were adjusted by ±Δ10-200 °C. The steady-state gains remained constant. The feed gas flow rate to the acid plant was adjusted by ±Δ5-20 $kNm^3 h^{-1}$. There was more variation in the steady-state gains for flow rate. This is due to a strong correlation between flow rate and outlet temperature (He J. , 2018). The average steady-state disturbance gains for the CGE/HGE and CIGE/HIGE heat exchanger networks are listed in Table 23 and Table 24, respectively. The steady-state gain for the gas composition at Node 6, which has an effect on the temperature at Node 7, was taken from previous work by He *et al.* (2019). The steady-state gain for feed gas SO_2 concentration is also listed in Table 23. From the results, for the CGE/HGE network of heat exchangers, the concentration of SO_2 at Node 6, which determined the temperature at Node 7 has the largest effect on the outlet temperatures. The feed gas flow rate also has a significant effect on the outlet temperatures. These results are consistent with those from Figure 35 and Figure 36. These disturbances are frequently encountered and one of the main challenges in efficient acid plant operation. For the CIGE/HIGE network of heat exchangers the effect of the disturbances on the outlet temperatures is not as severe with the exception of the temperature at Node 12, which is related to the concentration of SO_2 in the converter.

Table 23 Steady-state gains for the CGE/HGE heat exchanger network for disturbance variables

Controlled Variable	Disturbance Variable				
	Temperature			Flow Rate	SO_2 Volume Percent
	Node 2	Node 7	Node 32	Node 1	Node 6
Node 6	0.3287	0.4739	0.1975	-0.3805	12.5
Node 11	0.2629	0.5720	0.1652	0.3578	N/A

Table 24 Steady-state gains for the CIGE/HIGE heat exchanger network for disturbance variables

Controlled Variable	Disturbance Variable			
	Temperature			Flow Rate
	Node 12	Node 15	Node 24	Node 1
Node 13	0.5761	0.3011	0.1228	0.1702
Node 31	0.5476	0.3193	0.1331	-0.1657

Chapter 4: Dynamic Model Identification

This chapter describes how a dynamic model was identified for temperature of the heat exchangers in the sulfuric acid plant.

4.1 Process Dynamics

Industrial operating data are used to determine the dynamics of the process variables on the controlled variables. Examining the industrial data, the controlled variables do not vary simultaneously with the manipulated variables. The outlet temperatures of the HGE and HIGE are the inlet streams are the inlet streams to the catalytic converters and tight temperature control is crucial for efficient SO_2 conversion. Thus, knowing the dynamic response of the outlet temperatures to changes in valve positions is of interest. V1 on the HGE and V5 on the HIGE will be investigated since these valves have larger operating ranges and greater variation. Figure 41 shows the dynamic response of the outlet temperatures of the HGE to a change in the position of V1. To confirm the changes in the outlet temperatures are a result of manipulating V1, the position of V2 and the feed gas temperature and flow rate are also plotted in Figure 41 and remain relatively constant. From the steady-state model investigated in Chapter 3, for a decrease in the position of V1, the outlet temperatures of the HGE increase. From Figure 41 the position of V1 is reduced from 90 to 33% at 3 minutes and the temperature of the cold stream outlet begins to increase at 4 minutes. The temperature of the hot stream outlet is more sluggish and begins to increase at 9 minutes.

Figure 42 show the dynamic response of the outlet temperatures of the HIGE to a change in the position of V5. Again, the position of V6 and the feed gas temperature and flow rate are plotted in Figure 42 and remain constant during the manipulation of V5. From Chapter 3, for an increase in the position of V5, the outlet temperatures will decrease. The position of V5 is increased from 0 to 40% at 0 minutes and is held at approximately 40% after 2 minutes. From Figure 42 the temperature of the cold stream outlet begins to decrease at 8 minutes. The temperature of the hot stream outlet responds to the change in valve position much faster and begins to decrease at 4 minutes. Figure 41 and Figure 42 confirm that the controlled variables do not respond to changes in manipulated variables simultaneously.

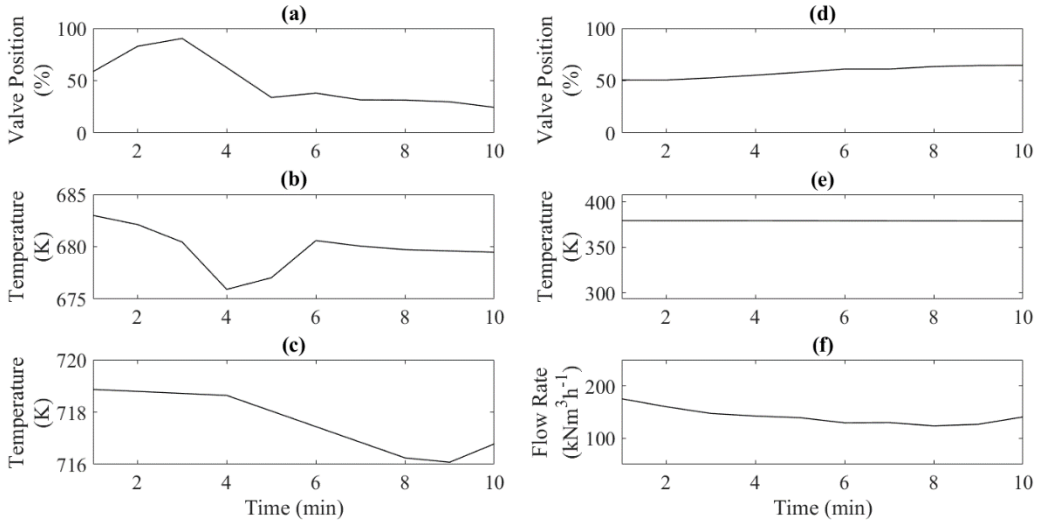

Figure 41 For a change in (a) V1 valve position, the dynamic response of the (b) cold stream and (c) hot stream outlet temperatures of the HGE with the (d) V2 valve position and the feed gas (e) temperature and (f) flow rate held relatively constant

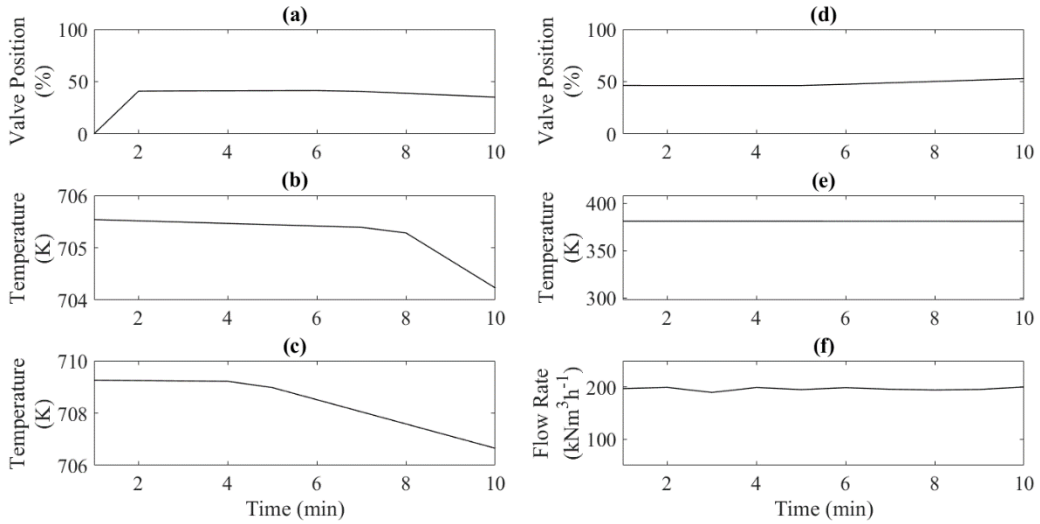

Figure 42 For a change in (a) V5 valve position, the dynamic response of the (b) cold stream and (c) hot stream outlet temperatures of the HIGE with the (d) V2 valve position and the feed gas (e) temperature and (f) flow rate held relatively constant

A correlation coefficient is a calculated number between -1 and 1 that represents the linear dependence of two variables. The correlation coefficient between controlled variables and manipulated and disturbance variables can be used as an indication of whether or not the manipulated and disturbances variables have a strong or weak influence on the controlled variables. Industrial operating data was used to determine the correlation coefficient between each controlled variables and the manipulated and disturbance variables. The industrial operating data collected over the 30-day sampling period was used to calculate the correlation coefficient. The correlation coefficients, based solely on industrial data, are listed in Table 25. A correlation coefficient close to unity suggests that the manipulated or disturbance variable has a strong influence on the controlled variable. The relationship between variables can be further investigated by examining the correlation with different time delays. From Table 25,

the industrial data suggests that the valve position V1 and the feed gas temperature and flow rate have the strongest influence on the temperature at Node 6. The correlation between these variables for different time delays is shown in Figure 43. The maximum correlation occurs at 2 minutes for a change in valve position and 0 minutes a change in feed gas temperature and flow rate. These results are an estimation of the process time constant. A similar investigation was carried out for the outlet temperatures at Node 13 and Node 31, which are most strongly influenced by the positions of V5 and V6 and the inlet temperatures to the CIGE/HIGE heat exchanger network. The resulting time delay plots are shown in Figure 44 and Figure 45 for Node 13 and Node 31, respectively. The correlation coefficients for the temperature at Node 11 suggest that none of the manipulated or disturbance variables has a strong effect on the controlled variable. This is due to the lack of variation in the industrial data at this measuring point, where control has been applied to maintain a tight temperature range. In reality, the manipulated and controlled variables would have a stronger influence on the temperature at Node 6 than the correlation coefficients suggest. The estimations of the process time constants, which are used as an initial guess for MATLAB's System Identification toolbox in are listed in Table 26.

Table 25 Correlation coefficients between controlled variables and manipulated and disturbance variables from industrial data

CGE/HGE				CIGE/HIGE			
Manipulated or Disturbance Variable		Controlled Variable (T)		Manipulated or Disturbance Variable		Controlled Variable (T)	
Location	Type	Node 6	Node 11	Location	Type	Node 13	Node 31
V1	V	-0.4876	0.2123	V5	V	-0.1068	0.6467
V2	V	-0.0372	-0.0529	V6	V	-0.4828	-0.7998
Node 2	T	-0.4602	0.0615	Node 12	T	0.5517	0.6942
Node 7	T	-0.2904	0.3479	Node 15	T	0.4683	0.6597
Node 32	T	-0.3259	0.3827	Node 24	T	0.0609	-0.0775
Node 1	F	-0.6242	0.1927	Node 1	F	0.2405	0.1315

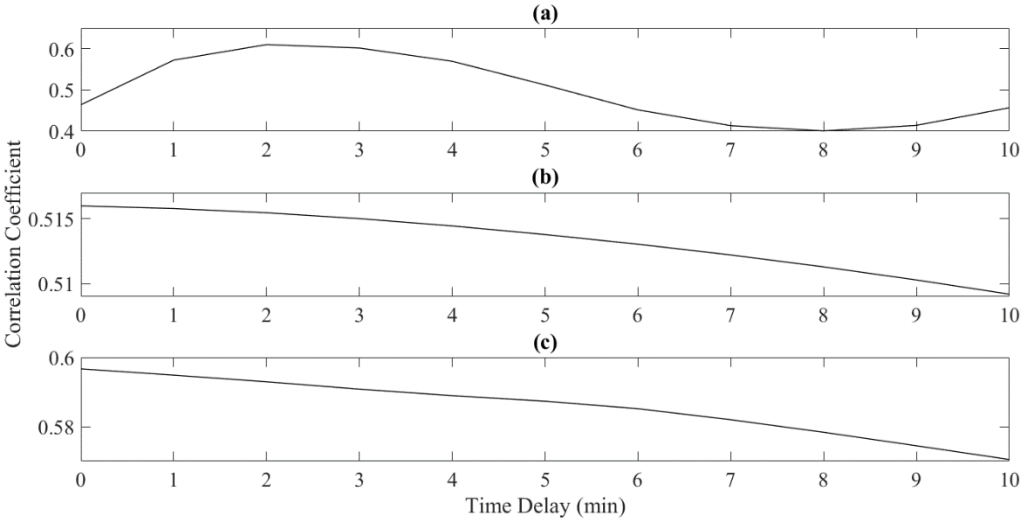

Figure 43 Correlation coefficient between temperature at Node 6 and (a) valve position at V1, (b) temperature at Node 2 and (c) flow rate at Node 1 with different time shifts

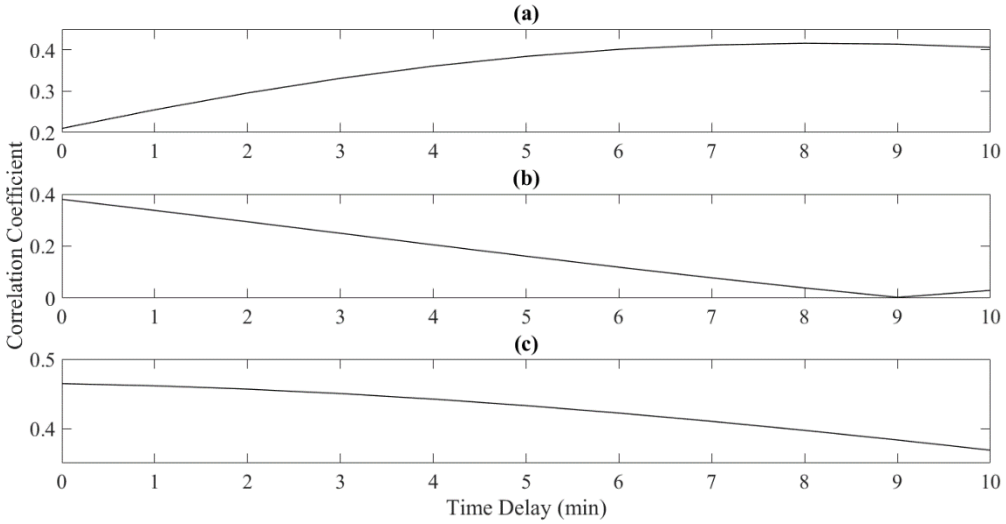

Figure 44 Correlation coefficient between temperature at Node 13 and (a) valve position at V5, (b) valve position at V6 and (c) inlet temperature at Node 12

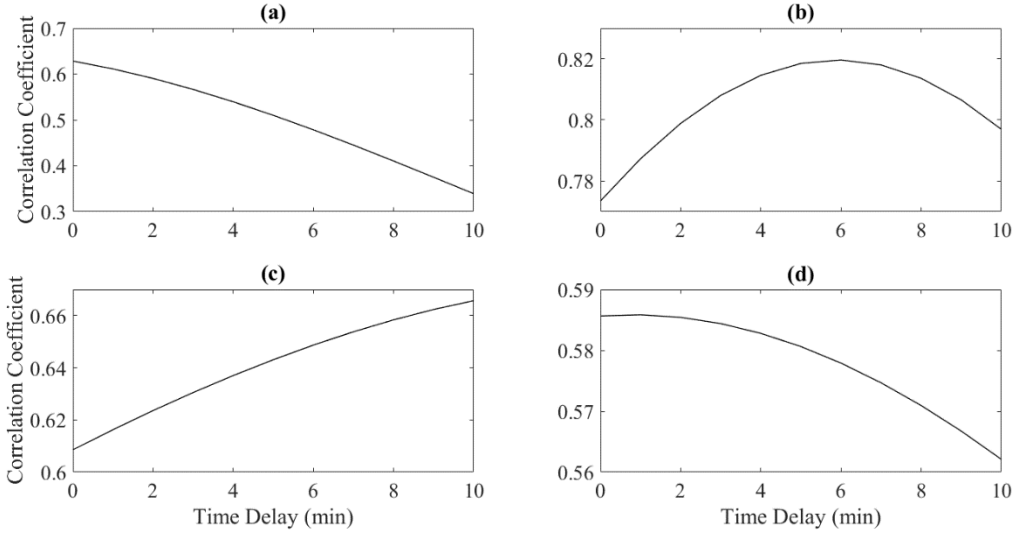

Figure 45 Correlation coefficient between temperature at Node 31 and (a) valve position at V5, (b) valve position at V6, (c) inlet temperature at Node 12 and (d) inlet temperature at Node 15

Table 26 Estimated time delay (min) between the controlled variables and manipulated and disturbance variables from the correlation coefficient

Manipulated or Disturbance Variable		Controlled Variable (T)	Manipulated or Disturbance Variable		Controlled Variable (T)
Location	Type	Node6/Node11	Location	Type	Node13/Node31
V1	V	2	V5	V	0
V2	V	N/A	V6	V	6
Node 2	T	0	Node 12	T	10
Node 7	T	N/A	Node 15	T	0
Node 32	T	N/A	Node 24	T	N/A
Node 1	F	0	Node 1	F	N/A

4.2 Dynamic Model Identification

Process identification is based on fitting the real process response data. Process identification can be utilized to establish a low-order model structure that effectively describes the process dynamics of the system (Liu & Geo, 2012). The identified dynamic model can be used for the purpose of control system design and analysis.

A transfer function is used to determine the dynamic behaviour of a process after changes are made to the input variables. The model characterizes the dynamic relationship of two process variables, an output variable and an input variable. Determining the dynamic behaviour of a process helps in designing and analyzing control systems. Equation 4.1 is the first-order form of a transfer function model plus dead time (FOPDT). Many industrial processes can be adequately approximated by first-order transfer functions.

$$G(s) = \frac{\mathrm{Y}(s)}{\mathrm{U}(s)} = \frac{Ke^{-\theta}}{\tau s + 1} \tag{4.1}$$

Where G is the transfer function, Y is the output (controlled variables), U is the input (manipulated or disturbance variables), K is the steady-state process gain, τ is the process time constant (min) and θ is the dead time (min).

4.2.1 System Identification

MATLAB's System Identification toolbox can be used to identify a dynamic model for the temperature of the outlet streams of the CGE/HGE and CIGE/HIGE heat exchanger networks. The identified model is based solely on industrial operating data supplied to the toolbox, which is supplied as an input or output. A FOPDT model (Equation 4.1) is selected as the model type. For a FOPDT model the toolbox will estimate values for gain, process time constant as well as dead time. For the CGE/HGE heat exchanger network, the outputs are the temperature at Node 6 and Node 11 and the inputs are the positions of V1 and V2, the feed gas temperature and flow rate and the input temperatures at Node 7 and Node 32. Table 27 lists the identified FOPDT model parameters for the outlet temperature at Node 6. The fit of the identified model is 73.66%. Although this model has a good fit and estimates the output from industrial operating data well, some of the values estimated by the toolbox are unrealistic. For example, the toolbox estimates that the process time constant for the feed gas temperature as 13,971 minutes. Based on industrial data and the correlation coefficient between the temperatures at Node 6 and Node 2, the process time constant would much smaller. Table 28 lists the identified

FOPDT model parameters for the outlet temperature at Node 11. The fit of the identified model is 4.928%. The temperature measurement data for Node 11 has very little variation since control has been applied to maintain a constant temperature at this measuring point. The quality of the data used for model identification is crucial as it is the only information that is supplied to the toolbox. Therefore, it can be concluded based on the very poor fit of the identified model that the industrial operating data for Node 11 is not suitable for model identification using the System Identification Toolbox.

Table 27 FOPDT model identified using MATLAB's System Identification Toolbox for the temperature at Node 6

Manipulated or Disturbance Variable Location	Type	Gain	Time Constant (min)	Dead Time (min)
V1	V	-0.3910	5.308	0
V2	V	-1.144	14.08	0
Node 2	T	-0.4754	13,971	30
Node 7	T	0.4492	6.671	0
Node 32	T	0.1156	0.014	30
Node 1	F	-0.1944	14.62	0

Table 28 FOPDT model identified using MATLAB's System Identification Toolbox for the temperature at Node 11

Manipulated or Disturbance Variable Location	Type	Gain	Time Constant (min)	Dead Time (min)
V1	V	-0.2051	14.33	1.215
V2	V	0.5548	13.75	4.968
Node 2	T	0.4240	0.3761	0
Node 7	T	0.3646	9.545	0
Node 32	T	0.1374	12.85	5.402
Node 1	F	0.0340	2.011	30

For the CIGE/HIGE heat exchanger network, the outputs are the temperature at Node 13 and Node 31 and the inputs are the positions of V5 and V6, the feed gas flow rate and the input temperatures at Node 12, Node 15 and Node 24. Table 29 lists the identified FOPDT model parameters for the outlet temperature at Node 13. The fit of the identified model is -1.061%. Similarly to Node 11, at Node 13 control has been applied to maintain a constant temperature. Consequently, there is very little variation in the industrial operating data for this measuring point which makes the data unsuitable for model identification using the System Identification toolbox.

Table 30 lists the model parameters identified for the outlet temperature at Node 31. The fit of the identified model is 54.09%. However, some of the model parameters identified are unrealistic. For example, the toolbox estimates that the process time constant for the feed gas flow rate is 650,776,296 minutes.

Table 29 FOPDT model identified using MATLAB's System Identification Toolbox for the temperature at Node 13

Manipulated or Disturbance Variable Location	Type	Gain	Time Constant (min)	Dead Time (min)
V5	V	-0.0786	1.097	7.413
V6	V	-0.0217	0.0345	29.16
Node 12	T	1.464	71,402	30
Node 15	T	2.054	168,084	0
Node 24	T	9.145	39,123	29.57
Node 1	F	0.0353	33,651	30

Table 30 FOPDT model identified using MATLAB's System Identification Toolbox for the temperature at Node 31

Manipulated or Disturbance Variable Location	Type	Gain	Time Constant (min)	Dead Time (min)
V5	V	-0.0853	2.980	20.96
V6	V	-0.2941	8.625	0
Node 12	T	0.7694	96.59	0
Node 15	T	-1.326	134.0	7.739
Node 24	T	-0.2845	1060	29.90
Node 1	F	706.4	650,776,296	30

Examining the FOPDT model parameters identified using the System Identification toolbox it can be concluded that the industrial operating data for the temperatures at Node 11 and Node 13 is not suitable for model identification. The models identified for temperature at these measuring points fit the industrial operating data poorly and did not estimate the outlet temperature well. The temperature at these measuring points is very tightly controlled and as a result there is very little variation in the measurement data. Thus, it is assumed that the cold and hot stream outlet temperatures for each of the heat exchanger networks behaves similarly. The industrial operating data for Node 6 will be used to estimate the model for Node 11. Similarly, the industrial operating data for Node 13 will be used to estimate the model for Node 31. It can also be concluded from the identified models that the estimation of dead time is unrealistic and should not be included in the model. Thus, the model in Equation 4.1 reduces to a first-order model with no time delay.

4.2.2 System Identification Incorporating Prior Information

To improve the FOPDT models identified, prior information about the system to be identified, such as the gain and process time constant, is supplied which can improve the quality of the model (Alenany *et al.*, 2010; Alenany & Shang, 2013). The steady-state process gains previously determined using the steady-state model (Table 21 - Table 24) were supplied to the toolbox. The time-delay values from Table 26, which were estimated using correlation coefficient time-delay plots, were supplied as an initial guess for the process time constants. The models identified by the toolbox for the temperature at Node 6/Node 11 and Node 13/Node 31 are listed in

Table *31*. The process time constants identified using prior information are much more realistic. For the CGE/HGE heat exchanger network, there is an additional disturbance variable. The concentration of SO_2 at Node 6 determines the temperature at Node 7, which is an inlet to the HGE. The process time constant for a change in SO_2 concentration at Node 6 is taken from He *et al.* (2019).

Table 31 Process time constants (min) determined by MATLAB System Identification toolbox

Manipulated or Disturbance Variable		Controlled Variable (T)	Manipulated or Disturbance Variable		Controlled Variable (T)
Location	Type	Node6/Node11	Location	Type	Node13/Node31
V1	V	1.846	V5	V	0
V2	V	0	V6	V	5.525
Node 2	T	0	Node 12	T	19.78

Node 7	T	0.0553	Node 15	T	0
Node 32	T	3491	Node 24	T	370.7
Node 1	F	0	Node 1	F	19.49

4.3 Comparison with Industrial Data

The model validation plots from MATLAB's System Identification toolbox show the measured and simulated outputs of the identified models. The identified models are fed with inputs from the validation data set and the output is calculated and plotted. This is the simulated model output, which is compared to the output in the validation data set. The plots show the deviation from mean temperature. The percent of the simulated output variations that is reproduced by the model is used to determine the goodness of fit. The model identified for temperature at Node 6 and Node 31 have a fit of 21.06% and 53.83%, respectively. The validation plots for the temperature at Node 6 and Node 31 are shown in Figure 46 and Figure 47, respectively.

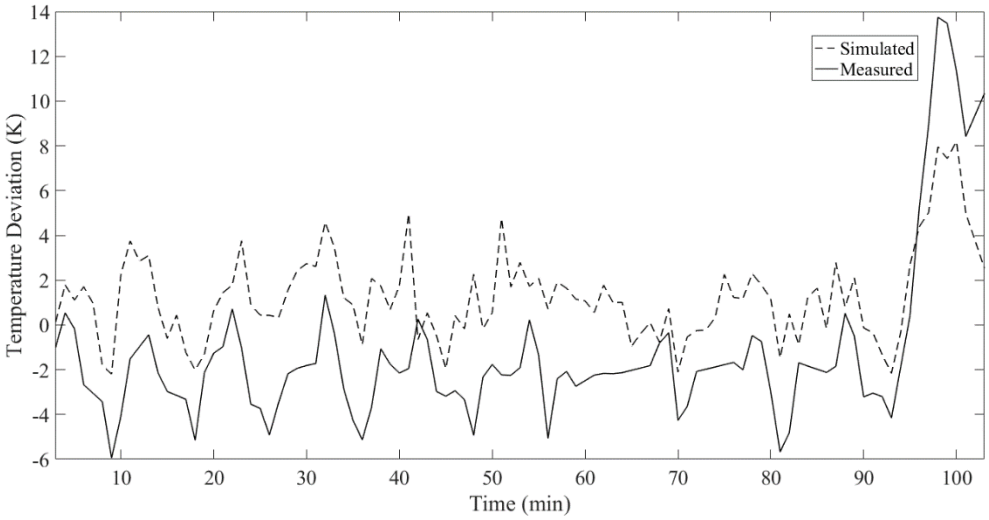

Figure 46 MATLAB System Identification validation plot for identified model for temperature at Node 6, fit of 21.06%

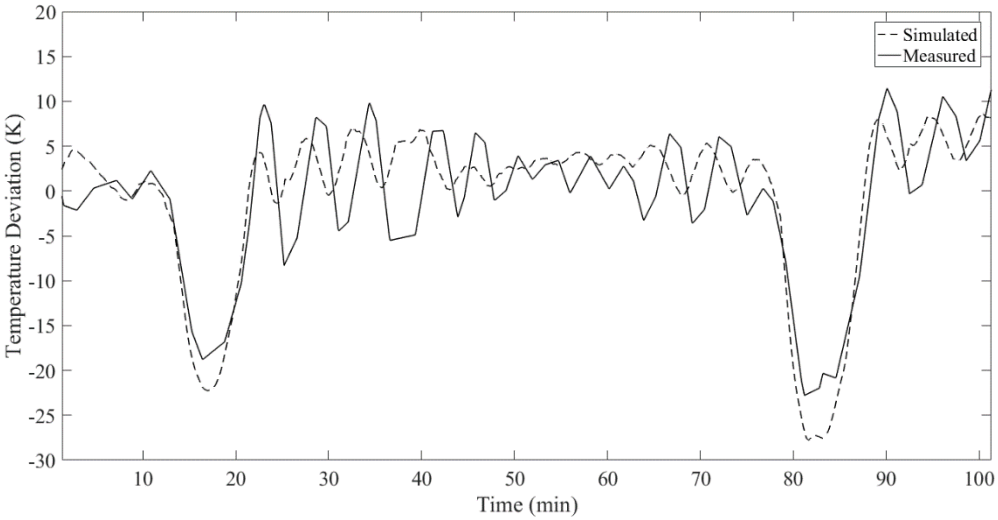

Figure 47 MATLAB System Identification validation plot for temperature at Node 31, fit of 53.83%

There are many limitations to using the industrial data in identifying the model parameters. The industrial data was collected for 30 operating days, under various operating conditions and during start-ups and shut-downs. The data for the outlet temperatures at Node 6, Node 11, Node 13 and Node 31 are the controlled variables of interest. However, the industrial data for these locations is controlled temperature data. Control techniques have been applied to regulate the temperature and so the data is not representative of the outlet temperatures with no control, which is the ideal case for control simulation. The industrial data was used to determine the correlation between process variables to gain understanding into variable interaction and estimate the dynamics of the process. From a correlation analysis it may be suggested that some process variables are highly correlated when in fact there is little or no correlation at all,

which can be explained from process knowledge. For example, during start-up the data would suggest that there is a strong correlation between the flow rate and SO_2 concentration in the feed gas. As the feed gas is blown into the acid plant the flow rate and SO_2 concentration increase. There is a strong correlation between the variables due to operating conditions but in reality the two variables are not dependent on each other.

MATLAB's System Identification toolbox and process knowledge were used in combination to explore the possibility of creating a first-order dynamic model of the process. For the purpose of control simulation and analysis a simple model is sufficient. From process knowledge the heat exchanger dynamics are not large, so the steady-state model developed in Chapter 3 and the process dynamics estimated in this chapter are a fair representation of the process, though the industrial data did not fit a first-order model as well as hoped.

Chapter 5: Control Configuration and Simulation

This chapter describes the control problem and a control analysis as well as the simulation results for the dynamic model identified in Chapter 4.

5.1 Control Problem

Multiple-input, multiple-output (MIMO) processes involve a number of input and output variables. MIMO control problems present an additional challenge due to the presence of unknown process interactions as each manipulated variable can have an effect on both controlled variables. In such a case, the most effective control configuration is not easily recognizable. For a process with n controlled variables and n manipulated variables, there are $n!$ possible multi-loop configurations. Figure 48 shows two control configurations for a two-by-two MIMO system using two feedback control. In (a) the output, y_1, is controlled by adjusting the manipulated variable, u_1, while y_2 is controlled by u_2. This configuration is referred to as a 1-1/2-2 controller pairing. The alternate controller pairing, (b), is 1-2/2-1, where y_1 is controlled by u_2, and y_2 is controlled by u_1. The control loop interactions result from the presence of a third hidden feedback loop. For a 1-1/2-2 controller pairing, if $y_1$moves away from its set-point due to a disturbance being the controller of loop 1, G_{c1}, adjusts u_1 to maintain y_1 at its set-point. This action affects y_2 via G_{21}. Since the action of G_{c1} has moved y_2 away from its set-point, the controller of loop 2, G_{c2}, adjusts u_2 to maintain y_2 at its set-point. This

action effects y_1 via G_{12}. These two controller actions proceed until a new steady-state is reached.

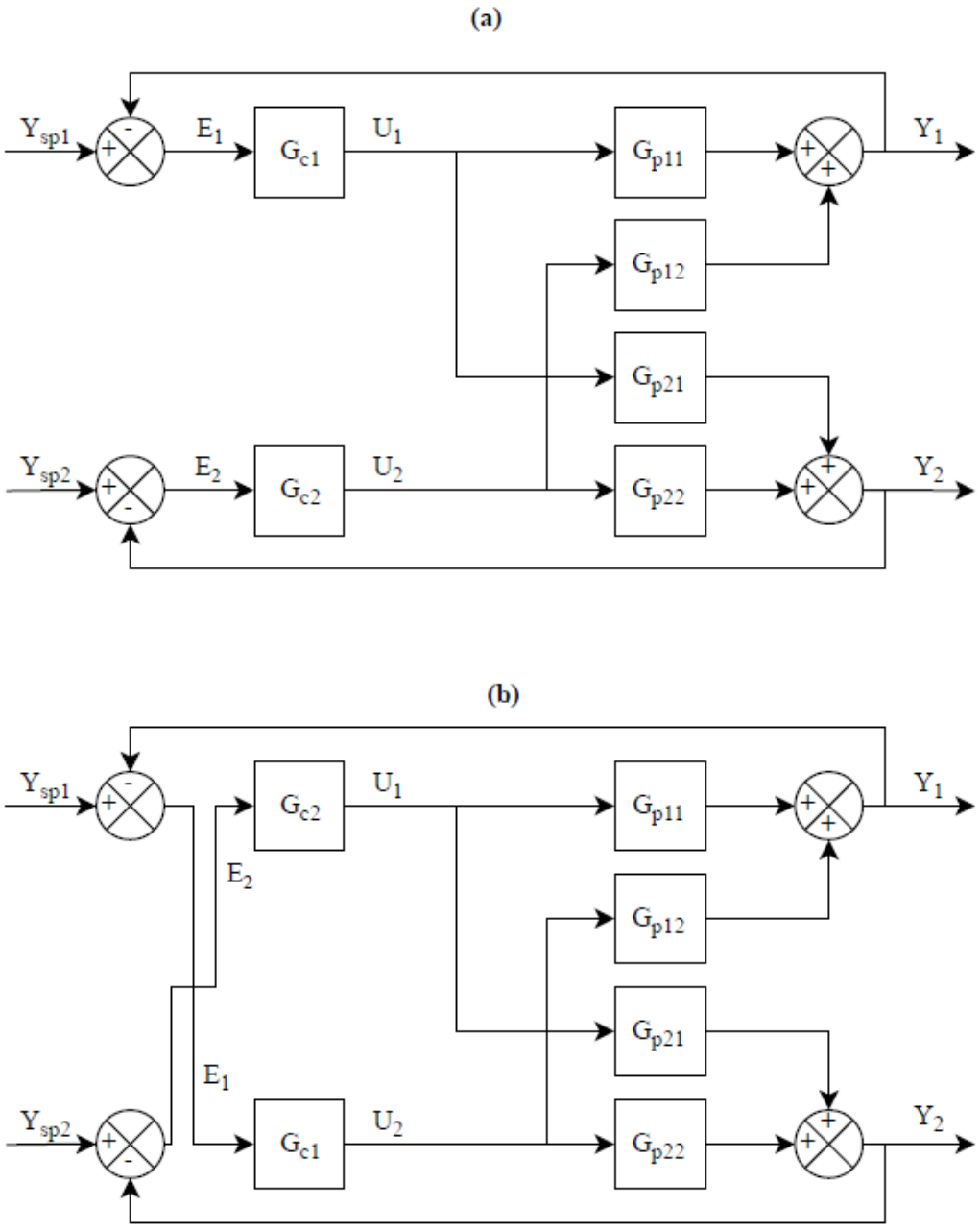

Figure 48 Block diagram for a MIMO control problem with two controlled variables and two manipulated variables. (a) 1-1/2-2 controller pairing and (b)1-2/2-1 controller pairing (Seborg et al., 2011)

For each of the CGE/HGE and CIGE/HIGE heat exchanger networks there are two controlled and two manipulated variables, so it is a two-by-two MIMO control problem. The controller two pairing options are listed in Table 32 for the CGE/HGE and CIGE/HIGE heat exchanger networks.

Table 32 Pairing options for each of the heat exchanger networks

Heat Exchanger Network	1-1/2-2 Controller Pairing		1-2/2-1 Controller Pairing	
	Controlled Variable (y)	Manipulated Variable (u)	Controlled Variable (y)	Manipulated Variable (u)
CGE/HGE	Node 6	V1	Node6	V2
	Node 11	V2	Node 11	V1
CIGE/HIGE	Node 13	V5	Node 13	V6
	Node 31	V6	Node 31	V5

5.2 Control Analysis

5.2.1 Bristol's Relative Gain Array

Bristol's relative gain array (RGA) matrix provides a measure of process interactions and a recommendation of the most effective pairing of manipulated and controlled variables (Ogunnaike, 1996). The approach requires only steady-state gain information and is based on the concept of relative gain. The relative gain is defined as (Bristol, 1996; McAvoy, 1981):

$$\lambda_{ij} \triangleq \frac{\left(\partial y_i/\partial u_j\right)_u}{\left(\partial y_i/\partial u_j\right)_y} = \frac{open-loop\ gain}{closed-loop\ gain} \tag{5.1}$$

where λ_{ij} is the relative gain of the element *(i,j)* of the steady-state gain matrix. The open-loop gain corresponds to the steady-state gain. The relative gains are arranged in a RGA matrix:

$$\Lambda = \begin{bmatrix} \lambda_{11} & \cdots & \lambda_{1,j} \\ \vdots & \ddots & \vdots \\ \lambda_{i,1} & \cdots & \lambda_{i,j} \end{bmatrix} \tag{5.2}$$

where Λ is the RGA matrix. Some important properties of the RGA: it is normalized, the relative gains are not effected by units and scaling since they are a dimensionless parameter and the relative gain is an indication of how changes in the gain can effect process control characteristics. For a 1-1/2-2 controller pairing shown in Figure 48 the steady-state gain matrix, $\boldsymbol{K}$, is:

$$\boldsymbol{K} = \begin{bmatrix} K_{11} & K_{12} \\ K_{21} & K_{22} \end{bmatrix} \tag{5.3}$$

The gain matrix has been arranged so that the diagonal elements correspond to the proposed controller pairing. The linearized steady-state model expressed in terms of deviation variables is:

$$y_1 = K_{11}u_1 + K_{12}u_2 \tag{5.4}$$

$$y_2 = K_{21}u_1 + K_{22}u_2 \tag{5.5}$$

From Equation 5.1 the open-loop steady-state gain, K_{11}, is equal to:

$$K_{11} = \left(\frac{\partial y_1}{\partial u_1}\right)_{u_2} \tag{5.6}$$

Rearranging Equation 5.5 for u_2 and setting y_2 equal to zero:

$$u_2 = -\frac{K_{21}}{K_{22}} u_1 \tag{5.7}$$

Substituting Equation 5.7 into Equation 5.4:

$$y_1 = K_{11} u_1 \left(1 - \frac{K_{12} K_{21}}{K_{11} K_{22}}\right) \tag{5.8}$$

Taking the partial derivative of Equation 5.8 with respect to u_1:

$$\left(\frac{\partial y_1}{\partial u_1}\right)_{y_2} = K_{11} u_1 \left(1 - \frac{K_{12} K_{21}}{K_{11} K_{22}}\right) \tag{5.9}$$

Substituting Equation 5.6 and Equation 5.9 into Equation 5.1 and rearranging, the expression for relative gain is:

$$\lambda_{11} = \frac{1}{1 - \frac{K_{12}K_{21}}{K_{11}K_{22}}} \tag{5.10}$$

The other relative gains are easily calculated:

$$\lambda_{12} = \lambda_{21} = 1 - \lambda_{11} \tag{5.11}$$

$$\lambda_{22} = \lambda_{11} \tag{5.12}$$

Thus, the RGA is always symmetric and can be expressed as:

$$\Lambda = \begin{bmatrix} \lambda & 1-\lambda \\ 1-\lambda & \lambda \end{bmatrix} \tag{5.13}$$

Assuming that y_2 is kept at its set-point of zero under closed-loop control, rearranging Equation 5.8:

$$\frac{y_1}{u_1} = K_{11}\left(1 - \frac{K_{12}K_{21}}{K_{11}K_{22}}\right) \tag{5.14}$$

Substituting Equation 5.10 into Equation 5.14:

$$\frac{y_1}{u_1} = K_{11}\left(\frac{1}{\lambda}\right) \tag{5.15}$$

Examining Equation 5.15, the relative gain can be interpreted as a divisor of the open-loop gain, K_{11}. For instance, if the relative gain is equal to 1, there is no correction to the gain and the open-loop and closed-loop gain are equal. If the relative gain is a large, positive value the closed-loop gain is substantially smaller than the open-loop gain. In this case u_1 has very little influence on y_1, which could have important operational implications (Seborg *et al.*, 2011). If the relative gain is negative the closed-loop gain has the opposite sign of the open-loop gain, which can make control difficult.

Based on the relative gain there are five pairing cases considered for a two-by-two process:

1. If $\lambda = 1$, the open-loop and closed-loop gains between y_1 and u_1 are identical and changes to u_2 has no effect on y_1. In this case, a 1-1/2-2 controller pairing should be employed (Seborg *et al.*, 2011).
2. If $\lambda = 0$, the open-loop gain between y_1 and u_1 is zero and u_1 has no direct effect on y_1. In this case, a 1-2/2-1 controller pairing should be employed (Seborg *et al.*, 2011).
3. If $0 < \lambda < 1$, the closed-loop gain between y_1 and u_1 is larger than the open-loop gain. The interaction between the two loops is largest when $\lambda = 0.5$. (Shinskey, 1996; McAvoy, 1981).
4. If $\lambda > 1$, there is interaction between the two control loops. As λ increases, the degree of interaction increases, becoming most severe when $\lambda \to \infty$. When λ is large, it is difficult to control both outputs independently (Skogestad & Postlethwaite, Multivariable Feedback Control, 2001).

5. If $\lambda < 0$, the open-loop and closed-loop gains between y_1 and u_1 have different signs and oscillations can occur when control is applied due to instability. A 1-1/2-2 controller pairing should not be employed (Shinskey, 1996; McAvoy, 1981).

The recommendations for pairing are based solely on steady-state information and dynamic behaviour should also be considered when choosing a controller pairing. For example, there may be a large time-delay or time constant between y_1 and u_1, or y_2 and u_2 so y_1 would response slowly to changes in u_1, in which case a 1-1/2-2 controller pairing is not desirable. Dynamic considerations should be considered especially when $\lambda > 1$ (McAvoy, 1981).

For a 1-2/2-1 controller pairing the steady-state gain matrix is:

$$\boldsymbol{K} = \begin{bmatrix} K_{12} & K_{11} \\ K_{22} & K_{21} \end{bmatrix} \tag{5.16}$$

And the expression for relative gain becomes:

$$\lambda_{11} = \frac{1}{1 - \frac{K_{11}K_{22}}{K_{12}K_{21}}} \tag{5.17}$$

RGA Stability

The RGA stability theorem provides useful information about the stability of a proposed controller pairing (Grosdidier *et al.*, 1985; Niederlinski, 1971). Like RGA, the theorem is based solely on steady-state information and is based on three assumptions:

1. The process transfer function matrix must be stable, rational and proper;
2. The feedback controllers must contain integral action;
3. Individual control loop is stable when any of the other loops are opened.

The closed-loop system is unstable if the inequality in Equation 5.18 is satisfied.

$$\frac{|\boldsymbol{K}|}{\prod_{i=1}^{n} K_{ii}} < 0 \tag{5.18}$$

where $|\boldsymbol{K}|$ is the determinant of the gain matrix.

The relative gain and RGA stability from the analysis are listed Table 33. Analyzing the results, the relative gain is ~0.5 for both the CGE/HGE and CIGE/HIGE networks of heat exchangers and each controller pairing option. As a result, the analysis gives little insight to which controlled and manipulated variables should be paired. However, it does suggest that there are strong interactions between the two control loops. Since the relative gains are similar, a 1-1/2-2 or 1-2/2-1 controller pairing would be acceptable. The RGA stability for the networks of heat

exchangers results do not satisfy the inequality in Equation 5.18. Therefore, both of the controller pairing options are stable.

Table 33 Relative gain and RGA stability

Heat Exchanger Network	1-1/2-2 Controller Pairing		1-2/2-1 Controller Pairing	
	Relative Gain	RGA Stability	Relative Gain	RGA Stability
CGE/HGE	0.5109	1.957	0.4891	2.045
CIGE/HIGE	0.5600	1.786	0.4400	2.273

5.2.2 Singular Value Analysis

Singular value analysis (SVA) aids in the selection of controlled, measured and manipulated variables, evaluates the robustness of a proposed control strategy and determines the multi-loop control configuration. SVA, like RGA, is also based on steady-state gain information. Considering the linear steady-state process described in Equation 5.4 and Equation 5.5, the gain matrix for a 1-1/2-2 controller pairing is:

$$\boldsymbol{K} = \begin{bmatrix} K_{11} & K_{12} \\ K_{21} & K_{22} \end{bmatrix} \tag{5.19}$$

A desirable property of the gain matrix is that the n linear equations and n unknowns in the set of equations are linearly independent. If not, not all of the n controlled variables can be independently regulated and control will be challenging. There are several methods to determine whether or not the gain matrix is linearly independent. The fist method is to

determine the determinant of the gain matrix. If the determinant is equal to zero, the matrix is singular and the n equations are not linearly independent. If the determinant is not equal to zero, the n equations are linearly independent. For a 1-1/2-2 controller pairing, the determinant of the steady-state gain matrix is equal to:

$$\det\begin{bmatrix} K_{11} & K_{12} \\ K_{21} & K_{22} \end{bmatrix} = K_{12}K_{21} - K_{11}K_{22} \tag{5.20}$$

The second method is to calculate the eigenvalues of the gain matrix. If any of the eigenvalues are zero, the gain matrix is singular, and it will be difficult to control the process. Also, if one eigenvalue is very small compared to the others, then large changes in one or more of the manipulated variables will be required to control the process. The eigenvalues of the gain matrix are the roots of the equation:

$$\left|\begin{bmatrix} K_{11} & K_{12} \\ K_{21} & K_{22} \end{bmatrix} - \Upsilon I\right| = 0 \tag{5.21}$$

where I is an identity matrix with the same dimensions as the gain matrix and Υ is the matrix of eigenvalues.

For a 1-2/2-1 controller pairing the same procedure is followed. However, the arrangement of the steady-state gains reflects controller pairing:

$$\boldsymbol{K} = \begin{bmatrix} K_{12} & K_{11} \\ K_{22} & K_{21} \end{bmatrix} \tag{5.22}$$

The results of the linear independence analysis are listed in Table 34. For both a 1-1/2-2 and 1-2/2-1 controller pairing for the CGE/HGE and CIGE/HIGE networks of heat exchangers the determinant is not equal to zero. In addition, neither of the eigenvalues are equal to zero. These results suggests that the gain matrix is linearly independent and the controlled variables can be independently regulated.

Table 34 Steady-state gain matrix determinant and eigenvalues to determine linear independence

Heat Exchanger Network	1-1/2-2 Controller Pairing		1-2/2-1 Controller Pairing	
	Determinant	Eigenvalues	Determinant	Eigenvalues
CGE/HGE	-0.1545	-0.2680 0.5764	0.1545	-0.3351+0.2055i -0.3351-0.2055i
CIGE/HIGE	0.0980	-0.2409+0.2000i -0.2409-0.2000i	-0.0980	0.3342 -0.2932

The singular values of the gain matrix is another important property. The singular values are the positive square roots of the eigenvalues of the product matrix $\boldsymbol{K}^T\boldsymbol{K}$.

$$|\boldsymbol{K}^T\boldsymbol{K} - \Upsilon I| = 0 \tag{5.23}$$

where Υ is the matrix containing the eigenvalues and I is an identity matrix. Usually, the non-zero singular values are ordered in a vector.

$$\sigma = \sqrt{\Upsilon} \tag{5.24}$$

$$\sigma = \begin{bmatrix} \sigma_1 \\ \vdots \\ \sigma_r \end{bmatrix} \tag{5.25}$$

where σ is the matrix of non-negative singular values, σ_1 being the largest and σ_r the smallest (r represents the rank of the matrix).

The last matrix property is the condition number (CN). For a non-singular gain matrix, the CN is a positive number defined by the ratio of the largest and smallest non-zero singular values:

$$CN = \frac{\sigma_1}{\sigma_r} \tag{5.26}$$

The CN is superior in providing a more reliable measure of ill-conditioning and sensitivity problems (Seborg *et al.*, 2011). The value of the determinant, eigenvalues and RGA give no indication of poor conditioning until the CN is determined. If the gain matrix is singular, then it is ill-conditioned, and $CN = \infty$. A large CN value indicates poor conditioning and as a result control with any controller pairing is difficult. A "large" CN is defined as being greater than 10 (Skogestad & Postlethwaite, 2001). The singular values and CN are equal for a 1-1/2-2 and 1-2/2-1 controller pairing, they are listed in Table 35. The CN number for each of the controller

pairings is less than 10, therefore neither pairing is poorly conditioned and both will be controllable.

Table 35 Singular values and condition number for a 1-1/2-2 and 1-2/2-1 controller pairing

Heat Exchanger Network	Singular Values	Condition Number
CGE/HGE	0.7096 0.2177	3.259
CIGE/HIGE	0.3784 0.2590	1.461

5.2.3 Stability

The minimum CN is defined as the "least conservative value" and can be calculated using the RGA matrix (Grosdidier *et al.*, 1985).

$$CN_{min} = \|\Lambda\|_1 + \sqrt{\|\Lambda\|_1{}^2 - 1} \tag{5.27}$$

where CN_{min} is the minimum CN and $\|\Lambda\|_1$ is the 1-norm of the RGA matrix. Diagonal and triangular RGA matrices as well as RGA matrices with an odd number of negative elements have a CN_{min} of 1. When the minimum CN is equal to 1, the system is well behaved and there are no sensitivity problems even when the relative gain is ~0.5 and there are strong interactions. Grosdidier *et al.* also suggests an alternate method of determining CN:

$$CN = \|\boldsymbol{K}\|_e \times \|\boldsymbol{K}^{-1}\|_e = \sigma_1 \times \frac{1}{\sigma_r} \tag{5.28}$$

where $\|\boldsymbol{K}\|_e$ and $\|\boldsymbol{K}^{-1}\|_e$ are the Euclidean norms of the gain and inverse gain matrix, respectively. The minimum and Euclidean CNs are equal for a 1-1/2-2 and 1-2/2-1 controller pairing, they are listed in Table 36. The minimum CN for each of the controller pairings is equal to 1, which indicates that control will be possible even with strong interactions between the control loops. The Euclidean CN are equal to those calculated using the SVA, Table 36.

Table 36 Minimum and Euclidean condition number for a 1-1/2-2 and 1-2/2-1 controller pairing

Heat Exchanger Network	Minimum Condition Number	Euclidean Norm Condition Number
CGE/HGE	1	3.259
CIGE/HIGE	1	1.461

5.3 Control Simulation

Feedback control is the dominant control strategy used in industry (Franklin *et al.*, 2010). In feedback control the controlled variable is measured and the measurement is sent to the controller to adjust the manipulated variable. The disturbance variables are not measured. Feedback control is advantageous because corrective action occurs as soon as the controlled variable deviates from its set-point, regardless of the source of the disturbance. However there is an inherent disadvantage is that no corrective action is taken until after a deviation in the controlled variable occurs. Thus, perfect control, where the controlled variable does not deviate

from its set-point during set-point and/or disturbance changes, is not realizable with feedback control. For processes with large time constants and/or long time delays, if large and frequent disturbances occur the process may operate in a continuous transient state under feedback control.

In feedforward control, disturbance variables are measured, but the controlled variables are not. The main advantage of feedforward control is that corrective action is applied before the disturbances upset the process. Typically, feedforward control is used in conjunction with feedback control, for processes where feedback control is not sufficient (Shinskey F. G., 1996). Used together, feedforward control reduces the effects of measurable disturbances while feedback control compensates for inaccuracies in the process model, measurement error and unmeasured disturbances. The block diagram for a feedforward-feedback control loop is shown in Figure 49.

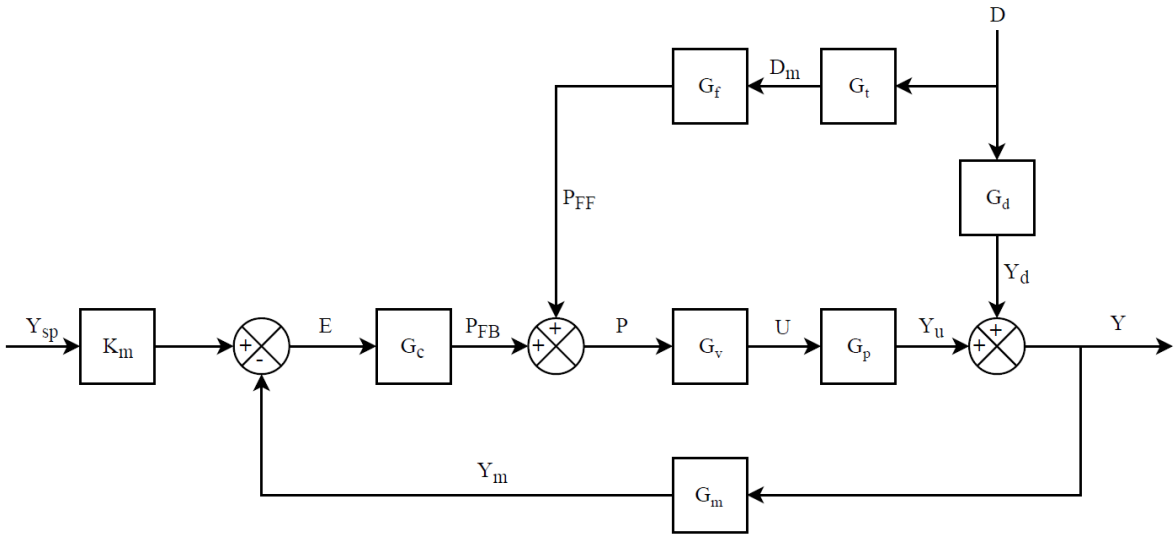

Figure 49 Standard block diagram of a feedforward-feedback control system based on deviation variables (Seborg et al., 2011)

Feedforward-feedback is the control scheme that will be investigated for the CGE/HGE and CIGE/HIGE heat exchanger networks using simulations. Two feedback controllers are used to control the outlet temperatures for each of the heat exchanger networks. For each heat exchanger network there are two pairings. The controlled variables of the CGE/HGE heat exchanger network are the outlet temperatures at Node 6 and Node 11. The outlet temperatures are controlled by adjusting V1 and V2. There are two pairing options: utilizing V1 to adjust the temperature at Node 6 and V2 to adjust the temperature at Node 11 or utilizing V2 to adjust the temperature at Node 6 and V1 to adjust the temperature at Node 11. The two feedback controller pairing options for the CGE/HGE heat exchanger network are shown in Figure 50. Similarly, for the CIGE/HIGE heat exchanger network the outlet temperatures at Node 13 and Node 31 are the controlled variables which are maintained at their set-points by adjusting V5 and V6. The two feedback controller pairing options for the CIGE/HIGE heat exchanger

network are shown in Figure 51. From Chapter 3 it was concluded that the disturbance variables that have the greatest impact on the controlled variables are the feed gas flow rate and the concentration of SO_2 in the feed gas. Thus, utilizing feedforward controllers to anticipate these disturbances can greatly improve process control. For the CGE/HGE heat exchanger network the feed gas flow rate and SO_2 concentration are measured and feedforward controllers are used to mitigate their effects on the process. The feedforward controllers are shown in Figure 50. For the CIGE/HIGE heat exchanger network only the feed gas flow rate is measured, shown in Figure 51. Feedforward control is not used for the feed gas SO_2 concentration for the CIGE/HIGE heat exchanger network since it has less of an impact on its outlet temperatures.

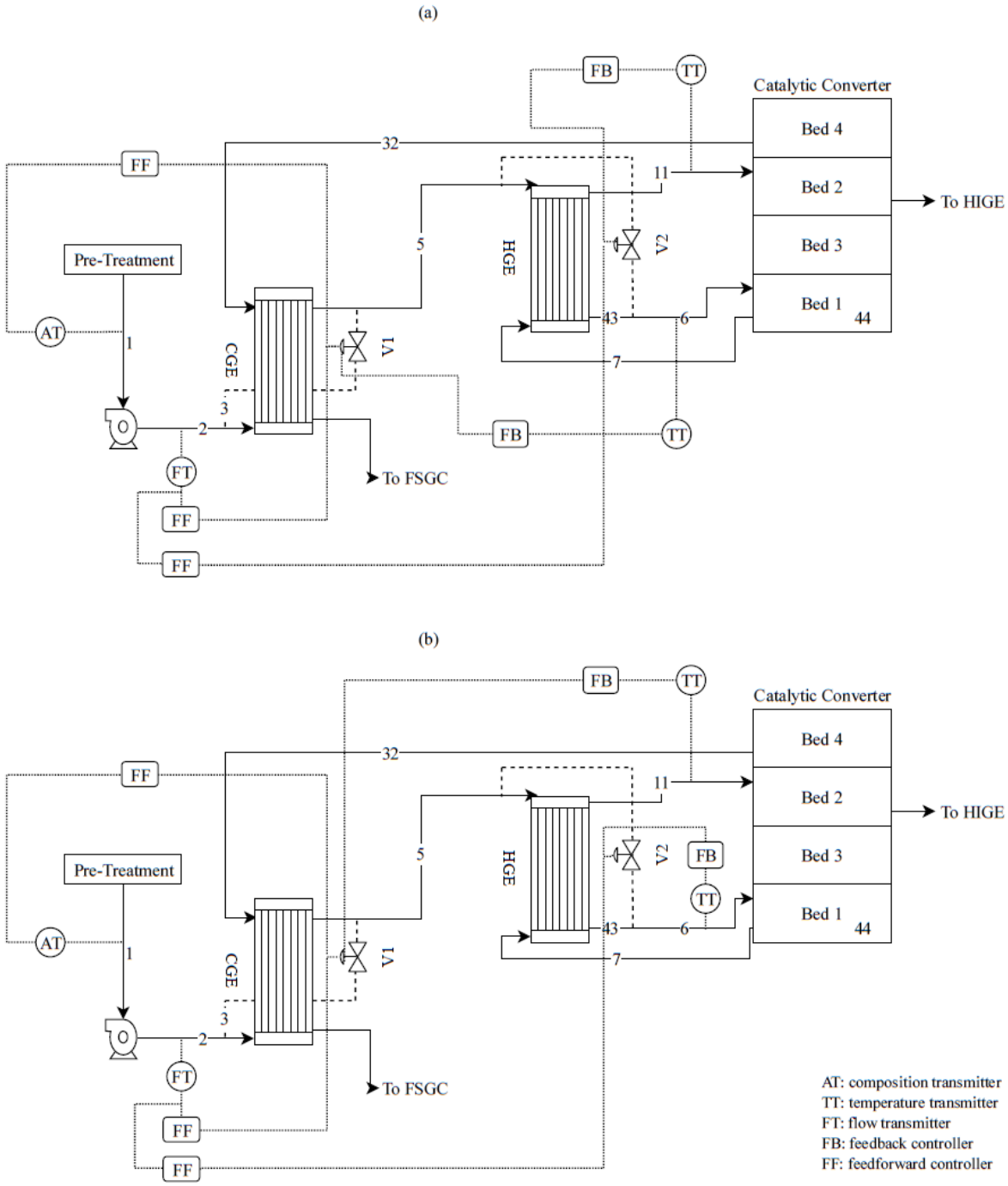

Figure 50 Feedforward-feedback controller pairing options for CGE/HGE heat exchanger network

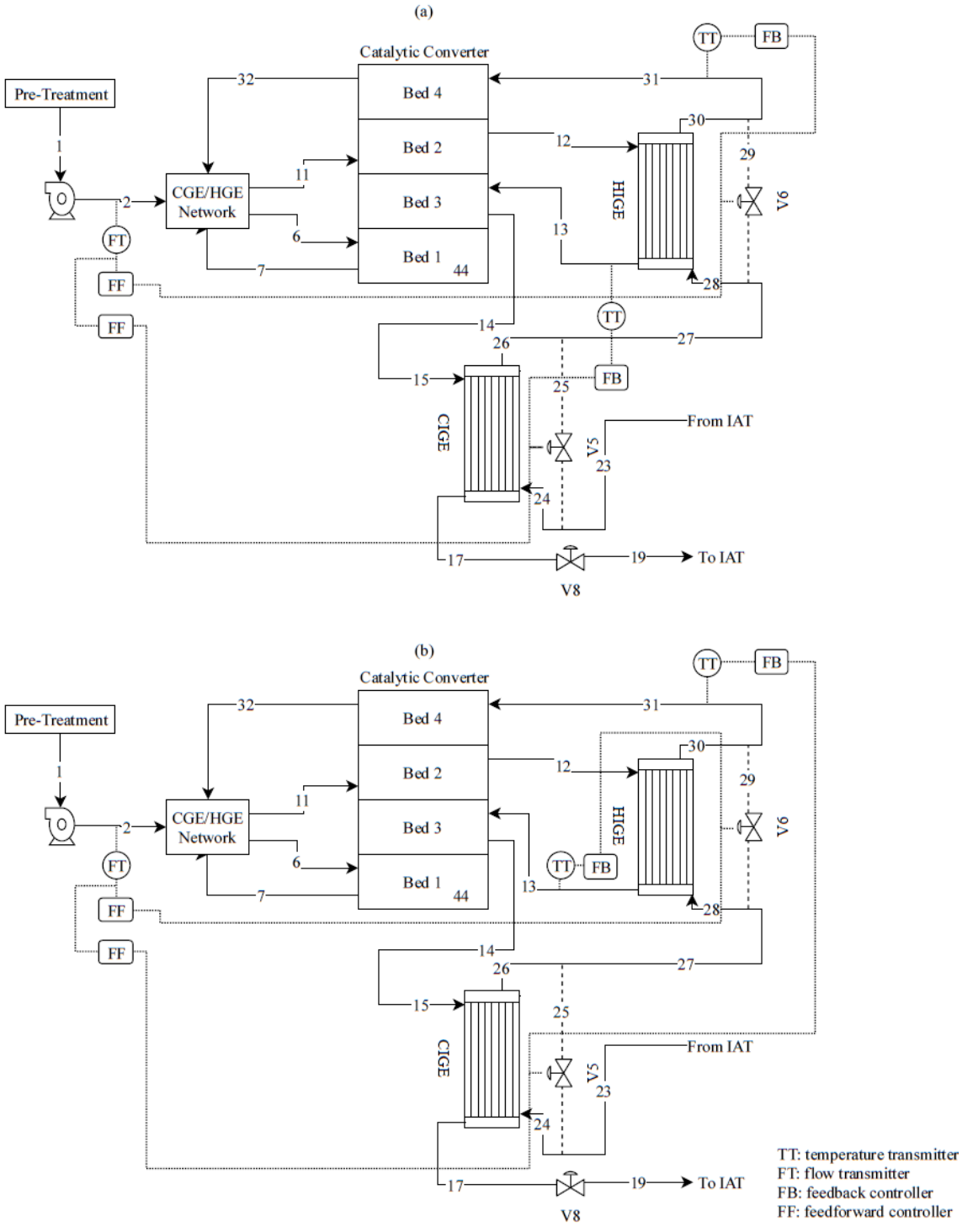

Figure 51 Feedforward-feedback controller pairing options for CIGE/HIGE heat exchanger network

Controllers

The dynamic model developed in Chapter 4 is a first-order model, which approximates the process well and is simple for industrial use. In most industrial processes, a PI controller is selected over a PID controller (Skogestad, 2003). Thus, in the control simulations PI controllers are used for the feedback controllers. Using the direct synthesis (DS) method, the controller design in based on a process model and a desired closed-loop transfer function. The internal model control (IMC) method is also based on an assumed process model, however the IMC method allows for uncertainty in the model. The final expression for the PI control derived using the DS and IMC methods is:

$$G_c = K_c\left(1 + \frac{1}{\tau_I s}\right) \tag{5.29}$$

where G_c is the controller, K_c is the controller gain, and τ_I (min) is the integral time. Examining the controller dervied using the DS and IMC methods, as τ_c decreases, K_c increases because a faster set-point response requires more strenuous control action by the controller. A more conservative controller would have a larger τ_c as K_c would decrease. Increasing the controller gain causes the process response to be less sluggish however, a large controller gain can cause undesirable oscillations and can cause instability. On the other hand, increasing the integral time makes the control action more conservative, as the amount of time is takes a controlled variable to return to its set-point increases.

Although there are only two parameters to be tuned for a PI controller, it is difficult to find the most appropriate values, which causes most industrial PI controllers to be poorly tuned (Skogestad, 2001). Poor tuning can lead to excessive control action, poor control performance and poor quality of products (Liu & Daley, 2001). PI controller tuning is complicated by non-linearities, model error and unmeasured disturbances (Liu & Daley, 2001). However, a well-tuned and adequately designed PI controller can meet or exceed most control objectives (Fruehauf *et al*, 1994). Controller tuning is subjective (Liu & Daley, 2001) as there is an inherent trade-off between the controller performance and robustness (Shinskey, 2002). A high degree of performance results in rapid and smooth response. Robustness describes the sensitivity of the closed-loop response to changes in dynamic parameters. A control system is robust if it provides a satisfactory response for a wide range of operating conditions and inaccuracy in the process model (Fruehauf *et al*, 1994). Conservative controller settings results in a more robust controller but results in poor performance. There is a second trade-off between disturbance rejection and set-point tracking. Controllers tuned for excellent disturbance rejection can produce a large offset for set-point changes. Conversely, controllers tuned for set-point tracking can cause the process' response to disturbances to be sluggish.

Several guidelines have been suggested for tuning feedback controllers (Rivera *et al.*, 1986; Fruehauf *et al.*, 1994; Skogestad, 2001; Skogestad, 2003; Liu & Daley, 2001). For a first-order model after a set-point change and/or process disturbance, a new steady-state is reached in approximately 5τ minutes (Seborg *et al.*, 2011). The feedback controllers were tuned with this in mind. The controller gain was selected so that it was inversely proportional to the product

of the other gains in the feedback loop, assuming that the sensors and transmitters have negligible dynamics and a steady-state gain equal to 1. Thus, the controller gain is inversely proportional to the steady-state process gain. Equation 5.29 was used to determine the time constant of the feedback controller. The feedback controller settings for a 1-1/2-2 and 1-2/2-1 controller pairing are listed in Table 37 and Table 38, respectively.

Table 37 Feedback controller settings for a 1-1/2-2 controller pairing

Heat Exchanger Network	Controller 1		Controller 2	
	Gain	Time Constant /min	Gain	Time Constant /min
CGE/HGE	-6.013	1.846	2.107	1.404
CIGE/HIGE	-5.411	0.9018	-3.368	5.525

Table 38 Feedback controller settings for a 1-2/2-1 controller pairing

Heat Exchanger Network	Controller 1		Controller 2	
	Gain	Time Constant /min	Gain	Time Constant /min
CGE/HGE	-1.900	0.95	-6.969	1.846
CIGE/HIGE	4.363	5.525	-5.313	1.025

From Figure 49, the closed-loop transfer function for disturbance changes is:

$$\frac{Y(s)}{D(s)} = \frac{G_d + G_t G_f G_v G_p}{1 + G_c G_m G_v G_p} \tag{5.30}$$

Ideally, the feedforward-feedback control system would produce perfect control. Under perfect control the action of the controller compensates exactly for changes in the disturbance variable so that the output is equal to 0 (deviation variable). Assuming perfect control the expression for the feedforward controllers is:

$$G_f = -\frac{G_d}{G_t G_v G_p} \tag{5.31}$$

For simplicity it is assumed that the transmitters and control valves have negligible dynamics and that the steady-state gains are equal to 1. Also, the dynamics of the disturbances are not considered when tuning the feedforward controllers. Feedforward controllers were included for the major disturbances: flow rate and SO_2 concentration of the feed gas. The feedforward controller gains are listed in Table 39.

Table 39 Feedforward controller gains for major disturbance variables

Heat Exchanger Network	Controlled Variable	Disturbance Variable	
	Temperature	Flow Rate	SO_2
CGE/HGE	Node 6	0.3805	-12.5
	Node 11	-0.3578	N/A
CIGE/HIGE	Node 13	-0.1702	N/A
	Node 31	0.1657	N/A

The steady-state gains calculated using the model developed in Chapter 3 and the dynamic parameters identified in Chapter 4 are used as the model for simulation using MATLAB's

Simulink. The large time constants estimated by MATLAB's System Identification toolbox were limited to 10 minutes.

5.3.1 Case 1: Feed Gas Flow Rate Disturbance

The first major disturbance that is commonly encountered in the acid plant is feed gas flow rate. Post-SFU and Clean AER process changes, there will be a highly varying flow rate of SO_2 laden off-gas to the acid plant. The variations in flow rate originate from the converter aisle where the Pierce-Smith converters operate in a batch-wise nature. The identified dynamic model can be used to simulate the response of the controlled variables to a flow rate disturbance before the process changes are implemented.

After 10 minutes of steady-state operation a feed gas flow rate disturbance of 100 $kNm^3\ h^{-1}$ is introduced. The simulation results for the controlled variables, outlet temperatures of the CGE/HGE and CIGE/HIGE heat exchanger networks, for a 1-1/2-2 controller pairing are shown in Figure 52. The results suggest that a flow rate disturbance has a greater effect on the CIGE/HIGE heat exchanger network. The temperatures at Node 6 and Node 11 reach a new steady-state less than 10 minutes after the disturbance is introduced and the temperature deviates approximately 10 K. Based on the mean values of temperature at Node 6 and Node 11 from the industrial operating data, a temperature deviation of 10 K would be well within the operating temperature of the catalyst in the converter. The small offset and settling time are desirable as the majority of SO_2 oxidation occurs in the first bed of the catalytic converter

and tight temperature control is crucial. The temperatures at Node 13 and Node 31 do not deviate from their set-point as much as the temperatures at Node 6 and Node 11. The temperature at Node 13 reaches steady-state relatively quickly, approximately 10 minutes. However, it takes the temperature at Node 31 substantially longer to reach a new steady-state, approximately 65 minutes.

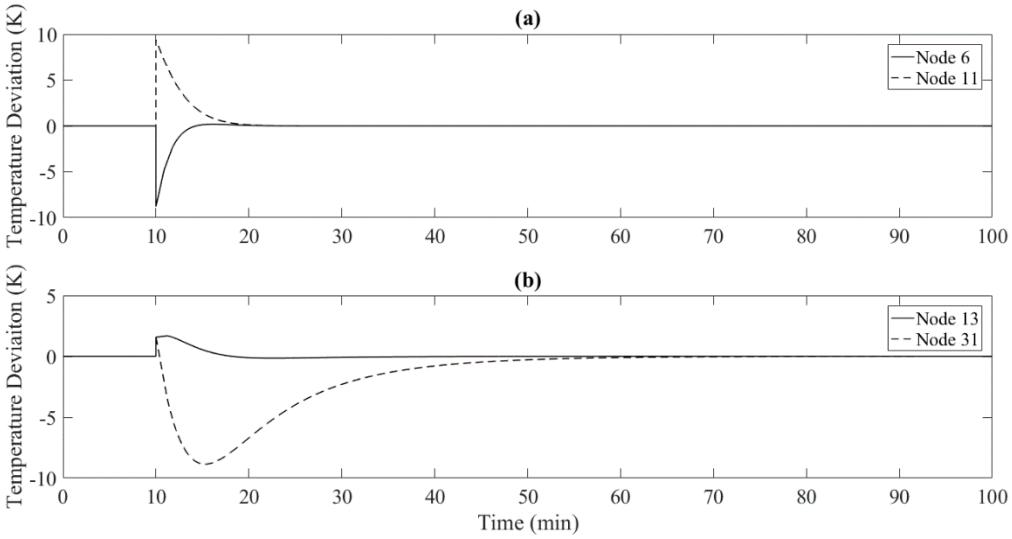

Figure 52 Outlet temperatures for (a) CGE/HGE and (b) CIGE/HIGE heat exchanger network for a feed gas flow rate disturbance of 100 $kNm^3\ h^{-1}$ with a 1-1/2-2 controller pairing

The simulation results for the controlled variables for a 1-2/2-1 controller pairing are shown in Figure 53. The results are similar to those observed for a 1-1/2-2 controller pairing. The temperatures at Node 6 and Node 11 reach a new steady-state quickly and the deviation is not large. The temperatures at Node 13 and Node 31 do not deviate from their set-point by more than 5 K. The temperature at Node 31 reaches steady-state relatively quickly however, it takes the temperature at Node 13 much longer. This is the opposite effect observed using a 1-1/2-2

controller pairing. It may be advantageous to have tighter temperature control at Node 31 which is the inlet stream to the final bed of the catalytic converter. This would ensure maximum SO_2 oxidation is taking place before the off-gas is released into the environment via the Superstack. This could be achieved using a 1-2/2-1 controller pairing.

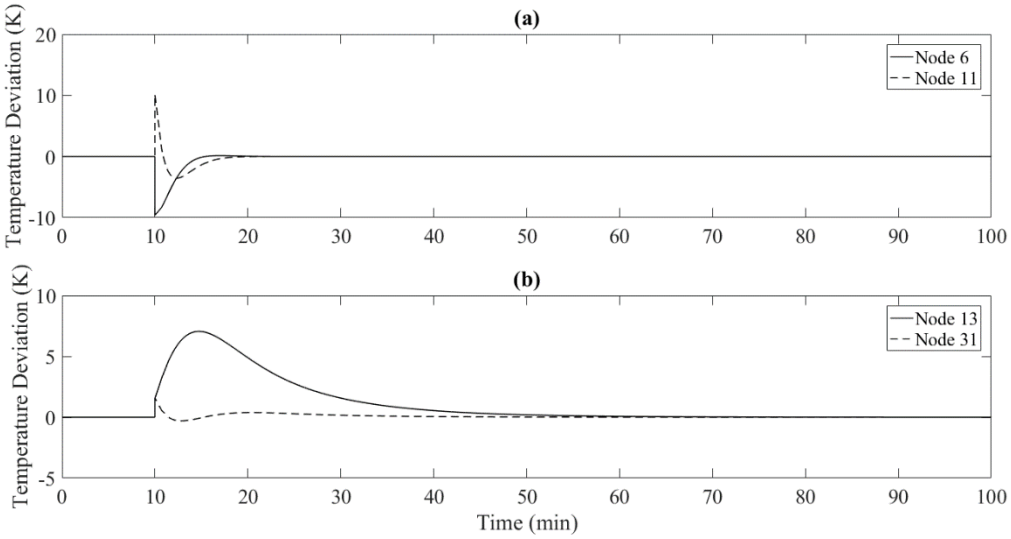

Figure 53 Outlet temperatures for (a) CGE/HGE and (b) CIGE/HIGE heat exchanger network for a feed gas flow rate disturbance of 100 kNm^3 h^{-1} with a 1-2/2-1 controller pairing

5.3.2 Case 2: Feed Gas Composition Disturbance

The second major disturbance that is commonly encountered in the acid plant is the concentration of SO_2 in the feed gas. The amount of SO_2 in the off-gas dictates the amount of SO_3 being produced in the converter and consequently the amount of heat evolving from the reaction. Temperature would need to be adjusted via the manipulated variable in order avoid a gas temperature that would irreversibly damage the catalyst and maintain a constant gas

temperature within the operating range of the catalyst. The identified dynamic model can be used to simulate the response of the controlled variables to a change in the SO_2 content in the feed gas. The outlet temperatures of the CGE/HGE heat exchanger are investigated, as these streams contain the highest amount of SO_2 and are the inlet streams to the first and second bed of the catalytic converter, where the majority of SO_2 oxidation occurs. From process knowledge, if the amount of SO_2 in the feed gas were increased, the amount of oxidation taking place in the first bed of the catalytic converter would consequently increase. Since more SO_3 is being produced the amount of heat evolved from the reaction would also increase. The temperature at the outlet stream of the first bed of the catalytic reactor, Node 7, is the hot stream inlet to the HGE. Since the hot stream of the HGE has increased more heat transfer would occur and the temperatures at Node 6 and Node 11 would be effected.

After 10 minutes of steady-state operation, the SO_2 content in the feed gas is increased by 2 vol%. The simulation results for the controlled variables, the outlet temperature of the CGE/HGE heat exchanger network, for a 1-1/2-2 controller pairing are shown in Figure 54. The results suggest that a SO_2 disturbance has a greater effect on the temperature at Node 6 than Node 11. The temperature at Node 6 deviates approximately 4 K and reaches a new steady-state after about 60 minutes. Again, similar to the flow rate disturbance, a 10 K deviation from mean temperature would still be within the optimal oxidation temperature range. Node 11 deviates less than 3 K and also reaches a new steady-state around 60 minutes after the disturbance was introduced. The response of the temperatures at Node 6 and Node 11 are similar for a 1-2/2-1 controller pairing, see Figure 55. It also takes around 60 minutes for

the temperatures to reach a steady-state, however, the temperature deviation is much smaller, which is desirable for the inlet streams to the catalytic converter.

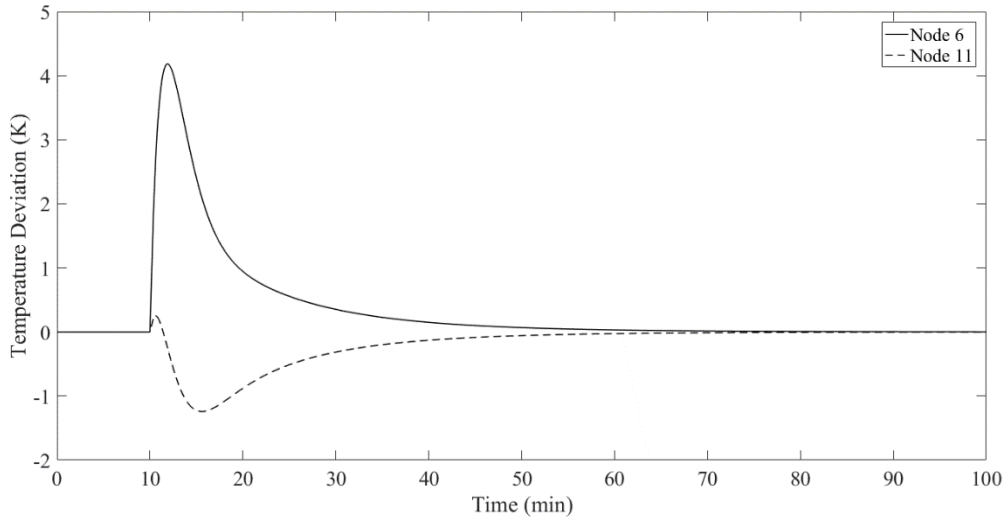

Figure 54 Outlet temperatures for CGE/HGE heat exchanger network for a feed gas composition disturbance of 2% with a 1-1/2-2 controller pairing

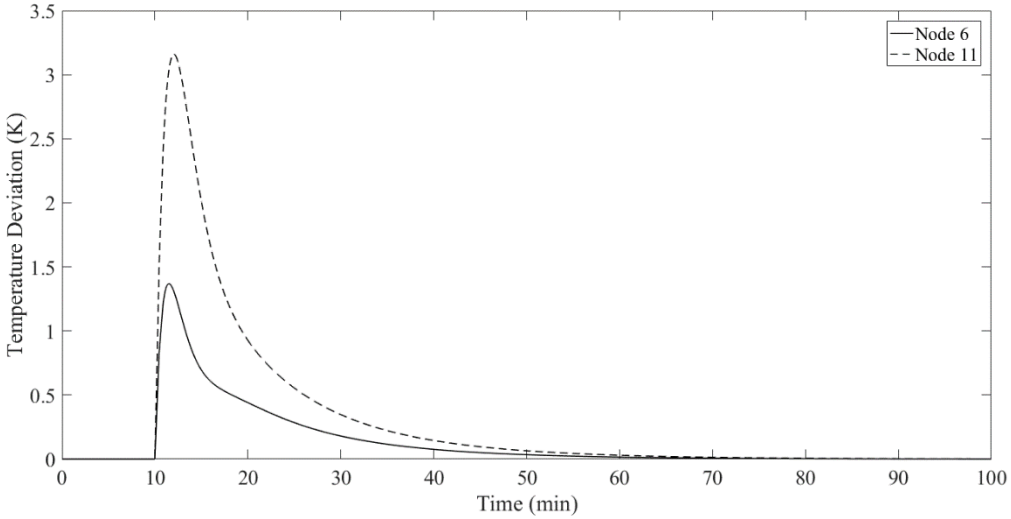

Figure 55 Outlet temperatures for CGE/HGE heat exchanger network for a feed gas composition disturbance of 2% with a 1-2/2-1 controller pairing

Chapter 6: Conclusions

This conclusion chapter summarizes the findings of this dissertations and discusses future work.

6.1 Summary of Results

In Chapter 3, a steady-state model for the temperature throughout the acid plant was developed. The steady-state model is based on fundamental mass and energy balances around the heat exchangers in the acid plant. In developing the steady-state model is was assumed that the heat exchanger were adiabatic, that the gas characteristics did not change from the inlet to the outlet of the heat exchangers and that absorption towers removed all of the SO_3 from the gas stream. The model contained two unknown parameters, β and UA, which were estimated using industrial operating data and a non-linear least squares solver. The model and estimated parameters were validated by comparing the measured temperatures from the industrial operating data to the model-predicted temperatures. The results show that the steady-state model estimates temperature trend well for the CIGE/HIGE heat exchanger network. There more disagreement between the model-predicted and measurement data for the CGE/HGE heat exchanger network since tight temperature control has been applied to the outlet temperatures of these heat exchangers. However, the model was successful in tracking temperature variations. The steady-state model was used to investigate the effects of process variables on the controlled variables. The temperatures of particular interest were the outlet streams of the HGE and HIGE, which are the inlet streams to the catalytic converter. Tight temperature

control within the operating range of the catalyst is the key variable in efficient SO_2 oxidation, and consequently acid plant operation. Two configurations were investigated: open-loop and closed-loop. The effects of the process variables on the controlled variables were amplified in a closed-loop configuration, which is expected since the outlet temperature of the catalytic converter would have an impact on the temperatures within the heat exchangers. It was concluded that the feed gas flow rate and SO_2 concentration in the feed gas had the largest effect on the controlled variables. These two disturbances will be greatly impacted with Clean AER project changes. Capturing the off-gas from the converter aisle, a major portion of the Clean AER project, will increase variation in feed gas flow rate and SO_2 concentration, which will make efficient acid plant operation difficult. The effects of the manipulated variables on controlled variables were also investigated which aided in identifying which valves have the greatest impact on outlet temperatures. This provides a better understanding of process interactions and can be used as a foundation of knowledge for process control. The steady-state gains were calculated, which quantify the observations of the open-loop configuration.

The dynamics of the process were investigated by examining industrial operating data, which suggested that the response of the controlled variables to operating changes and disturbances is sluggish and a steady-state model does not accurately represent the process. The correlation coefficient between the controlled variables and the manipulated and disturbance variables was calculated using industrial operating data. The correlation coefficient provides an estimate of how influential a disturbance and/or manipulated variable is on the controlled variable. For highly correlated variables correlation coefficient time-delay plots were constructed. The time-

delay plots provide a good estimate of the process time constant. Utilizing industrial operating data, the System Identification toolbox was used to identify a FOPDT model. The resulting model contained some unrealistic parameter estimates. The fit of the model identified for the temperatures at Node 11 and Node 13 was also very poor. This is a result of the industrial operating data at Node 11 and Node 13 which has very little variations since control has been applied to maintain tight temperature control. Thus the data at these measuring points is not suitable for model identification. Therefore, it was assumed that the cold and hot outlet temperatures of the CGE/HGE and CIGE/HIGE heat exchanger networks behaved similarly and only industrial operating data for Node 6 and Node 31 was used for model identification. The steady-state gains and time-delays plots were supplied to the System Identification toolbox, which improved the fit of the identified models. The resulting model fits the process well and can be used for control simulation, although the industrial operating data does not fit a simple, low-order dynamic model as well as hoped.

In Chapter 5, a control analysis was and a feedforward-feedback control scheme was simulated. The outlet temperatures of the CGE/HGE and CIGE/HIGE heat exchanger networks are regulated using the bypass valves located on each of the heat exchangers. Since there are multiple inputs and multiple outputs, temperature regulation in the acid plant is a MIMO control problem and the best controller pairing was not easily identifiable. Using steady-state information, a control analysis was carried out using RGA and SVA methods. Although RGA and SVA could not pinpoint the most effective controller pairing, it was concluded that the process is controllable even though there are strong process interactions. MATLAB's Simulink

was used to simulate a feedforward-feedback control scheme for two major disturbances: feed gas flow rate and SO_2 concentration. The controllers were tuned using the DS and IMC methods and the stability of the control loops was confirmed. Simulations were carried out for two alternative controller pairings. Examining the response of the outlet temperatures to major disturbances, both controller pairings produced similar results. Both pairings were successful in maintaining a temperature within the operating range of the catalyst and all of the temperatures reached a steady-state after the introduction of the disturbances.

6.2 Future Work

Temperature is a key variable in the efficient oxidation of SO_2 in the catalytic converter of a sulfuric acid plant and ultimately dictates the amount of SO_2 removed from an off-gas and prevented from being released into the environment. There are many manipulated and disturbance variables in sulfuric acid making process, which may have an influence on the temperature throughout the acid plant. Modeling temperature throughout the acid plant, is therefore, an important tool for process understanding, control and simulation that can be used to investigate various operational and disturbance changes. In this dissertation, a steady-state model was developed and used to identify a dynamic model. The resulting simple, first-order model fits industrial operating data fairly well and is sufficient for control analysis and simulation. To improve the steady-state model, the effects of process variables on the CIGE/HIGE heat exchanger network should be investigated using a closed-loop configuration. In addition, the steady-state gains of the process should be calculated using a closed-loop

configuration, which would improve the accuracy of the open-loop steady-state gains listed in this dissertation. A higher-order dynamic model, developed from first-principles rather than semi-empirical modeling should be explored by future research. The improved dynamic model would represent the temperature throughout the acid plant with a higher degree of accuracy. The model would be useful for investigating and validating operating changes, disturbance effects and exploring more advanced control schemes. A steady-state model should also be developed for temperature of the absorption towers. Lastly, the steady-state and dynamic models should be applied to industrial operating data post-SFU and Clean AER changes.

Nomenclature

Below is a list of all acronyms, substances, notations and variables and their units used throughout the dissertation.

Acronyms

Acronym	Description
AER	Atmospheric Emission Reduction
CGE	Cold gas exchanger
CIGE	Cold interpass gas exchanger
FAT	Final absorption tower
FSGC	Final SO_3 gas cooler
HGE	Hot gas exchanger
HIGE	Hot interpass gas exchanger
IAT	Interpass absorption tower
ISGC	Interpass SO3 gas cooler
MIMO	Multiple-input, multiple-output
NIST	National Institute of Standards and Technology
NPRI	National Pollutant Released Inventory
O.Reg.	Ontario Regulation
PI	Proportional-integral control
PD	Proportional-derivative control
PID	Proportional-integral-derivative control
RGA	Relative gain array
SFU	Surface Facility Upgrade
SRD	Standard Reference Database
SSE	Sum of squared errors
SVA	Singular value analysis

Substances and Compounds

Formula	Description
CO	Carbon monoxide
CO_2	Carbon dioxide
Cs	Caesium
$CuFeS_2$	Chalcopyrite
Fe	Iron
FeO	Iron oxide
Fe_8S_9	Pyrrhotite
Fe_2SiO_4	Silicate slag
H2O	Water
H_2SO_4	Sulfuric acid
K	Potassium
N_2	Nitrogen
Na	Sodium
NH_3	Ammonia
Ni	Nickel
NiO	Nickel oxide
NiS	Nickel matte
$(Ni,Fe)_9S_8$	Pentlandite
NO_x	Nitrogen oxides
O_2	Oxygen
$PM_{2.5}$	Fine particulate matter
S	Sulfur
SiO_2	Silica
SO_2	Sulfur dioxide
SO_3	Sulfur trioxide
SO_x	Sulfur oxides
V	Vanadium
VOC	Volatile organic compounds
V_2O_5-K_2SO_4	Vanadium-oxide catalyst

Block Diagram Notation

Variable	Description
D	Disturbance variable
D_m	Measurement of the disturbance variable
E	Error signal
G_c	Controller transfer function
G_d	Disturbance transfer function
G_f	Feedforward controller transfer function
G_m	Transmitter transfer function
G_p	Process transfer function
G_t	Disturbance transmitter transfer function
G_v	Final control element transfer function
K_c	Controller steady-state gain
K_m	Transmitter steady-state gain
P	Controller output
P_{FB}	Feedback controller output
P_{FF}	Feedforward controller output
U	Manipulated variable
Y	Controlled variable
Y_d	Change in Y due to D
Y_m	Measurement of the controlled variable
Y_{sp}	Controlled variable set-point
Y_u	Change in Y due to U

Variables

Variable	Description, units
A	Heat transfer area, m^2
A, B, C, D, E	Shomate equation parameters
a, b	Empirical constants related with SO_2 oxidation reaction
C_m	Molar heat capacity, J mol^{-1} K^{-1}
$C_{m,i}$	Molar heat capacity of component i, J mol^{-1} K^{-1}
CN	Condition number
CN_E	Euclidean condition number
CN_{min}	Minimum condition number
C_p	Mass heat capacity, J g^{-1} K^{-1}
$\bar{C}_p$	Mean mass heat capacity, J g^{-1} K^{-1}
$C_{p,c}$	Mass heat capacity of cold stream, J g^{-1} K^{-1}
$C_{p,h}$	Mass heat capacity of hot stream, J g^{-1} K^{-1}
I	Identity matrix
k	Instant in time, min
K	Steady-state gain
K_E	Equilibrium constant
K_c	Controller gain
M	Molar mass of gas stream, kg mol^{-1}
M_i	Molar mass of component i, g mol^{-1}
$\dot{m}$	Mass flow rate, kg s^{-1}
$\dot{m}_c$	Mass flow rate of cold stream, kg s^{-1}
$\dot{m}_h$	Mass flow rate of hot stream, kg s^{-1}
N	Flow rate, kNm^3 h^{-1}
P	Pressure, mmWG
P_{E_i}	Partial pressure at equilibrium of component i, atm
q	Rate of heat transfer, W
R	Ideal gas constant, 8.314 J $mol^{-1}K^{-1}$
t	Time, min
T	Temperature, K
$T_{c,i}$	Cold inlet temperature, K
$T_{c,o}$	Cold outlet temperature, K
T_E	Equilibrium temperature, K
T^f	Feed gas temperature, K
$T_{h,i}$	Hot inlet temperature, K
$T_{h,o}$	Hot outlet temperature, K
T_{int}	Intermediate temperature, K
U	Heat transfer coefficient, W m^{-2} K^{-1}
UA	Unknown parameter, W K^{-1}

V	Valve positon, %
V_i	Volume percentage of component *i*, vol%
X	Volume percentage of SO_2, vol%
X_i	Molar fraction of component *i*
X_i^f	Molar fraction of component *i* in feed
y_F	Filter output
y_m	Filter input/measured value
α	Bypass fraction
β	Unknown parameter
∂	Partial derivative
ΔH	Enthalpy of reaction, MJ $kmol^{-1}$
Δt	Sampling time, min
ΔT	Temperature difference, K
ΔT_{am}	Arithmetic mean temperature difference, K
ΔT_{lm}	Log-mean temperature difference, K
ε	Dimensionless parameter
θ	Dead time, min
λ	Relative gain
Λ	Relative gain matrix
ξ	Equilibrium parameter
σ	Matrix of singular values
σ_1	Largest, non-negative singular value
σ_r	Smallest, non-negative singular value
τ	Process time constant, min
τ_c	Controller time constant, min
τ_F	Filter time constant, min
Υ	Matrix of eigenvalues
Φ	Conversion ratio
Φ_E	Equilibrium conversion ratio
ω	Derivative filter constant

Matrix Operations

Notation	Operation
$\mathrm{X}_{i,j}$	*(i,j)* element of matrix **X**
$\boldsymbol{X}^{T}$	Transverse of matrix **X**
$\mathbf{X}^{-1}$	Inverse of matrix **X**
$\lvert\mathbf{X}\rvert$	Determinant of matrix **X**
$\lVert\mathbf{X}\rVert_{\mathrm{e}}$	Euclidean norm of matrix **X**
$\lVert\mathbf{X}\rVert_{1}$	1-norm of matrix **X**

References

Alenany, A., & Shang, H. (2013). Recursive subspace identification with prior information using the constrained least squares approach. *Computers and Chemical Engineering, 54*, 174-180.

Alenany, A., Shang, H., Soliman, M., & Ziedan, I. (2010). Subspace Identification with Prior Steady-State Information. *The 2010 International Conference on Computer Engineering & Systems*, (pp. 103-108). Cairo, Egypt.

Bergh, L. G., Muquillaza, V., & Chacana, P. B. (2004). Control Analysis of the Operation of a Copper Smelter and Two Sulphuric Acid Plants. *11th IFAC Symposium on Automation in Mining, Mineral and Metal Processing. 37*, pp. 227-232. Nancy: Elsevier.

Bristol, E. H. (1996). On a New Measure of Interactions for Multivariable Process Control. *IEEE Transactions on Automatic Control, 11*, 133-134.

Chase, M. W. (1998). NIST-JANAF Thermochemical Tables. *Journal of Physical and Chemical Refernce Data*, 1-1951.

Craig, N., & Vinal, G. W. (1940). Thermodynamic Properties of Sulfuric-Acid Solutions and Their Relation to the Electromotive Force and Heat of Reaction of the Lead Storage Battery. *Journal of the National Bureau of Standards, 24*, 475-490.

Crawford, G. A. (1995). Environmental improvements by the mining industry in the Sudbury Basin of Canada. *Journal of Geochemical Exploration*, 267-284.

Crundwell, F. K., Moats, M. S., Ramachandran, V., Robinson, T. G., & Davenport, W. G. (2011). *Extractive Metallurgy of Nickel, Cobalt and Platinum Group Metals.* Oxford, United Kingdom: Elsevier.

Davenport, W. G., & King, M. J. (2013). *Sulfuric Acid Manufacture.* Oxford: Elsevier.

Davenport, W. G., & Partelpoeg, E. H. (2015). *Flash Smelting: Analysis, Control and Optimization.* Oxford, United Kingdom: Pergamon Press.

Environment and Climate Change Canada. (2019, May). *Air pollutant emissions.* Retrieved from Government of Canada: https://www.canada.ca/en/environment-climate-change/services/environmental-indicators/air-pollutant-emissions.html

Fenton, M., Armstrong, K., & Huebsch, J. (2016). Convertible Lump Sum EPS Contracting Model - How to get the plant you need now and still enjoy in 20 years? *Procedia Engineering, 138,* 206-219.

Franklin, C. A., Burnett, R. T., Paolini, R. J., & Raizenne, M. E. (1985). Health Risks from Acid Rain: A Canadian Perspective. *Environmental Health Perspectives, 63*, 155-168.

Franklin, G. F., Powell, J. D., & Emami-Naeini, A. (2010). *Feedback Control of Dynamic Systems* (6th ed.). Toronto: Pearson.

Fruehauf, P. S., Chien, I.-L., & Lauritsen, M. D. (1994). Simplified IMC-PID tuning rules. *ISA Transactions, 33*, 43-59.

Gosiewski, K. (1993). Dynamic modelling of industrial so2 oxidation reactors part I. model of 'hot' and 'cold' start-ups of the plant. *Chemical Engineering and Processing: Process Intensification, 32*(2), 111-129.

Government of Canada. (2006, April 29). *Canadian Environemtal Protection Act: Notice Requiring the Preparation and Implementation of Pollution Prevention Plans in Respect of Specified Toxic Sudbstanes Released from Base Metals Smelters and Refineries and Zinc Plants.* Retrieved from Canada Gazette: http://www.gazette.gc.ca/rp-pr/p1/2006/index-eng.html

Government of Canada. (2018, September 13). *Vale Canada Limited - Copper Cliff Smelter 2017.* Retrieved from National Pollutant Release Inventory: https://pollution-waste.canada.ca/national-release-inventory/archives/index.cfm?do=facility_substance_summary&lang=en&opt_npri_id=0000000444&opt_report_year=2017

Government of Ontario. (2017, July 28). *O. Reg. 194/05: Industry Emissions - Nitrogen Oxides and Sulphur Dioxide.* Retrieved from Government of Ontario: https://www.ontario.ca/laws/regulation/050194

Government of Ontario. (2019, January 1). *Air Pollution - Local Air Quality.* Retrieved from Government of Ontario: https://www.ontario.ca/laws/regulation/050419

Grosdidier, P., Morari, M., & Holt, B. R. (1985). Closed-Loop Properties from Steady-State Gain Information. *Industrial and Engineering Chemistry Fundamentals, 24*, 221-235.

Günther, R., Schöneberger, J. C., Arellano-Garcia, H., Thielert, H., & Wozny, G. (2012). Design and modeling of a new periodical-steady state process for the oxidation of

sulfur dioxide in the context of an emission free sulfuric acid plant. *Computer Aided Chemical Engineering, 31,* 1677-1681.

He, J. (2018, April 16). *Dynamic Modelling of Catalytic SO2 Converter in a Sulfuric Acid Plant of an Industrial Smelter (Doctoral dissertation).* Retrieved June 14, 2019, from Research Repository: https://zone.biblio.laurentian.ca/handle/10219/3113

He, J., & Shang, H. (2017). A soft sensor for the sulphur dioxide converter in an industrial smelter. *Canadian Journal of Chemical Engineering, 95*(6), 1093-1100.

He, J., Zhang, J., & Shang, H. (2019). Two-Phase Dynamic Modeling and Simulation of Transport and Reaction in Catalytic Sulfur Dioxide Converters. *Industrial & Engineering Chemistry Research, 58*(25), 10963-10974.

Husnil, Y. A., Andika, R., & Moonyoung, L. (2017). Optimal plant-wide control of the wet sulfuric acid process in an integrated gasification combined cycle power plant. *Journal of Process Control*.

King, M. J. (1999, May 13). *Control and optimization of metallurgical sulfuric acid plants (Doctoral dissertation).* Retrieved June 14, 2019, from UA Theses and Dissertations: https://repository.arizona.edu/handle/10150/284812

Kiss, A. A., Bildea, C. S., & Grievink, J. (2010). Dynamic modeling and process optimization of an industrial sulfuric acid plant. *Chemical Egineering Journal, 158,* 241-249.

Linstrom, P. J., & Mallard, W. G. (2018, October). *NIST Standard Reference Database Number 69.* Retrieved from NIST Chemistry WebBook: https://webbook.nist.gov/chemistry/#Search

Liu, G. P., & Daley, S. (2001). Optimal-tuning PID control for industrial systems. *Control Engineering Practice, 9,* 1185-1194.

Liu, T., & Geo, F. (2012). *Industrial Process Identification and Control Design.* New York: Spinger.

Mann, R., Gardner, I. J., & Morris, C. (1980). Reactor dynamics and strtegies for minimising SO2 emissions during start-up of a contact sulphuric acid plant. *Chemical Engineering Science, 35,* 185-192.

Mann, R., Stavridis, E., & Djamarani, K. (1986). Experimental fixed-bed reactor dynamics for SO2 oxidation. *Chemical Engineering Research and Design, 64*(4), 248-257.

McAvoy, T. J. (1981). Connection between Relative Gain and Control Loop Stability and Design. *AIChE Journal, 27*(4), 613-619.

Moats, M. S., & Davenport, W. G. (2014). Chapter 2.2 - Nickel and Cobalt Production. In S. Seetharaman (Ed.), *Treatise on Process Metallurgy* (pp. 625-669). Oxford, United Kingdom: Elsevier.

Niederlinski, A. (1971). A Heuristic Approach to the Design of Linear Multivariable Interacting Control Systems. *Automation, 7*, 691-701.

Ogunnaike, B. A. (1996). A contemporary industrial perspective on process control theory and practice. *Annual Reviews in Control, 20*, 1-8.

Read, A. (2016, April 26). *Sulphur Dioxide and Health.* Retrieved from Pembina Institute: https://www.pembina.org/pub/sulphur-dioxide-and-health

Ripley, E. A., Redmann, R. E., & Crowder, A. A. (1996). *Environmental Effects of Mining.* Delray Beach, United States: St. Lucie Press.

Rivera, D., Morari, M., & Skogestad, S. (1986). Internal Model Control. 4. PID CONTROLLER DESIGN. *Industrial & Engineering Chemistry, Process Design and Development, 25*(1), 252-265.

Seborg, D. E., Edgar, T. F., Mellichamp, D. A., & Doyle III, F. J. (2011). *Process Dynamics and Control* (3rd ed.). John Wiley & Sons, Inc.

Shinskey, F. G. (1996). *Process-Control Systems.* Toronto: Mc-Graw Hill.

Shinskey, F. G. (2002). Process Control: As Taught vs as Practiced. *Industrial and Engineering Chemistry, 41*, 3745-3750.

Silveston, P. L., Hudgins, R. R., Bogdashev, S., Vernijakovskaja, N., & Matros, Y. S. (1994). Modelling of a periodically operating packed-bed SO2 oxidation reactor at high conversion. *Chemical Engineering Science, 49*(3), 335-341.

Skogestad, S. (2001). Probably the best simple PID tuning rules in the world. *AIChE Annual meeting* (pp. 1-28). Reno: Norwegian University of Science and Technology.

Skogestad, S. (2003). Simple analytic rules for model reduction and PID controller tuning. *Journal of Process Control, 13*(4), 291-309.

Skogestad, S., & Postlethwaite, I. (2001). *Multivariable Feedback Control* (2nd ed.). Toronto: Wiley.

Sørensen, P. A., Møllerhøj, M., & Christensen, K. A. (2015). New dynamic models for simulation of industrial SO2 oxidation reactors and wet gas sulfuric acid plants. *Chemical Engineering Journal, 278*, 421-429.

Vale. (2012). *Toxic Reduction Plan Summaries.* Copper Cliff: Vale.

Vale Canada Limited. (n.d.). *Ontario Operations.* Retrieved from Greater Sudbury Air Quality: www.airquality-sudbury-vale.com/ontario-operations/index.asp

Vale. (n.d.). *Clean AER Project.* Retrieved from Vale: http://www.vale.com/canada/EN/aboutvale/communities/sudbury/Clean-AER/Pages/default.aspx

WBK & Associates Inc. (2003, March 1). *Sulphur dioxide: environmental effects, fate and behaviour.* Retrieved from Alberta Government: https://open.alberta.ca/publications/077853216x